

UCSF

UC San Francisco Electronic Theses and Dissertations

Title

Studies of TMEM16A Calcium Activated Chloride Channel Structure and Function

Permalink

<https://escholarship.org/uc/item/26s2m1z3>

Author

Tien, Jason

Publication Date

2014

Peer reviewed|Thesis/dissertation

**Studies of TMEM16A Calcium Activated Chloride Channel
Structure and Function**

by

Jason Tien

DISSERTATION

Submitted in partial satisfaction of the requirements for the degree of

DOCTOR OF PHILOSOPHY

in

Neuroscience

in the

GRADUATE DIVISION

of the

UNIVERSITY OF CALIFORNIA, SAN FRANCISCO

Copyright 2014

by

Jason Tien

Acknowledgements

This work would not have been possible without the generous support of mentors, colleagues, family, and friends.

I first need to thank Drs. Lily and Yuh Nung Jan for the unparalleled training and research opportunities that they have offered me over the course of my graduate career. They have taught me to ask creative questions and to think critically about scientific results. I have been privileged to interact with extremely talented colleagues and to have access to tremendous resources in their lab. They have given me the freedom to pursue my own scientific interests and have encouraged me to follow my passions wherever they may take me.

I also thank my colleagues in the Jan lab. The lab would not be the same place without the scientific energy of these superb scientists. In particular, I need to acknowledge Drs. Hye Young Lee, Christian Peters, and Huanghe Yang for their patient mentorship. My research is possible only because of their tutelage over the years. I have learned so much over the course of our collaboration and have benefited from our numerous discussions.

My studies would also not have been possible without the help of the Minor lab. The members of the Minor lab have taught me everything I know about protein biochemistry. In particular, Drs. Daniel Minor, David Shaya, Gabriel Mercado Besserer, and Marco Lolicato have been endlessly generous with their time and expertise.

This dissertation would also not be possible without the support and advice of my Thesis Committee. I thank Drs. Peter Sargent, David Agard, and Yuriy Kirichok for their time and dedication to my graduate training. It has been a privilege to be advised by such

incredible scientists, and many of the experiments contained within this work started as topics of discussion at this Committee.

I want to thank the scientists who mentored me during my early academic training. Drs. Oliver Hobert and Sarah Chang taught me how to hold a pipette for the first time and patiently trained a novice high school student. Drs. Roger Reeves and Lisa Olson mentored me through my first scientific project as an undergraduate and encouraged me to publish a manuscript for the first time. Dr. Richard Haganir and Richard Johnson were responsible for my later undergraduate research where I worked on my first independent project. It is because of the encouragement of these mentors that I have pursued a graduate degree.

I also need to acknowledge all the people outside of the lab who have made my training at UCSF such an exceptional experience. First, I thank Drs. Leslie King and Deneb Karentz at the University of San Francisco who gave me the opportunity and training to teach undergraduate students. Second, I thank the UCSF Innovation, Technology, & Alliances office for introducing me to entrepreneurship and teaching me everything I know about patents and licensing. Third, I thank Dean Elizabeth Watkins and President Joseph Castro for supporting me during my tenure as the president of the Graduate Students Association. My work in these different offices and institutions have enhanced my academic experience and has prepared me for a career as an independent scientist.

Lastly, I want to acknowledge my family who have been ever encouraging of my efforts to pursue an advanced degree. My parents, Yung and Hsiaowen Tien, and my sister, Joanne Tien, have been there to support my academic aspirations since elementary school. In addition, my partner, Eric Lusford, has been there daily for me in graduate school and has made every day I spend in San Francisco brighter and happier.

Contributions

Lily Y. Jan directed and supervised the research that forms the basis for this dissertation. This dissertation contains modifications of previously published materials. Chapter 1 is a modified reprint of “Molecular properties of ion channels” by Jason Tien, David Matthew Young, Yuh Nung Jan, and Lily Y. Jan appearing in John H. Byrne, Ruther Heidelberger, and M. Neal Waxham’s 3rd edition of *From Molecules to Networks* (2014). Chapter 2 is a modified reprint of “Identification of a dimerization domain in the TMEM16A calcium-activated chloride channel (CaCC)” by Jason Tien, Hye Young Lee, Daniel L. Minor Jr., Lily Y. Jan, and Yuh Nung Jan appearing in volume 110 of the *Proceedings of the National Academy of Sciences of the United States of America* (2013). Chapter 3 is a reprint of a manuscript “A comprehensive search for calcium binding sites critical for TMEM16A calcium-activated chloride channel activity” by Jason Tien, Christian J. Peters, Xiu Ming Wong, Tong Cheng, Yuh Nung Jan, Lily Y. Jan, and Huanghe Yang currently under review at *eLife*. Individual author contributions are noted at the end of each respective chapter.

This work is comparable to work for a standard thesis awarded by the University of California, San Francisco.

Lily Y. Jan

Abstract

TMEM16A is a novel calcium-activated chloride channel first cloned in 2008. It is responsible for regulating secretions from the epithelium, excitability of smooth muscle, membrane potential of neurons, and cellular proliferation. This work describes two studies investigating the structure and function of TMEM16A ion channels. In the first, I report a series of experiments that show that TMEM16A channels have a homodimeric architecture facilitated by its cytoplasmic N-terminus. This dimerization domain is important for channel assembly in eukaryotic cells, and the *in vitro* association of peptides containing the dimerization domain is consistent with a homotypic protein-protein interaction. Amino acid substitutions in the dimerization domain affect functional TMEM16A-CaCC channel expression as expected from its critical role in channel subunit assembly. In the second, I describe the identification of four acidic amino acid residues as putative calcium-binding sites. Alterations of the charge, polarity, and size of amino acid side chains at these sites alter the ability of different divalent cations to activate the channel. Furthermore, gating of TMEM16A mutants containing double cysteine substitutions at these residues are sensitive to the redox potential of the internal solution, providing evidence for their physical proximity and solvent accessibility.

Table of Contents

Chapter 1. Introduction.....	1
An overview of ion channels.....	1
Physiological Function of the TMEM16A Family of Transmembrane Proteins	16
Structural Mechanism of TMEM16A Function	19
Chapter 2. Identification of a Dimerization Domain in the TMEM16A Calcium- Activated Chloride Channel (CaCC)	22
Introduction.....	22
Results.....	23
Discussion	32
Materials and Methods	34
Acknowledgments	39
Author Contributions	39
Chapter 3. A comprehensive search for calcium binding sites critical for TMEM16A calcium-activated chloride channel activity.....	40
Introduction.....	40
Results.....	42
Discussion	52
Methods	55
Acknowledgments	58
Author Contributions	58
Figure Legends.....	60

References 72

List of Figures

Figure 1.1. Examples of ion channel pores from various potassium channels	96
Figure 1.2: Several major families of ion channels use similar designs	97
Figure 1.3: Voltage-gated Ca ²⁺ and K ⁺ channels share a 6-TM architecture	98
Figure 1.4: Voltage dependent block of K _{ir} channels	99
Figure 2.1. TMEM16 family proteins form dimeric protein complexes	100
Figure 2.2. The TMEM16A N-terminal domain is sufficient for subunit interaction	101
Figure 2.3. A region in the cytoplasmic N-terminus is responsible for subunit dimerization.....	102
Figure 2.4. Residues 117–179 are sufficient for a homotypic dimer interaction	103
Figure 2.5. Replacement of the TMEM16A dimerization domain with that of TMEM16F yields functional channels.....	104
Figure 2.6. A Segment of 19 Residues is necessary for TMEM16A function.....	105
Figure 2.S1. Dendrogram showing sequence conservation between TMEM16 homologues in mouse (m) and Xenopus (x)	106
Figure 2.S2. Sequence alignment between mTMEM16A, xTMEM16A, mTMEM16B and mTMEM16F calculated using ClustalW2	107
Figure 2.S3. Cysteine residue in the TMEM16A dimerization domain is dispensable for subunit dimerization.....	108
Figure 2.S4. Alignment from Figure S2 of region replaced in chimera mutants between mTMEM16A and mTMEM16F.....	109
Figure 2.S5. Same cells from Figure 6 with ER-specific label shown	110

Figure 3.1. Calmodulin (CaM) is not responsible for the calcium-dependent activation of TMEM16A calcium-activated chloride channels (CaCC).....	111
Figure 3.2. Screen for potential calcium-binding residues in TMEM16A-CaCC	112
Figure 3.3. Systematic alanine scan of highly conserved intracellular acidic residues identified five mutations that dramatically reduced the apparent calcium sensitivity of TMEM16A-CaCC	113
Figure 3.4. The effects of different amino acid side chains on the calcium sensitivity of mutant TMEM16A-CaCC channels indicate that E698, E701, E730 and D734 might be directly involved in binding calcium	114
Figure 3.5. TMEM16A channel sensitivity to strontium ions is disrupted by mutations of the identified calcium-binding sites	115
Figure 3.6. TMEM16A channel sensitivity to cadmium ions is disrupted by mutations at the identified calcium-binding sites	116
Figure 3.7. Cysteine crosslinking suggests that the calcium-binding residues in TMEM16A-CaCC form a metal ion binding pocket that is exposed to the cytoplasm	117
Figure 3.S1. Calmodulin (CaM) is not involved in the calcium-dependent activation of TMEM16A-CaCC	118

Chapter 1. Introduction

The cell membrane is a hydrophobic bilayer of lipids lined with negative phosphate charges on both sides and is normally impermeable to all but small, uncharged molecules. In order to allow important physiological ions to cross this barrier, cells express ion channels that serve as highly selective passageways through which ions can pass. In the nervous system, the activity of ion channels results in the resting membrane potential of neurons and controls the firing pattern and waveform of action potentials. To fulfill these functions, ion channels are selectively permeable to only certain ions and are regulated by chemical, electrical, or sensory signals (Hille, 2001).

This work examines the structural features of the TMEM16A calcium-activated chloride channel. I begin with a brief introduction describing several classes of well-characterized ion channels and review the existing scholarship pertaining to TMEM16A proteins. I then describe a study that shows that TMEM16A proteins are dimers composed of identical subunits. Lastly, I present a series of experiments that identify several acidic amino acids to be sites of calcium-TMEM16A interaction. This research provides insights into the mechanism by which TMEM16A channels function and contributes toward a structural understanding of TMEM16A activity.

AN OVERVIEW OF ION CHANNELS

Ion channels are distinguished by two major functional characteristics. First, they form a pore through which ions traverse the membrane (see Figure 1.1). The pore is made up of transmembrane segments organized to form a hole through the lipid bilayer, and the unique arrangement of amino acids and transmembrane segments determines the

selectivity, conductivity, and permeability of the channel. Second, most channels can regulate the movement of ions through the pore with a gate that can open or close depending on stimuli. The stimulus can be in the form of voltage depolarization, extracellular ligands, or intracellular second messengers. This gating mechanism is responsible for the activation, deactivation, and inactivation of the channel. Structural elements from different parts of the protein may be involved in each of these functional features and can often be regulated by interactions with the environment, other proteins, or post-translational modifications. As a result, biological systems can precisely tune the activity of ion channels to meet their physiological needs.

Ion channels are grouped into several families based on similarities in their structure and mechanism of action. Channels in the same family typically share the same membrane topology for their pore-lining α subunits and display significant sequence similarity. In addition to forming the ion permeation pathway, α subunits often also contain other domains to support the pore and influence its dynamics. Auxiliary or β subunits can confer regulatory or modulatory effects on channel function.

Pore-Loop Channels

The group of pore-loop (“p-loop”) channels is a large superfamily of evolutionarily related proteins that share a similar architecture characterized by four homologous subunits each contributing two transmembrane helices joined by a p-loop toward the pore-lining region of the channel. This protein family contains over a hundred different gene members, including channels in the voltage-gated sodium (Na_v), voltage-gated calcium (Ca_v), voltage-gated potassium (K_v), calcium-activated potassium (K_{Ca}), cyclic nucleotide gated (CNG), transient receptor potential (TRP), inwardly-rectifying potassium (K_{ir}) and

two-pore potassium (K_{2P}) channel subfamilies (Yu and Catterall, 2004). Crystallographic studies of these proteins have revealed an “inverted teepee” topology (Figure 1.1) with the p-loop located at the wider end of the teepee facing the extracellular solution and the narrower portion of the teepee pointing toward the cytoplasm. The p-loop and the transmembrane helices flanking it form the narrowest portion of the ion permeation pathway (Doyle et al., 1998), and the order and identity of the amino acid residues in the p-loop determine the precise ion selectivity properties of the channel (Heinemann et al., 1992, Lu et al., 2001).

Voltage-gated sodium, calcium, and potassium channels. The founding members of this family of proteins are the voltage-gated channels, including Nav, Cav, and Kv (Figures 1.2A and 1.3A–B) (Catterall, 1998, Catterall, 2000, Jan and Jan, 1997). Voltage-gated channels are opened by changes in membrane potential detected by a voltage sensor connected to the pore domain. In the voltage-gated potassium channel, four homologous subunits assemble post-translationally into a pore-forming protein complex; in sodium and calcium channels, four homologous pseudosubunits are linked together in a long polypeptide to form a large α subunit. Each subunit or pseudosubunit contains six transmembrane segments organized with a four-transmembrane voltage sensor N-terminal to the two-transmembrane pore domain. By responding to changes in membrane potential, these channels play critical roles in shaping action potentials and facilitating neuronal responses to depolarization. Voltage-gated sodium channels initiate and propagate action potentials, voltage-gated potassium channels hyperpolarize the cell and modulate the duration of the action potential, and voltage-gated calcium channels regulate the influx of second messengers important for downstream signaling events following

action potentials (Kandel, 2012). Although most voltage-gated channels are activated by depolarization, other family members include hyperpolarization-activated cation channels involved in rhythmic activities (Lüthi and McCormick, 1998) and plant potassium channels activated by hyperpolarization (Gaymard et al., 1996, Marten et al., 1999, Schachtman et al., 1992).

Calcium-activated potassium channels. As its name suggests, calcium-activated potassium channels have potassium-selective pores that are gated by calcium (Berkefeld et al., 2010). These channels can be divided into two groups: large-conductance BK channels (Atkinson et al., 1991, Lee and Cui, 2010) and small-conductance SK channels (Köhler et al., 1996, Weatherall et al., 2010). BK channels, to facilitate the termination of action potentials, are maximally activated by simultaneous depolarization and micromolar intracellular calcium. Similar to the voltage-gated potassium channel, BK channels are complexes of four subunits that each contains six transmembrane segments forming a voltage sensor and a pore domain. In addition, BK channels have an extra S0 domain that places the N-terminus on the extracellular side and a large cytosolic calcium-sensing domain that uses the free energy of calcium interaction with acidic residues arranged in a “calcium gating ring” to drive changes in gate conformation (Figure 1.3C) (Yuan et al., 2010). SK channel topology is also similar to that of the voltage-gated potassium channel, with six transmembrane segments per subunit and four subunits per channel. Unlike the BK channel, however, the SK channel is not gated by voltage and its calcium-sensing domain is an auxiliary calmodulin subunit. The calmodulin molecule is constitutively associated with the cytosolic calmodulin-binding domain of the SK channel, and the binding

of calcium to calmodulin causes conformational changes that are transmitted to the SK protein gate (Schumacher et al., 2001).

Cyclic nucleotide gated channels. CNG channels are a cation-selective species that play a critical role in signal transduction pathways that use cGMP or cAMP as second messengers (Biel and Michalakis, 2009, Mazzolini et al., 2010). Although they share the six-transmembrane topology of Kv channels and have a functional voltage sensor (Tang and Papazian, 1997), CNG channels are largely insensitive to changes in membrane potential and are gated only by cyclic nucleotides. Ligand binding is facilitated by a cytosolic cyclic nucleotide binding domain located at the C-terminus of each subunit. Cyclic nucleotide binding to each subunit triggers centripetal movement of the gating ring to open the channel (Taraska and Zagotta, 2007).

Other channels with architecture similar to CNG channels include the hyperpolarization-activated and cyclic nucleotide gated (HCN) channels (Wahl-Schott and Biel, 2009) and the ether-a-go-go (EAG) potassium channels (Bauer and Schwarz, 2001). HCN channels are sodium- and potassium-permeable membrane proteins that are activated by hyperpolarization and are important for the regulation of the pacemaker current in the heart. Ligand interaction with its cyclic nucleotide domains modulates HCN channel activity by shifting its activation curves toward depolarizing potentials. EAG, along with eag-related (ERG) and eag-like (ELK) channels, are potassium-selective channels activated by depolarizing membrane potentials. Although these channels have a cyclic nucleotide binding domain, ligand binding does not seem to have a pronounced functional effect on channel gating.

Transient receptor potential channels. The transient receptor potential (TRP) channels are a diverse class of nonselective cation channels that are important for sensory transduction. They share a 6 transmembrane architecture with the Kv channels, but are generally not voltage sensitive and may be permeable to divalent cations like calcium (Montell, 2005). TRP channels may be activated by a variety of stimuli and thus serve a key signal transduction role in several sensory modalities. Different subtypes of TRP channels have been shown to be necessary for thermo-, mechano-, chemo-, and photosensation. In some cases, such as in the TRPV family responsible for thermosensation and mechanosensation, the ion channel is the physical sensor responsible for transducing environmental stimuli to electrochemical reactions. In other cases, such as in the TRPC family which responds to second messengers of the phospholipase C (PLC) pathway and to calcium efflux from internal stores, the channel acts as intermediaries in the signal transduction pathway. This is the case in the pheromone chemosensing pathway in the mammalian vomeronasal organ and the photon detection pathway of *Drosophila* photoreceptor cells, where environmental stimuli is converted to neuronal depolarization by activating G protein-coupled receptors that signal through second messengers to activate TRP channels (Venkatachalam and Montell, 2007). Notwithstanding its prominence in sensory transduction, the mechanism by which TRP channels gate their pores remains poorly understood. Recent research has suggested that channel gating may involve several structural elements, including the N-terminal ankyrin repeats (Cordero-Morales et al., 2011), the pore turret (Yang et al., 2010), the C terminal cytoplasmic domain (Brauchi et al., 2006), and the transmembrane pore domain (Salazar et al., 2009).

Inwardly rectifying potassium channels. The inwardly rectifying potassium (K_{ir}) channels are also members of the p-loop superfamily. Although the concentration of potassium ions is usually much higher inside the cell than outside the cell, K_{ir} channels are named for their ability to allow much larger potassium influx than efflux. Like K_v channels, K_{ir} channels have four α subunits lining the pore, but they only contain two transmembrane segments, which correspond to the pore domain of the K_v channel alpha subunit without the voltage sensor (Figure 1.2B) (Jan and Jan, 1997). The observed inward rectification arises from a voltage-dependent block of the pore by the strong interaction of divalent cations with several acidic residues in the second transmembrane domain (Figure 1.4). At hyperpolarizing potentials, extracellular cations – most of which are monovalent ions – tend to flow into the cell. Because the p-loop selectivity filter is selective for potassium over sodium, the inward flow of current consists mostly of potassium ions. However, since the cytoplasm contains high concentrations of magnesium and other di- and polyvalent cations, multivalent cations enter the pore at depolarizing potentials and clog the pore to block current in the outward direction (Nichols and Lopatin, 1997).

Channels in the classical Kir2 subfamily are constitutively open while channels in the Kir3 G-protein gated potassium channel (GIRK) and Kir6 ATP-sensitive potassium channel (K_{ATP}) subfamilies open in response to ligand interaction. GIRK channels are activated by interaction of their cytoplasmic C-terminal domain directly with $G\beta\gamma$ subunits. Their activation allows inhibitory transmitters such as GABA to generate slow inhibitory postsynaptic potentials (IPSPs) in the brain, and the parasympathetic transmitter acetylcholine to slow the heart rate (Lüscher et al., 1997, Wickman et al., 1998). K_{ATP} channels are inactivated by ATP interaction with Kir6's cytoplasmic domains and are

activated by ADP interaction with the nucleotide-binding domain of an auxiliary sulphonylurea receptor (SUR) subunit that associates 1:1 with Kir6 subunits (Hibino et al., 2010). Besides regulating insulin release from the pancreas in response to changes in blood glucose levels, ATP-sensitive potassium channels are present in the brain, the heart, and skeletal and smooth muscles (Ashcroft and Gribble, 1998, Ashcroft, 2000, Babenko et al., 1998, Quayle et al., 1997). In the central nervous system, these channels may be responsible for regulating food intake and metabolism (Yang et al., 2012b). In addition, metabolic stress may activate these channels to protect neurons from death (Yamada et al., 2001).

Two-pore potassium channels. Two-pore potassium (K_{2P}) channels, unlike other channels in this family, contain two pore-loop domains. Each pore-lining α subunit of these channels appears to be a tandem dimer of two Kir-like, or one Kir-like and one Kv-like, α subunits (Figure 1.2C) (Lesage and Lazdunski, 2000). Because of their unique two-pore architecture, each subunit actually contributes two p-loops to the channel pore and channels assemble as dimers instead of tetramers. These channels are thought to be “leak” potassium channels that are active at rest, determining the resting membrane potential with their activities. Although many of these channels are constitutively active, their activity can be modulated by various environmental stimuli, which makes them ideal candidates for sensory receptors. Among these candidates are the TREK channel subtype that can be modulated by mechanical perturbation of the membrane and by changes in temperature and pH, the TASK channel subtype that is sensitive to acid, and the TALK channel subtype that is sensitive to alkaline. Additional channels in the K_{2P} family include the TWIK, THIK, and TRESK groups (Enyedi and Czirjak, 2010). Channel gating in the K_{2P}

family may be mediated by alpha helices near the inner opening of the pore domain or in the plasma membrane bilayer (Miller and Long, 2012, Brohawn et al., 2012). In addition, many of these channels may have novel pharmacological profiles due to the presence of a “cap” that blocks access to their pore domain from the extracellular side (Patel et al., 1999).

Voltage-Gated Proton Channel

Members of the voltage-gated proton channel family have a voltage-sensor domain homologous to that of the Kv channels (Figure 1-2D). Instead of having a separate pore domain, however, movement of the voltage sensor in response to depolarization opens a proton permeation pathway in the voltage-sensor domain itself (Berger and Isacoff, 2011). This pathway is filled with a continuous “wire” of water molecules that extend from the intracellular to the extracellular side, and protons are conducted along this wire by jumping from one water molecule to the next (Ramsey et al., 2010). Each proton channel is a dimer composed of two separate voltage-sensor domains, each with its own independent pore that is allosterically coupled to the other so that channel gating exhibits positive cooperativity (Tombola et al., 2010). In excitable cells, these channels are responsible for extruding acid during action potentials, presumably in response to excess protons produced as a result of metabolic activity (Decoursey, 2003).

Ionotropic glutamate receptors

The ionotropic glutamate receptors (iGluRs) are a group of ligand-gated non-selective cation channels that open in response to external glutamate (Cull-Candy and Leszkiewicz, 2004, Mayer, 2011). Depending on their differential sensitivity to different pharmacological agents, they are divided into three major classes: N-methyl D-aspartate

(NMDA) receptors, α -amino-3-hydroxy-5-methylisoxazole-4-propionic acid (AMPA) receptors, and kainate receptors. Members of the iGluR channel family are tetrameric protein complexes assembled from four homologous subunits. Each subunit has an ligand-binding domain important for agonist interaction and a transmembrane domain containing the selectivity filter and the activation gate (Mayer and Armstrong, 2004). The transmembrane domain consists of three membrane-spanning alpha helices (M1, M3, and M4) that line the pore and a reentrant loop (M2) that forms the selectivity filter of the channel (Figure 1.2E) (Kuner et al., 2001). Glutamate interaction with iGluRs triggers a rotation of the ligand-binding domain “clamshell” and pulls apart the M3 gating transmembrane helices to open up the pore (Sobolevsky et al., 2009, Madden, 2002). The pore-lining domain of these ligand-gated ion channels is topologically equivalent to an “upside-down” K_{ir} α subunit (Wo and Oswald, 1995) and a prokaryotic potassium-selective glutamate receptor with this membrane topology (Chen et al., 1999) has been identified as a missing link between potassium channels and eukaryotic glutamate receptors. The channels in this family are perhaps best known for their role in a learning and memory process called long-term potentiation (LTP) where NMDA receptors act as coincidence detectors whose activation signals the insertion of AMPA receptors into the postsynaptic membrane (Kerchner and Nicoll, 2008).

Cys-Loop Channels

The cys-loop channels are an unrelated group of ligand-gated ion channels (Karlin, 2002, Sine and Engel, 2006). The founding members of this family are the cationic nicotinic acetylcholine receptors (nAChR) that are responsible for various forms of cholinergic signaling in the nervous system, including receiving input at the neuromuscular junction

and mediating reward circuitry in the mesocorticolimbic dopamine system. nAChRs are assembled combinatorially as a heteropentameric protein complex from various possible subunits. There are seventeen different nAChR subunits grouped into five different types (α , β , γ , ϵ , and δ). Each subunit contains four transmembrane segments (Figure 1.2F) and an amino-terminal ligand-binding domain. The ligand-binding domains of an α subunit and an adjacent subunit work cooperatively to bind one acetylcholine molecule at the cleft between the two subunits, and two bound acetylcholine molecules are necessary for full channel activation. Upon agonist binding, the second transmembrane segment (M2), the pore-lining helix, rotates to open the channel (Unwin, 1995, Miyazawa et al., 2003).

Other members of the cys-loop channel family include the cation-permeable 5-HT₃ serotonin receptor that mediates fast excitatory synaptic transmission (Maricq et al., 1991) and the anion-permeable glycine (Lynch, 2004) and GABA_A (Olsen and Sieghart, 2009) receptors that mediate fast inhibitory synaptic transmission. Mutations in a series of polar amino acid residues in the pore-lining M2 helix of the nAChR channel are necessary to convert the channel from a cation-selective type to an anion-selective type (Galzi et al., 1992, Imoto et al., 1988, Konno et al., 1991).

Intracellular calcium channels

Cation channels composed of four subunits, each with large cytoplasmic domains and six transmembrane segments, are responsible for releasing calcium from internal stores such as the endoplasmic reticulum (ER) (Mikoshiha, 1997, George et al., 2004). Members of this family include the inositol 1,4,5-trisphosphate (IP₃) receptors that are activated by interaction with IP₃ second messengers and the ryanodine receptors (RyR) that can be activated by direct interaction with voltage-gated calcium channels on the

plasma membrane (Figure 1.2G). No crystallographic structure of these channels has yet been resolved, but high-resolution electron microscopy has revealed a “square-mushroom” shape with a pore extending down the central axis. Similar to pore-loop potassium channels, the selectivity filter is thought to be a narrow constriction in the pore formed by TM5 and TM6 and is gated by the bending and rotation of a bundle of transmembrane helices located at the cytoplasmic surface (Foskett et al., 2007). In IP₃ receptors, the free energy used to drive channel activation comes from the interaction between phosphate groups on the IP₃ ligand and basic residues in the clam-shaped IP₃ binding core domain (Taylor and Tovey, 2010). Although the allosteric activation mechanism for ryanodine receptors is not well understood, gating for RyR channels is likely to be complex and to involve several modulators such as Cav channels, calmodulin, calsequestrin, CaMKII, and FK506 binding proteins that dock onto its large cytoplasmic domain (Lanner et al., 2010).

Epithelial Sodium Channels

Epithelial sodium channels (ENaC) are voltage-independent, amiloride-sensitive, trimeric protein complexes that contain two membrane-spanning segments per subunit (Figure 1-2H) and are responsible for the detection of a variety of sensory stimuli (Ben-Shahar, 2011). Members of the ENaC family include FMRamide-activated sodium channels that are gated by ligands (Coscoy et al., 1998), acid sensing ion channels (ASIC) that are activated by protons (Waldmann et al., 1997), chemosensory channels that respond to salt (Chandrashekar et al., 2010), and mechanosensory channels responsible for touch sensation (O'Hagan et al., 2005). The pore of these channels is lined by the second transmembrane helix of each subunit and is gated by a kink in the helix that rotates away from the central axis to open the ion permeation pathway. Ion selectivity is most likely

achieved by the negative electrostatic potential of the pore vestibule and a narrow selectivity filter on the cytoplasmic side of the gate. A large extracellular domain is poorly conserved between different ENaC channels and acts as the sensor for the various stimuli detected by different ENaC channels (Kashlan and Kleyman, 2011, Jasti et al., 2007).

Purinergic Cation Channels

Non-metabotropic purinergic signaling is mediated by the P2X class of ATP receptors, a family of nonselective cation channels that typically depolarize cells under physiological conditions (Valera et al., 1994, Burnstock, 2007). In the central nervous system, these channels may be found postsynaptically at glutamatergic and GABAergic synapses, where co-released ATP molecules modulate synaptic responses. In addition, P2X channels may be found presynaptically, where it increases the probability of neurotransmitter release by elevating calcium influx (Khakh and North, 2012), and on glial cells, where P2X channel activation triggers the release of gliotransmitters to facilitate glia-neuron communication (Sperlágh et al., 2006). In the periphery, these channels may be responsible for the fast synaptic transmission of sensory information in the gustatory, olfactory, auditory, and pain pathways (Surprenant and North, 2009).

P2X channels are chalice-shaped, trimeric protein complexes with a large ATP-binding extracellular domain and two transmembrane segments per subunit (Figure 1-2I). The pore is formed by the second transmembrane helix of each subunit and is lined by electronegative oxygen atoms that interact directly with permeant ions. In the closed state, the pore helices cross each other to constrict the pore. The ATP-binding site is formed at the interface between two adjacent subunits, and agonist interaction causes the extracellular domains to move toward each other, rotating the transmembrane segments

outwards and opening the pore in an iris-like motion. Ions enter the channel through lateral fenestrations in the extracellular domain and ion selectivity is partially achieved by the presence of acidic residues near the channel entrance in the extracellular domain (Hattori and Gouaux, 2012, Kawate et al., 2009).

ClC Chloride Channels

ClC chloride channels are widely expressed throughout the body and, in the nervous system, are responsible for regulating the excitability of neuronal membranes as well as the acidification of synaptic vesicles (Jentsch et al., 2005). These channels evolved from prokaryotic chloride/proton exchangers, and many of them remain voltage and pH sensitive. Structurally, ClC channels are dimeric proteins containing one pore per subunit (Figure 1.2J). Each subunit is a two-fold symmetrical polypeptide with eighteen transmembrane segments. The C-terminal half of the polypeptide is homologous to the N-terminal half, but oriented in the opposite, anti-parallel direction. The two halves of each subunit fold around a central pore running down the axis of symmetry, each orienting the N termini of two alpha-helices toward the ion permeation pathway and creating two positive electrostatic sites in the pore that selectively interact with chloride (Dutzler et al., 2002). The pore is gated by the side chain of a negatively charged glutamate residue that occludes the pore in the closed state and swings out of the way when it is protonated by low pH to reveal a third chloride binding site (Dutzler et al., 2003). The movement of chloride into this site is voltage dependent, and the competition between the ion and the glutamate side chain for this site is responsible for the voltage-dependent gating of ClC channels (Pusch et al., 1995, Pusch, 2004).

Cystic Fibrosis Transmembrane Regulator

The Cystic Fibrosis Transmembrane Regulator (CFTR) protein is a member of the ATP-binding cassette (ABC) superfamily that forms chloride channels in the heart, airway epithelium, and exocrine tissue (Sheppard and Welsh, 1999). Encoded by a single polypeptide, the CFTR protein contains a regulatory R domain in addition to the two transmembrane domains and two nucleotide binding domains found in other ABC proteins (Gadsby et al., 2006). Full channel activation requires the phosphorylation of the R domain by protein kinase A (Cheng et al., 1991) followed by the interaction of the nucleotide binding domains with ATP (Vergani et al., 2005). This interaction drives the dimerization of the nucleotide binding domains, sandwiching two ATP molecules between them to open the gate. Simultaneously, a Walker motif in the second nucleotide binding domain begins to hydrolyze its ATP, which returns the channel to the closed state (Gunderson and Kopito, 1995, Berger et al., 2005). Each transmembrane domain contains six membrane-spanning segments (Figure 1.2K), and homology models based on non-channel ABC transporters as well as site-directed mutagenesis studies suggest that lysine and arginine residues in transmembrane segments 1, 5, and 6 form a positively-charged environment in the pore and are important for ion selectivity (El Hiani and Linsdell, 2012).

TMEM16 Calcium-Activated Channels

There are ten genes in the mammalian genome that code for integral membrane proteins of the TMEM16 family (Figure 1.2L) (Duran and Hartzell, 2011). Although not all of these genes have been characterized yet, at least three of them are calcium-activated ion channels. TMEM16A and TMEM16B are chloride channels that are responsible for

regulating mucus secretion in the airway epithelium and membrane excitability in central and peripheral neurons (Huang et al., 2012c, Huang et al., 2012a), while TMEM16F is a non-selective cation channel that is involved in plasma membrane lipid scrambling in platelets (Yang et al., 2012a). As of this writing, biochemical studies have described these channels as dimeric proteins (Fallah et al., 2011, Sheridan et al., 2011, Tien et al., 2013), but other structural mechanisms responsible for calcium sensitivity and ion selectivity remain largely unknown.

PHYSIOLOGICAL FUNCTION OF THE TMEM16A FAMILY OF TRANSMEMBRANE PROTEINS

Since it was first cloned in 2008, research in the past half decade has revealed the importance of TMEM16A activity in regulating the physiology of biological systems. TMEM16A was first discovered to be a calcium-activated chloride channel in epithelial cells of the murine trachea (Rock et al., 2008, Rock et al., 2009) where it is responsible for a purinoceptor (UTP)-regulated chloride secretion that is important for mucus secretion and the maintenance of airway surface liquid (Huang et al., 2012b, Ousingsawat et al., 2009). In addition to the airways, TMEM16A-CaCC is also found in several other types of epithelia. It is responsible for mediating secretions from the pancreatic duct (Wang et al., 2013), the biliary epithelium (Dutta et al., 2011), and the salivary glands (Romanenko et al., 2010). By responding to metabotropic signaling and altering the rate of electrolyte export, TMEM16A regulates the amount of fluid secreted from epithelial cells and its molecular composition (Jang and Oh, 2014). In addition, TMEM16A is expressed in the intestines (Yang et al., 2014) and is responsible for rotavirus toxin NSP4-induced diarrhea (Ousingsawat et al., 2011).

Beyond mediating secretions from epithelia, TMEM16A-CaCC is important for smooth muscle function. TMEM16A functions as an excitatory signal for vasoconstriction in blood vessels (Forrest et al., 2010, Manoury et al., 2010, Ohshiro et al., 2014) and contributes to excitability of both urethra (Sancho et al., 2012) and airway (Zhang et al., 2013) smooth muscle cells. In the gastrointestinal tract (Zhu et al., 2009), kidney (Iqbal et al., 2012), bladder (Yu et al., 2012b), and oviduct (Dixon et al., 2011), TMEM16A regulates the pace-making activity of the interstitial cells of Cajal. Although the individual steps of these rhythmic currents have not yet been directly observed, it is likely that depolarization of the interstitial cells of Cajal opens voltage-gated calcium channels that increase intracellular calcium to activate calcium-activated chloride channels which repolarize the cell (Sanders et al., 2012). Separately, TMEM16E, another member of the TMEM16A family, appears to be important for skeletal muscle development and mutations in this gene is associated with muscular dystrophy (Bolduc et al., 2010, Liewluck et al., 2013).

As ion channels, TMEM16A and its homologue TMEM16B also play important roles in modulating electrical signaling in the nervous system. TMEM16A has been proposed to be a sensor for noxious heat in the peripheral nervous system (Cho et al., 2012, Kanazawa and Matsumoto, 2014) and may contribute to nerve-injury induced hypersensitivity (Lee et al., 2014). In nociceptive sensory neurons, it has been implicated in the bradykinin inflammation pathway by depolarizing DRG neurons (Liu et al., 2010). Expression of TMEM16A is also found in the cochlea (Yi et al., 2013, Jeon et al., 2011), olfactory epithelium (Dauner et al., 2012), vomeronasal organ (Dibattista et al., 2012), and retina (Jeon et al., 2013). Similarly, TMEM16B has been found in the rod photoreceptor (Dauner et al., 2013), olfactory neurons (Rasche et al., 2010), and hippocampal pyramidal cells

(Huang et al., 2012c). Not many studies have yet explored how TMEM16 proteins contribute to the function of each of these populations, although available research suggests that its role is likely modulatory in most cases. TMEM16B function is not required for olfaction even though it contributes a calcium-activated chloride current in the nasal epithelium (Billig et al., 2011). In the hippocampus, TMEM16B raises the threshold for action potential generation and shortens action potential duration (Huang et al., 2012c).

Other TMEM16 proteins have also been implicated in nervous system function even though there is no evidence that they are ion channels. TMEM16C has been proposed to reduce nociceptive neuron excitability in the DRG by interacting with the sodium-activated potassium channel Slack (Huang et al., 2013). Mutations in TMEM16C is linked with primary torsion dystonia (Zech et al., 2014) and dominant craniocervical dystonia (Charlesworth et al., 2012). In the central nervous system, mutations in TMEM16K have been shown to cause cerebellar ataxia (Chamova et al., 2012).

Unlike TMEM16A and TMEM16B, TMEM16F is not an anion channel. Instead, it is a dual function phospholipid scramblase (Suzuki et al., 2010) and nonselective cation channel (Yang et al., 2012a). Mutations of the TMEM16F gene result in Scott syndrome, a bleeding disorder caused by defects in platelet phosphatidylserine exposure, an integral step in the blood coagulation cascade (Castoldi et al., 2011). Although there appears to be only one calcium sensor, TMEM16F scramblase and ion channel function through independent mechanisms (Terashima et al., 2013).

The family of TMEM16 proteins has also been implicated in regulating cellular proliferation. The first report of this was a study associating missense mutations of TMEM16E (GDD1) with gnathodiaphyseal dysplasia, a disease characterized by the extra

growth of bone in the face (Tsutsumi et al., 2004). Since then, TMEM16A has been found in prostatic adenocarcinomas (Liu et al., 2012), head and neck squamous cell carcinomas (Ruiz et al., 2012), esophageal tumors (Fei et al., 2014), and gastrointestinal stromal tumors (West et al., 2004). It may increase cell proliferation and migration by signaling through the NF κ B (Liu et al., 2014), MAPK (Duvvuri et al., 2012), and EGFR (Britschgi et al., 2013) pathways. In contrast, TMEM16F regulates cell apoptosis (Juul et al., 2014), proliferation (Zhao et al., 2014), and migration (Jacobsen et al., 2013, Szteyn et al., 2012). The signaling pathway by which TMEM16F regulates these functions is not known.

STRUCTURAL MECHANISM OF TMEM16A FUNCTION

TMEM16A is a calcium-activated chloride channel. As its name suggests, its gate is activated by micromolar concentrations of intracellular calcium and its pore is selective for chloride ions (Yang et al., 2008, Schroeder et al., 2008, Caputo et al., 2008). It is distinguished from other calcium-activated chloride channels such as CLCA and the bestrophins by several biophysical signatures. First, TMEM16A channels are small-conductance chloride channels with single channel conductances in the low picoSiemens range (Yang et al., 2008). Second, TMEM16A CaCCs are outwardly rectifying at low concentrations of internal calcium and are ohmic at higher concentrations of calcium (Schroeder et al., 2008, Xiao et al., 2011). Third, membrane depolarization and calcium sensitivity of TMEM16A CaCCs are interdependent and the degree of activation modulates the gating kinetics of the channel (Ferrera et al., 2009, Yu et al., 2012a, Cenedese et al., 2012). Fourth, conductance of ions through TMEM16A channels is modulated by the

species of the permeant ion (Xiao et al., 2011), and it preferentially permeates large anions over smaller anions (Schroeder et al., 2008).

Few studies to-date have explored the structural features of TMEM16A in detail, and mapping the key residues responsible for its biophysical properties remains an important goal. From the data available, it appears that the pore-forming region of the channel is located somewhere between transmembrane segments 5 and 7. Early on, Yang et al. (2008) found that modification of cysteine mutations at residues 625, 630, and 635 by MTSET blocks TMEM16A channel activity. In addition, substitution of positively-charged residues at R617 and K664 with acidic residues reduced the selectivity of the channel for anions. Similarly, Yang et al. (2012a) found that exchanging K584 in TMEM16A with the glutamine found in TMEM16F increased the permeability of TMEM16A for sodium. Thus, it appears that a cluster of residues near the fifth and seventh transmembrane segments form the pore of TMEM16A CaCCs. Beyond the effects of these six residues on ion permeability, however, it is unknown how these residues mediate ion selectivity and whether other residues also play a role in TMEM16A pore formation.

Research regarding the activation mechanism of TMEM16A has focused on the possible role of calmodulin and several intracellular acidic residues in sensing calcium. Several groups have suggested that calmodulin is responsible for the calcium sensitivity of TMEM16A. Calmodulin inhibitors (Tian et al., 2011) and mutations that interfere with TMEM16A-calmodulin interactions (Vocke et al., 2013) were shown to reduce TMEM16A-dependent currents. However, more recent data suggest that calmodulin may not be responsible for gating the TMEM16A pore (Terashima et al., 2013). Instead, TMEM16A channels appear to be gated by the direct interaction of calcium ions with acidic residues at

E698 and E701. These residues appear to be required for calcium sensitivity and neutralizing these charges substantially increases the EC₅₀ of channel activation (Yu et al., 2012a, Yu et al., 2014).

In addition to these sites, several other mechanisms responsible for regulating channel activity have been identified. Alternative splicing can modulate the calcium sensitivity, voltage dependence, rectification, and kinetics (Xiao et al., 2011, Ferrera et al., 2009, Ferrera et al., 2011, Caputo et al., 2008, Mazzone et al., 2011) of the channel. Interaction with calmodulin may alter the anion selectivity (Jung et al., 2013) while interaction with phosphatidylinositol 4,5 biphosphate may inhibit chloride currents (Pritchard et al., 2014). In addition, several putative phosphorylation sites have been proposed to be involved in regulating TMEM16A function, although no direct observations of this have yet been reported (Yu et al., 2014, Tian et al., 2011).

Chapter 2. Identification of a Dimerization Domain in the TMEM16A

Calcium-Activated Chloride Channel (CaCC)

Jason Tien, Hye Young Lee, Daniel L. Minor, Yuh Nung Jan, and Lily Yeh Jan

INTRODUCTION

Recent identification of TMEM16A as the calcium-activated chloride channel (CaCC) first described in the frog oocyte has enabled molecular studies of this novel ion channel family (Hartzell et al., 2005, Huang et al., 2012a). Homologues of this channel have been identified in organisms throughout the evolutionary lineage, including yeast, plants, invertebrates, and vertebrates (Berg et al., 2012). In the mouse, TMEM16A-CaCC regulates smooth muscle contraction and fluid secretion. In addition, TMEM16A and its close homologue TMEM16B contribute to nervous system functions ranging from the modulation of signal transduction in sensory neurons to the control of action potential duration in hippocampal neurons (Stöhr et al., 2009, Huang et al., 2012c). Another member of this family, TMEM16F, is a small-conductance calcium-activated non-selective cation channel (SCAN) that is important for a calcium-activated scramblase activity associated with Scott syndrome's defects in blood coagulation (Suzuki et al., 2010, Yang et al., 2012a).

The quaternary structure of many ion channels are known to be oligomeric membrane protein complexes assembled from multiple identical or closely related pore-forming subunits. For example, the NMDA-type glutamate receptor is a tetramer assembled from two obligate NR1 subunits and a choice of two NR2 subunits ranging from NR2A through NR2D (Cull-Candy and Leszkiewicz, 2004), and studies of homologous ionotropic glutamate receptors implicate a cytosolic domain at the amino terminus in tetramerization

(Madden, 2002). Similarly, the pentameric cys-loop receptors (Yu and Hall, 1991), the tetrameric potassium channels (Li et al., 1992), and the gap junctions formed by hexameric hemichannels (Lagree et al., 2003) are all protein complexes composed of subunits whose assembly is driven by channel-specific oligomerization domains.

Several groups have recently used biochemical methods to characterize the quaternary structure of TMEM16A channels as homodimers (Fallah et al., 2011, Sheridan et al., 2011). These previous studies on channel stoichiometry have raised the following questions: Is dimerization necessary for channel function? What is the TMEM16A dimerization domain that directs subunit assembly? To address these open questions, we have mapped the TMEM16A dimerization domain to a region within the cytoplasmic N-terminus of TMEM16A. We show that this region is necessary and sufficient for dimerization, which is important for functional calcium-activated chloride channel expression.

RESULTS

TMEM16 Family Proteins Form Dimeric Protein Complexes

TMEM16A belongs to a family of ten members in vertebrates (Milenkovic et al., 2010). Recent studies have characterized TMEM16A, TMEM16B, and TMEM16F as functional calcium-activated ion channels. These channels are closely related, with TMEM16B and TMEM16F sharing 61% and 37% amino acid identity to TMEM16A in the mouse, respectively (Figures 2.S1 and 2.S2). Since mouse TMEM16A immunoprecipitates TMEM16A and forms homodimers (Fallah et al., 2011, Sheridan et al., 2011) in biochemical studies including our own (Figures 2.1A–C), we asked whether mouse TMEM16B and

TMEM16F are also capable of forming oligomers when expressed in human embryonic kidney (HEK 293) cells. Indeed, GFP-tagged TMEM16B co-immunoprecipitated with mCherry-tagged TMEM16B and GFP-tagged TMEM16F co-immunoprecipitated with mCherry-tagged TMEM16F when each pair was co-expressed in HEK 293 cells (Figure 2.1A). Non-denaturing polyacrylamide gel electrophoresis (PAGE) of GFP-tagged TMEM16B or TMEM16F revealed the presence of dimers that were converted to the monomeric form upon denaturation in increasing concentrations of SDS (Figure 2.1B). These dimeric species also appeared on denaturing SDS-PAGE when membrane complexes were stabilized by treating living cells with increasing concentrations of the amine-reactive chemical crosslinkers DTSSP or DSP (Figure 2.1C), suggesting that the dimeric protein is present in physiologically intact cells.

Since the similar quaternary structure of these proteins may arise from the conservation of a specific dimerization domain of TMEM16 family members, we wondered whether these homologues are able to form heterodimers *in vitro*. We therefore attempted to co-immunoprecipitate mCherry-labeled mouse TMEM16A with other mouse TMEM16 family members co-expressed in HEK 293 cells. We found that TMEM16A co-immunoprecipitated with the more-closely related homologue, TMEM16B, but not the more distant homologue, TMEM16F (Figure 2.1D). Similarly, TMEM16B co-immunoprecipitated with TMEM16A but not TMEM16F (Figure 2.1E). Moreover, TMEM16F did not co-immunoprecipitate with either TMEM16A or TMEM16B (Figure 2.1F). The ability for close-homologues to interact extended even across species, as *Xenopus* TMEM16A was co-immunoprecipitated by both mouse TMEM16A and TMEM16B (Figure 2.1G), with which it shares 75% and 61% sequence identity (Figure 2.S1). Thus, ion

channels in the TMEM16 family are dimeric proteins, and the interactions responsible for channel assembly appear to be well-conserved specifically in other calcium-activated chloride channels of the TMEM16 family.

Identification of the TMEM16A Dimerization Domain

Having found that TMEM16A assembles into dimeric complexes, we next sought to identify the region responsible for this interaction. Because several other channel proteins (Madden, 2002, Li et al., 1992, Lagree et al., 2003) oligomerize via their cytosolic regions, we began by purifying each of the five predicted cytosolic domains (Das et al., 2007) from mouse TMEM16A on glutathione-conjugated beads and mixing them with lysate from HEK 293 cells expressing GFP-tagged TMEM16A (Figures 2.2A and B). Only the GST-tagged peptide containing the very N-terminal domain of TMEM16A was able to pull-down the full-length TMEM16A protein from mammalian cells (Figure 2.2B).

We next verified this N-terminal domain interaction using two further assays. First, hypothesizing that a truncation mutant containing the N-terminal domain and a transmembrane segment would insert into the endoplasmic reticulum (ER) membrane and interfere with the assembly and membrane trafficking of TMEM16A channels, we expressed the first 366 residues containing the entire N-terminal domain along with the first transmembrane segment of TMEM16A in a HEK 293 cell line that stably expressed mCherry-tagged TMEM16A. The population of mCherry-tagged TMEM16A proteins on the cell surface and accessible to labeling by a membrane impermeable amine-reactive biotin was progressively reduced in cells transfected with increasing concentrations of this truncation mutant (Figure 2.2C). This led to a reduction in functional channel expression as detected in electrophysiological recordings of calcium-activated chloride currents in HEK

293 cells co-transfected with this mutant and wildtype TMEM16A ($p < 0.01$, unpaired t -test, Figures 2.2D–F). Second, we also tested whether this interaction could be detected using co-immunoprecipitation assays. We found that mCherry-tagged TMEM16A co-immunoprecipitated with not only the truncation mutant containing residues 1–366, but also mutants containing only residues 1–321 without a transmembrane segment (Figure 2.3A and B).

We next attempted to map the dimerization domain by shortening the truncation mutant further. Since the first 116 residues of the N-terminal domain is not well-conserved between TMEM16A and TMEM16B (Figure 2.S2) and since Ferrera et al. (2011) has reported that the first half of the N-terminal domain is not necessary for TMEM16A function, we hypothesized that the first 116 residues are also not required for protein dimerization. Indeed, when the first 116 residues were removed, residues 117–321 remained sufficient for co-immunoprecipitation with full-length TMEM16A (Figure 2.3C). This dimerization domain appears to interact homotypically since residues 117–321 also co-immunoprecipitated with just the N-terminal domain (residues 1–321) and with itself (residues 117–321) (Figure 2.3D).

To further define the dimerization domain, we made a series of smaller truncation mutants based on the predicted secondary structure (Cole et al., 2008, Combet et al., 2000, Cheng et al., 2005) and the sequence conservation in the N-terminal domains of the TMEM16A and TMEM16B homologues (Figure 2.3A). We tested each with co-immunoprecipitation experiments to identify the minimally-necessary region for protein-protein interaction. Constructs spanning residues 117–296, residues 117–266, and residues 117–231 were able to interact with both the full-length TMEM16A protein (Figure

2.3E) and residues 117–321 (Figure 2.3F) while residues 117–151 could not, suggesting that the 78 amino acids corresponding to residues 152–231 are critical for TMEM16A dimerization. In fact, not only are these 78 residues necessary for dimer interaction, they are also sufficient, since peptides containing these residues tagged with GFP or mCherry were able to co-immunoprecipitate (Figure 2.3G). Focusing on this critical region, we made another series of truncations (Figure 2.4A) and found that while residues 117–218, residues 117–204, and residues 117–179 were able to interact with full-length TMEM16A, constructs containing only residues 117–160 could not (Figure 2.4B). The interaction in this minimal region appears to be homotypic since residues 117–179 not only bound to all other truncation mutants containing residues 117–179 (Figure 2.4C), it also bound to itself (Figure 2.4D).

Since residues 117–179 are sufficient to interact with wildtype TMEM16A channels in co-immunoprecipitation assays, we wondered whether overexpression of this fragment would also act as a dominant negative in electrophysiological assays of channel function. When wildtype TMEM16A was co-transfected into HEK 293 cells with a construct containing only residues 117–179, functional channel expression was decreased relative to cells co-transfected with an empty vector ($p < 0.01$, unpaired t -test, Figures 2.4E–G). The decrease in whole-cell current was smaller than that observed when residues 1–399 were co-transfected (Figure 2.2D), possibly because a fragment containing only residues 117–179 is expected to be cytosolic and would therefore interact with wildtype TMEM16A subunits less efficiently than constructs containing a transmembrane segment.

Because this region contains a cysteine at residue 166 (Figure 2.S3A), we performed further mutagenesis experiments to test the role of C166 and disulfide bond formation in

subunit dimerization. Mutant N-terminal domains with triple alanine substitutions scanning the region including C166 were still able to co-immunoprecipitate with full-length TMEM16A proteins as well as truncation mutants containing only residues 117–204 (Figures 2.S3B–C). This result is consistent with the location of the dimerization domain in the cytoplasmic N-terminus where it is exposed to the reducing intracellular environment and thus unlikely to form disulfide bonds. In addition, C166 is poorly conserved across TMEM16A/B/F homologues, suggesting that it is dispensable for channel oligomerization.

The TMEM16A Dimerization Domain Is Responsible for Specific Subunit Interactions

Having observed that TMEM16F subunits normally form homodimers even though TMEM16A subunits do not heterodimerize with TMEM16F subunits (Figures 2.1D and F), we wondered whether the TMEM16F dimerization domain is also in its N-terminal region and whether the dimerization domain is responsible for this specificity in subunit interactions. To test these questions, we engineered chimera mutants by substituting residues 117–179 in TMEM16A's dimerization domain with the homologous sequence from TMEM16F (A/F chimera 117–179) (Figure 2.S4). The dimerization domain in these mutants appeared to be sufficient for homodimerization in the context of the TMEM16A protein and facilitated functional channel assembly when expressed in HEK 293 cells (Figures 2.5A–C). However, the whole-cell calcium-activated chloride currents generated by these channels were smaller than wildtype currents ($p < 0.05$, Dunn's test, Figure 2.5A).

Hypothesizing that the reduction in current may be the result of inefficient protein folding due to mutation of such a large region within the N-terminal domain of TMEM16A, we engineered a second chimera protein targeting a smaller region for mutagenesis. Since truncation mutants containing residues 117–179 and residues 152–231 were able to form

homodimers *in vitro* (Figure 2.4D), we reasoned that residues 152–179 could be a critical region sufficient for protein-protein interaction. We therefore replaced TMEM16A residues 152–179 with the homologous region from TMEM16F (A/F chimera 152–179) (Figure 2.S4). This smaller mutation was able to efficiently form homodimers when expressed in HEK 293 cells and produced whole-cell calcium-activated chloride currents with amplitudes similar to those observed with wildtype TMEM16A channels (Figures 2.5A–C).

Having found that both chimera mutants were able to form homodimers when expressed in HEK 293 cells, we next tested the ability of these mutants to form heterodimers. As expected, neither chimera mutant co-immunoprecipitated with wildtype TMEM16A or TMEM16B subunits (Figures 2.5D and E), suggesting that the dimerization domains of TMEM16F and TMEM16A are not compatible for heterodimeric interactions despite their homology (Figure 2.S4). Thus, we have identified a dimerization domain within the TMEM16A protein that facilitates specific intersubunit assembly among TMEM16 family members.

A Conserved Peptide of 19 Residues Within the Dimerization Domain is Necessary for TMEM16A Assembly

We noticed that the region spanning residues 161–179 in the dimerization domain is predicted to form alpha helical structures in solution. Hypothesizing that this region might form the core structure of the dimerization domain, we wondered whether disruption of this segment might impede TMEM16A-CaCC channel assembly and activity. Transfection of TMEM16A mutants where residues 161–179 (Δ 161-179) have been deleted did not result in the expression of calcium-activated chloride currents in HEK 293 cells ($p < 0.001$, Dunn's test with respect to wildtype channels, Figures 2.6A–C), suggesting

that TMEM16A is unable to assemble into functional channels without this segment of its dimerization domain. The loss of functional channel expression is likely caused by the failure of TMEM16A subunits to properly assemble into quaternary structures since mutants lacking residues 161–179 failed to bind to other TMEM16A subunits in co-immunoprecipitation assays (Figure 2.6D) and also mislocalized from the plasma membrane to the ER (Figures 2.6E and 2.S5). This deficit was likely specific for higher-order protein assembly since the fluorescent tags placed at the C-terminus of the deletion mutant protein were well-folded and functional, suggesting that the protein was translated and did not trigger an unfolded-protein response for degradation. This phenomenon has been observed in previous studies of transmembrane proteins (Zerangue et al., 2000, VanSlyke et al., 2000) and may be attributed to quality-control mechanisms in the ER that prevent the export of proteins until they can be folded into a native conformation and fully assembled or tagged for degradation (Ellgaard and Helenius, 2003).

Because the deletion of 19 residues is a large mutation that may cause major conformational rearrangements and protein misfolding, we also tested several smaller mutations to preserve as much of the native structure as possible while still disrupting the dimerization domain's intermolecular associations. Since the peptide of 19 residues within the dimerization domain is predicted to be alpha helical, we mutated A169 at the center of this peptide to proline (A169P), an amino acid known to have low helix-forming propensities (O'Neil and DeGrado, 1990). Substitution of alanine 169 with proline completely abolished calcium-activated chloride currents ($p < 0.001$, Dunn's test with respect to wildtype channels, Figures 2.6A–C), eliminated protein-protein interaction

(Figure 2.6D), and blocked channel trafficking to the plasma membrane (Figures 2.6E and 2.S5), similar to what we observed for the $\Delta 161-179$ mutant.

Another helix disrupting mutation of A169, namely substitution with glycine (A160G), appears to be more benign, as the mutation tended to reduce the observed current by only 74% (Figures 2.6A–C). This is likely caused by a disruption in channel assembly and trafficking as the A169G mutant protein showed a reduced ability to interact with wildtype TMEM16A (Figure 2.6D) and to localize to the cell surface (Figure 2.6E). Further disruptions of this domain by the introduction of glycine substitutions at V164 and L174 (V164G/A169G/L174G) eliminated the remainder of the chloride current ($p < 0.001$, Dunn's test with respect to wildtype channels, Figures 2.4A–C), protein-protein interactions (Figure 2.6D), and trafficking to the cell membrane (Figures 2.6E and 2.S5).

The predicted helical domain within the dimerization domain also contains the cysteine residue at position 166. Since our immunoprecipitation experiments showed that C166 is dispensable for TMEM16A dimerization (Figure 2.S3), we wondered whether small perturbations of this region such as substituting this cysteine with serine would have any effect on channel assembly or function. The C166S mutation of the dimerization domain tended to reduce the whole cell calcium-activated chloride current in HEK 293 cells (Figures 2.6A–C). However, this reduction in channel activity was not statistically significant, consistent with the observations that the mutant channel still co-immunoprecipitated with other TMEM16A subunits (Figure 2.6D) and transported to the plasma membrane (Figures 2.6E and 2.S5). Thus, C166 does not appear to be required for channel assembly and substitution of C166 with either serine or alanine (Figure 2.S3) does not compromise protein interactions in the N-terminal dimerization domain.

DISCUSSION

Many ion channels are assembled as modular complexes of identical or closely homologous pore-forming subunits. In addition to interactions of the membrane-spanning regions of these channel subunits, their cytosolic regions often harbor interaction domains that are important for channel assembly. Our study of the TMEM16A calcium-activated chloride channel extends this trend with a dimerization domain in the cytosolic N-terminal region crucial for channel assembly and function. We identify a region that is necessary and sufficient for homotypic protein-protein interactions in biochemical and electrophysiological assays. Perturbation of this domain interferes with channel subunit assembly and disrupts channel function. Replacement of this segment with homologous residues from TMEM16F alters the specificity of subunit interactions.

In TMEM16A-CaCC, this domain resides in a region highly conserved among the TMEM16 homologues, with the predicted helical segment (residues 161–179 of mTMEM16A) varying at just three residues in species that are as evolutionary divergent as rats, turkeys, chimpanzees, and zebrafish. The domain that we have identified is similar in size compared to the homotypic interaction domains found in other proteins. The T1 domain of K_v1 channels is approximately 87 residues long (Kreusch et al., 1998) while the A-domain tail of the K_v7 channels is approximately 41 residues long (Howard et al., 2007). Despite its short length, this region of the TMEM16A protein contains a segment that is predicted with high probability to be in an alpha-helical conformation (Cheng et al., 2005, Cole et al., 2008, Combet et al., 2000), possibly forming a core for protein-protein interactions. It is conceivable that these interactions are further stabilized by other parts of the protein.

Even though our data show that this N-terminal domain is necessary and sufficient for dimerization, it is unlikely to be the only inter-subunit contact present in the TMEM16A-CaCC channel. The interaction between TMEM16A subunits are probably additionally facilitated by the high effective concentration of proteins embedded in the lipid bilayer, the favorable energetic of side-chain packing in the transmembrane domains, as well as the other protein-protein interfaces present in other portions of the channel (Adam and Delbruck, 1968). These disparate sources of interaction are well established in the channel structure literature and each channel family seems to adopt a unique strategy for protein oligomerization (Li et al., 1992, Martínez et al., 2011, Ayalon and Stern-Bach, 2001, Howard et al., 2007). Since the dimerization domain identified in our studies exhibits no homology to any other known protein according to protein BLAST algorithms, further investigation of this channel will likely reveal unique oligomerization strategies that may not have been evident from these previously described models.

The calcium-activated chloride channel TMEM16A plays an important physiological role in many different cell types (Huang et al., 2012a). In addition, its close homologues TMEM16B and TMEM16F have been implicated in sensory transduction and modulation of central neuronal signaling (Stöhr et al., 2009, Huang et al., 2012c) and blood coagulation diseases (Suzuki et al., 2010, Yang et al., 2012a), respectively. To gain mechanistic insights to the function of this family of calcium-activated ion channels, it is important to probe the structural features of these novel proteins. Our study here continues this effort by identifying a region critical for directing proper channel assembly. These results will have implications for understanding the molecular interactions that regulate ion conductance through the channel as well as for developing chemical modulators of this channel.

MATERIALS AND METHODS

Immunoprecipitation

Transfected HEK 293 cells were lysed by homogenization in PBS (1.5 mM KH_2PO_4 , 4.3 mM Na_2HPO_4 , 2.7 mM KCl, 137 mM NaCl at pH 7.4) supplemented with 1% cholic acid, 1% Triton X-100, and 1x Complete protease inhibitor (Roche) with brief sonication. Insoluble matter was removed by centrifuging at $20,000\times g$ for 40 minutes at 4°C . Supernatants were incubated with mouse monoclonal antibodies raised against GFP (Neuromab) overnight at 4°C and then pulled-down with protein A-conjugated sepharose beads (Invitrogen) for 2 hours at 4°C . Beads were washed three times with lysis buffer and once with PBS before elution with SDS-PAGE running buffer.

Western Blot Analysis

Proteins denatured by heating for 5–10 minutes at 95°C in Laemmli sample buffer (Laemmli, 1970) were separated by SDS-PAGE and transferred to nitrocellulose membranes. After blocking in TTBS buffer (10 mM Tris-HCl, pH 7.5, 150 mM NaCl, 0.05% Tween-20, and 5% skim milk powder), the membranes were incubated with primary antibodies overnight at 4°C followed by horseradish peroxidase (HRP)-conjugated secondary antibodies for 1 hour at room temperature. Detection was performed using enhanced chemiluminescence kit and hyperfilm MP (Amersham).

Electrophysiology

HEK 293 transiently transfected for 14–20 hours were plated onto poly-L-lysine coated coverslips 2–3 hours prior to recording. Whole-cell recordings were performed at room temperature on transfected cells using an Axopatch 200B patch-clamp amplifier and

pClamp9 software (Molecular Devices) following conditions modified from Schroeder et al. (Schroeder et al., 2008). External solutions contained 140 mM NaCl, 5 mM KCl, 2 mM CaCl₂, 1 mM MgCl₂, and 10 mM HEPES and 300 nM free Ca⁺⁺ internal solutions contained 140 mM NaCl, 10 mM HEPES, 7.4 mM CaCl₂, and 12 mM EGTA. Free calcium concentrations were determined using Maxchelator software (<http://maxchelator.stanford.edu>) and the pH-metric method (Tsien and Pozzan, 1989). All solutions were titrated with NaOH to pH 7.2.

Materials

The ECL kit, hyperfilm MP, and glutathione-Sepharose 4B were purchased from GE Healthcare (Piscataway, NJ); EZ-Link Sulfo-NHS-LC-Biotin and Streptavidin agarose resin from Thermo Scientific (Rockford, IL); Lipofectamine™ 2000, Alexa fluor 647-streptavidin, DAPI, and Prolong Gold antifade reagent from Invitrogen (Carlsbad, CA); cholic acid from USB (Cleveland, OH); complete EDTA-free protease inhibitor cocktail from Roche (Indianapolis, IN); PBS, DMEM, L-glutamine, sodium pyruvate, and 0.25% trypsin from UCSF Cell Culture Facility (San Francisco, CA); all other chemicals were purchased from Sigma (St. Louis, MO).

Antibodies

Mouse monoclonal GFP antibody was purchased from NeuroMab (Davis, CA); rabbit polyclonal dsRed antibody from Clontech (Mountain View, CA); HRP-goat anti-rabbit IgG (H+L), HRP-goat anti-mouse IgG (H+L), rhodamine-goat anti-rabbit IgG (H+L) from Jackson ImmunoResearch Laboratories, Inc. (West Grove, PA).

DNA Constructs

Mouse-derived TMEM16A (30547439), TMEM16B (5357763), and TMEM16F (6409332) cDNAs were obtained from Open Biosystems, and *Xenopus*-derived TMEM16A cDNA was obtained from Schroeder et al. (2008). cDNAs were cloned into pEGFP-N1 and pmCherry-N1 vectors (Clontech) for mammalian expression and into pGEX-4T-1 (GE Healthcare) for bacterial expression. Truncation mutants were generated by PCR, chimera mutants were generated by overlap extension PCR, and site-directed mutagenesis was performed using the QuikChange kit (Stratagene) using primers listed in SI Table 1.

Cell Culture and Transfection

HEK 293 cells were cultured in Dulbecco Modified Eagle Medium (DMEM) supplemented with 4.5 g/L D-glucose, 110 mg/L sodium pyruvate, 584 mg/L L-glutamine, and 10% fetal bovine serum (FBS). Cell culture media was supplemented with 200 µg/mL Geneticin and 100 µg/mL hygromycin to maintain selection pressure for stably transfected TMEM16A cell lines. Cells were maintained at 37°C in a humidified incubator with 5% CO₂ and were transfected using Lipofectamine 2000 (Invitrogen).

Native Gel Electrophoresis

Transfected cells were washed twice with ice-cold PBS and harvested with 2X native sample buffer (Invitrogen). Cells were homogenized by brief sonication and insoluble material was precipitated at 20,000 × *g* for 20 min at 4°C. Supernatants were treated with differing concentrations of SDS for 30 min at RT, resolved using the NativePAGE kit (Invitrogen), and detected by Western blotting.

Cross-linking

Transfected cells were cooled on ice, washed twice with ice-cold PBS, and washed with different concentrations of DSP or DTSSP in PBS for 20 min on ice. Unreacted reagent was removed with four ice-cold PBS washes and quenched with two 100 mM glycine in ice-cold PBS washes. Cultures were harvested in buffer A (PBS, 1% Triton X-100, 1% cholic acid, and protease inhibitor cocktail). The homogenates were centrifuged at $12,000 \times g$ for 15 min at 4°C. The resulting complexes were resolved by SDS-PAGE and identified by Western blot analysis.

Surface Biotinylation

Transfected cells were cooled on ice, washed twice with ice-cold PBS, and incubated with 1 mg/mL Sulfo-NHS-S-S-Biotin in PBS for 20 min on ice. Unreacted biotinylation reagent was removed with four ice-cold PBS washes and quenched with two 100 mM glycine in ice-cold PBS washes. Cultures were harvested in buffer A. The homogenates were centrifuged at $12,000 \times g$ for 15 min at 4°C. The resulting supernatant was incubated with 50 μ L streptavidin-beads for 3 hr at 4°C. The resulting complexes were washed three times with 1 ml of buffer A and once with PBS without detergent, resolved by SDS-PAGE and identified by Western blot analysis.

Protein Purification

Peptides cloned into pGEX-4T-1 vectors were expressed in *Escherichia coli* (*E. coli*) BL21(DE3) in 2XYT broth at 25°C and induced at 0.6–0.8 OD₆₀₀ with 1 mM IPTG for 4 hr. Cells were lysed by sonication in buffer A and insoluble matter was cleared by centrifugation. Cleared supernatants were equilibrated with glutathione-conjugated

sepharose beads (GE Healthcare) and washed with PBS. Purified peptides on the beads were added directly to cell lysates for GST-pulldown experiments.

GST Pull-down

Membrane proteins were extracted by sonication from HEK 293 cell cultures in buffer A. Cleared lysates were allowed to equilibrate with GST-tagged peptides on glutathione-conjugated sepharose beads (GE Healthcare) for two hr at 4°C. Beads were washed three times with buffer A and once with PBS without detergent, and co-purifying proteins were separated by SDS-PAGE and identified by Western blot analysis and Ponceau S staining.

Immunocytochemistry

HEK 293 cells plated onto poly-L-lysine coated coverslips were allowed to express transiently transfected proteins for 48 hours. To visualize the ER compartment, HEK 293 cells were co-transfected with an ER-localized CD4-KKXX-GFP marker (Zerangue et al., 1999). Membrane proteins were labeled with a membrane-impermeable amine-reactive biotinylation reagent. Cells were fixed with 4% paraformaldehyde and 4% sucrose, permeabilized and blocked with 5% normal donkey serum in PBS containing 0.1% Triton X-100, and equilibrated overnight with rabbit antibodies raised against mCherry/dsRed (Clontech). Labeled proteins were detected by incubation with a rhodamine-conjugated anti-rabbit antibody (Jackson ImmunoResearch) and an Alexa Fluor 647-conjugated avidin (Invitrogen) for 1 hour at room temperature and examined under a Leica TCS SP2 confocal microscope (Leica Microsystems, Bannockburn, IL).

ACKNOWLEDGMENTS

We thank Dr. Sung Ho Ryu and Dr. Jae Yoon Kim of Pohang University of Science and Technology (POSTECH), Pohang, Korea for GST-tagged protein purification protocols. This work was supported by the National Institutes of Health Grants NS069229 (to L.Y.J.) and DC007664 (to D.L.M.), and the American Asthma Foundation 09-0051 (to D.L.M.). L.Y.J. and Y.N.J. are investigators of the Howard Hughes Medical Institute.

AUTHOR CONTRIBUTIONS

Jason Tien, Hye Young Lee, Daniel L. Minor, Yuh Nung Jan, and Lily Yeh Jan contributed to this work. J.T. and H.Y.L. contributed equally to this work.

J.T., H.Y.L., and L.Y.J. designed research; J.T. and H.Y.L. performed research; D.L.M. contributed new reagents/analytic tools; J.T., H.Y.L., D.L.M., Y.N.J., and L.Y.J. analyzed data; and J.T., H.Y.L., and L.Y.J. wrote the paper.

Chapter 3. A comprehensive search for calcium binding sites critical for

TMEM16A calcium-activated chloride channel activity

Jason Tien, Christian J. Peters, Xiu Ming Wong, Tong Cheng, Yuh Nung Jan, Lily Yeh Jan, and
Huanghe Yang

INTRODUCTION

Transmembrane proteins of the TMEM16 family include a number of calcium-dependent ion channels, such as the TMEM16A (Schroeder et al., 2008, Caputo et al., 2008, Yang et al., 2008) and TMEM16B (Stöhr et al., 2009, Schroeder et al., 2008) calcium-activated chloride channels (CaCCs) and the TMEM16F (Yang et al., 2012a) small conductance calcium-activated nonselective cation (SCAN) channel. These proteins have been implicated in a wide range of physiological activities (Berg et al., 2012, Huang et al., 2012a, Scudieri et al., 2012, Hartzell et al., 2009, Kunzelmann et al., 2011) including the control of fluid secretion in epithelia (Huang et al., 2012b, Romanenko et al., 2010), the regulation of membrane excitability in neurons (Huang et al., 2012c, Billig et al., 2011), the scrambling of membrane lipids in platelets (Suzuki et al., 2010, Yang et al., 2012), and the metastasis of certain cancers (Duvvuri et al., 2012, Katoh, 2003). Despite their important physiological roles, the mechanism by which calcium activates these proteins is still extensively debated.

Based on studies of calcium-activated potassium channels (K_{CaS}) (Maylie et al., 2004, Salkoff et al., 2006), two models have been proposed to account for the calcium sensitivity of TMEM16A-CaCC (Figure 3.1A). In one model resembling that of the small-conductance K_{Ca} (SK) channels (Xia et al., 1998, Schumacher et al., 2001), calcium ions interact with

calmodulin (CaM), and the physical association of calmodulin with TMEM16A is required to transduce the free energy of ion-protein interaction into movements of the channel gate (Vocke et al., 2013, Tian et al., 2011). In a second model similar to that of the large-conductance K_{Ca} (BK) channels (Schreiber and Salkoff, 1997, Shi et al., 2002, Xia et al., 2002, Wu et al., 2010, Yuan et al., 2010), calcium binds directly to TMEM16A, and this interaction drives channel activation (Yu et al., 2012, Terashima et al., 2013, Yu et al., 2014).

In this study, we performed a series of experiments designed to clarify the mechanism by which TMEM16A-CaCCs are gated by calcium. First, with multiple lines of evidence, we confirmed that CaM is not required for TMEM16A-CaCC activation. Then, we performed a comprehensive alanine mutagenesis screen of all highly conserved acidic residues in TMEM16A that are predicted to be accessible to the cytoplasm. Based on our measurements of these mutants' apparent calcium sensitivity in inside-out excised patches, we identify four acidic residues (including two acidic residues that were recently implicated in the calcium-dependent activation of TMEM16A-CaCCs (Yu et al., 2012)) that satisfy several criteria characteristic of calcium-binding sites. Substitution of each of these residues with various amino acids shifts the apparent sensitivity of TMEM16A-CaCC for different divalent cations, and cysteine residues at these sites can be cross-linked by oxidizing intracellular solutions. Our results thus demonstrate that direct binding of calcium to TMEM16A triggers channel activation independently of calmodulin and identify novel interaction sites between calcium ions and TMEM16A.

RESULTS

Calmodulin is not required for calcium-dependent TMEM16A-CaCC activation

We began our study of TMEM16A-CaCC's calcium-dependent activation by testing whether CaM is required for channel activity. Reasoning that apparent calcium sensitivity is the most direct measurement of TMEM16A function, we recorded CaCC currents from GFP-tagged TMEM16A channels at fixed test potentials using an inside-out excised patch configuration. CaCC current amplitudes increased in a calcium-dependent manner until channels reach maximum open probability in our recordings (Figure 3.1B). By fitting the dose-response curve to the Hill equation (Figure 3.1C), apparent calcium sensitivity was derived as the half maximal effective concentration (EC_{50}) of calcium required for channel activation. With rapid application of internal solutions, this patch clamp protocol effectively minimized the effect of channel desensitization on our analysis of TMEM16A-CaCC apparent calcium sensitivity (Figure 3.1B). In addition, deriving the apparent calcium sensitivity from individual inside-out patches allowed us to control for variations in protein expression that complicate the interpretation of data derived from other electrophysiology configurations such as whole-cell patch clamp.

Since overexpression of mutant CaM molecules whose E-F hand calcium-binding motifs are destroyed has a dominant negative effect on the ability of SK channels to detect changes in intracellular calcium (Xia et al., 1998), we tested the effects of these CaM mutations on TMEM16A-CaCCs. We found that co-expression of mutant CaM molecules without functional calcium-binding sites in the N-terminal lobe (CaM₁₂), C-terminal lobe (CaM₃₄), or both lobes (CaM₁₂₃₄) did not reduce the apparent calcium sensitivity of the

endogenous TMEM16A-CaCC in *Xenopus* oocytes (Figure 3.1D), in agreement with a recent study (Yu et al., 2014).

Because the failure of CaM mutants to reduce TMEM16A calcium sensitivity could conceivably be due to the inability of the mutant CaM molecules to sufficiently displace endogenous CaM from the putative TMEM16A-CaM complexes, we further clarified the role of CaM in TMEM16A-CaCC gating by conducting four additional experiments to manipulate the potential interaction between CaM and TMEM16A. First, we tried to sequester endogenous CaM molecules by directly applying anti-CaM antibodies to the cytoplasmic side of inside-out patches from *Xenopus* oocytes. In contrast to its potent inhibitory effect on CaM-dependent TRPV1 tachyphylaxis (Lishko et al., 2007), the CaM-antibody had no effect on TMEM16A-CaCC currents (Figure 3.1E). Second, we treated endogenous *Xenopus* TMEM16A channels with W7, a potent CaM antagonist that can prevent CaM from binding to its targets. We found that neither acute nor sustained applications of this drug disrupted the calcium sensitivity of TMEM16A channels (Figures 3.S1A–B). Third, consistent with previous reports (Xiao et al., 2011, Yuan et al., 2013, Ni et al., 2014), we found that barium, a divalent cation that cannot bind to CaM (Chao et al., 1984), can still potently activate TMEM16A channels in a dose-dependent manner (Figures 3.1C–D). Fourth, mutating three residues (V310, Y314, and L319) that were recently reported to be necessary for CaM-TMEM16A interactions (Vocke et al., 2013) did not reduce the apparent calcium sensitivity of the mouse TMEM16A channel expressed in HEK 293 cells (Figure 3.1F). Similar to the results reported by Vocke et al. (2013), the current amplitudes of these mutant channels were much smaller compared to wildtype channels in our inside-out patch recordings

(data not shown). However, the absence of any rightward shift in the dose-response curves suggests that these residues do not contribute toward TMEM16A-CaCC calcium sensitivity.

Because we were unable to alter TMEM16A-CaCC activity by inhibiting CaM function, could activate TMEM16A-CaCCs with barium, and could not shift channel EC_{50} by mutating the putative CaM-TMEM16A binding interface, we conclude that CaM is not responsible for the calcium sensitivity of TMEM16A-CaCCs.

Alanine mutagenesis screen identifies five acidic residues that are important for the calcium-dependent activation of TMEM16A channels

After excluding CaM as the calcium sensor for TMEM16A-CaCCs, we hypothesized that calcium might directly bind to TMEM16A itself. A recent study by Yu et al. (2012) found that mutations altering the charge at E698 and E701 (numbered E702 and E705 in the splice variant of TMEM16A used in their experiments) reduced the amplitude of whole-cell currents and altered channel activation and deactivation kinetics, suggesting that a ligand responsible for channel activation may interact with these sites. To test whether the apparent calcium sensitivities of E698Q and E701Q mutant channels are reduced, we measured their steady-state EC_{50} of calcium-dependent channel activation (Figures 3.2A and B). We found that their EC_{50} s were shifted to much higher calcium concentrations compared to the EC_{50} of wildtype TMEM16A channels, suggesting that these two acidic residues might be important for a direct interaction between calcium ions and TMEM16A-CaCC.

In proteins, calcium ions tend to bind to the carboxylate moieties of acidic amino acid residues (Pidcock and Moore, 2001) and typically require six to eight coordinates (Dudev and Lim, 2003). For a comprehensive survey of putative calcium binding residues

in TMEM16A, we identified 38 acidic residues (including E698 and E701) that are conserved in all known calcium-activated ion channels in the TMEM16 family (including a *Drosophila* calcium-activated chloride channel (Wong et al., 2013)) and that are hypothesized to be solvent accessible from the intracellular compartment (Figure 3.2C). We then systematically replaced each of these residues in the mouse TMEM16A channel with alanine and measured their apparent calcium sensitivity using inside-out patches excised from HEK 293 cells (Figure 3.3). We found that alanine substitutions at E698 and E701 greatly reduced the apparent calcium affinity of TMEM16A-CaCC (Figure 3.3), similar to the effects of glutamine substitutions at these residues (Figures 3.2A and B). Moreover, our screen identified three additional acidic residues (E650, E730, and D734) that were critical for the calcium sensitivity of TMEM16A channels (Figure 3.3). Similar to E698A and E701A, alanine mutations of these three acidic residues resulted in at least a ten-fold reduction of apparent calcium sensitivity. Interestingly, these five residues identified by our screen are confined to the region between the fifth and seventh putative transmembrane segments (Figures 3.2C and 3.7C) (Yu et al., 2012).

Altering the side chains of E650, E698, E701, E730, and D734 differentially changes the calcium sensitivity of TMEM16A-CaCCs

Calcium ions interact with different chemical moieties with different affinities depending on the coordination chemistry of the calcium ion (Sóvágó and Várnagy, 2013). In order to understand the role of E650, E698, E701, E730, and D734 in TMEM16A-calcium interactions, we replaced the side chains at each of these five potential calcium-binding residues with charge-neutralizing (Cys, Asn, or Gln), charge-reversing (Arg), and charge-

conserving (Asp or Glu) groups and measured their effects on the apparent calcium sensitivity of TMEM16A channels (Figure 3.4).

Introduction of cysteine substitutions at these sites replaces the glutamate or aspartate side chain with a small, hydrophobic methyl sulfhydryl group. Understandably, these manipulations had effects comparable to those of alanine substitutions (Figure 3.3C) and reduced the apparent calcium sensitivity of the channel (Figure 3.4F).

Similarly, we reasoned that charge-reversing arginine substitutions would have dramatic effects on calcium binding due to the introduction of a positively charged guanidinium group. Indeed, E698R, E701R, E730R and D734R were much less sensitive to internal calcium. Compared to wildtype (WT) channels (EC_{50} : $1.0 \pm 0.1 \mu\text{M}$), the EC_{50} s of E698R and E701R were increased by several thousand-fold to $5.0 \pm 0.3 \text{ mM}$ and $3.3 \pm 0.5 \text{ mM}$, respectively, while the effects of E730R were milder, increasing EC_{50} to $0.6 \pm 0.3 \text{ mM}$. The most substantial changes were observed in D734R mutants, where EC_{50} was increased to such a great extent that 10 mM intracellular calcium, the highest concentration of calcium used in this study, was unable to activate the mutant channel. The lack of CaCC current in D734R mutants was not due to defects in protein expression or folding because cadmium ions could still robustly activate the channel (see Figure 3.6F). In contrast, the arginine substitution in E650R mutants only produced a small reduction in calcium sensitivity (EC_{50} : $6.5 \pm 0.8 \mu\text{M}$), suggesting that the side chain at position 650 may not be directly involved in calcium coordination.

Because calcium ions tend to be coordinated by oxygen atoms, we also made several mutations to test the role of carboxylate and carbonyl moieties in TMEM16A-CaCC calcium sensitivity. First, we made charge-preserving mutations (Asp or Glu) that alter the length of

the amino acid side chain without removing the carboxylate group. If carboxylate moieties are important for TMEM16A-calcium interaction, these mutations may partially preserve TMEM16A-CaCC calcium sensitivity even if the change in side chain length alters the position of the carboxylate group. Second, we made charge-neutralizing mutations (Asn or Gln) that remove the charge of the amino acid side chain without changing its size. If carbonyl groups are involved in calcium coordination, these mutations may maintain the orientation of the amino acid residue and allow carbonyl groups to continue interacting with calcium ions.

We found that the shifts in EC_{50} caused by mutations at E698, E701, and D734 were consistent with these acidic residues playing a direct role in calcium coordination (Figure 3.4F). Charge-preserving mutations in E698D and E701D resulted in only a 3 to 10-fold increase in channel EC_{50} ($3.3 \pm 0.9 \mu\text{M}$ and $10.4 \pm 3.4 \mu\text{M}$, respectively), suggesting that side chain length is not critical for calcium binding, while mutations in D734E shifted the EC_{50} by about 800-fold to $0.8 \pm 0.3 \text{ mM}$, suggesting that calcium binding may be sensitive to the precise spatial arrangement of the carboxylate group at this position. Although calcium activation was compromised by substituting the acidic residue with a longer side chain, D734E was still more sensitive to calcium than other mutants possessing substitutions at this residue (Figure 3.4E).

In addition, replacing these acidic residues with glutamine or asparagine also increased channel EC_{50} , suggesting that the negatively-charged carboxylate group is important for calcium-binding. E698Q mutations resulted in a relatively small decrease in calcium sensitivity (EC_{50} : $0.03 \pm 0.01 \text{ mM}$) while E701Q and D734N had larger effects (EC_{50} : $2.9 \pm 0.3 \text{ mM}$ and $2.3 \pm 0.3 \text{ mM}$, respectively). This data, combined with a dramatic loss of

calcium sensitivity in mutants containing arginine, alanine or cysteine mutations at these three sites, supports the idea that side chain carboxylate groups at position E698, E701 and D734 might be directly involved in binding calcium.

Similarly, the mutations at E730 suggest that calcium ions may interact with this residue, although not necessarily with its side-chain carboxylate moiety (Figures 3.4D and F). In this case, charge-preserving aspartate mutations increased EC_{50} to 0.8 ± 0.2 mM even though charge-neutralizing asparagine mutations only increased EC_{50} to 0.09 ± 0.08 mM. Since channels bearing mutations that preserve the shape but not the charge of this acidic residue are more sensitive to calcium, it appears that TMEM16A-calcium interactions require the proper conformation of residues at this position, possibly to orient the carbonyl oxygen of the peptide backbone.

The effects of the mutations at E650 suggest that this residue may not be directly involved in binding calcium. In contrast to the mild effects of a charge-reversing arginine substitution (EC_{50} : 6.5 ± 0.8 μ M), the charge-preserving aspartate and charge-neutralizing glutamine substitutions increased EC_{50} to 0.8 ± 0.2 mM and 4.3 ± 0.9 mM, respectively, suggesting that neither E650's carboxylate nor carbonyl group is involved in calcium coordination. It thus seems likely that E650 might be involved in gating processes downstream of calcium binding while E698, E701, E730, and D734 may interact directly with calcium.

Mutations also alter channel sensitivity to other divalent cations

To further test whether E698, E701, E730, and D734 are involved in divalent cation coordination, we asked whether mutations of these residues also shift the EC_{50} of TMEM16A channel activation by ions other than calcium. Strontium ions are chemically

similar to calcium ions and are also able to robustly activate TMEM16A channels (Yuan et al., 2013, Ni et al., 2014) even though they have a larger atomic radius. Since both strontium and calcium are “hard” metal ions that prefer coordination with oxygen-containing ligands such as carboxylates and are typically coordinated by six ligands (Dudev and Lim, 2003, Rubin, 1963), we would expect our various mutations to shift the EC₅₀ of strontium and calcium activation in similar directions.

Indeed, compared to the low micromolar strontium sensitivity (EC₅₀: 7.7 ± 0.3 μM) of wildtype channels (Figures 3.5A and B), we found that alanine mutations at E698, E701, and D734 increased the EC₅₀ of channel activation by strontium to at least the hundred micromolar range (EC₅₀: 750 ± 70 μM, 7.6 ± 1.0 mM, 400 ± 100 μM, respectively). The strontium sensitivity of TMEM16A-CaCCs was drastically reduced by charge-reversing arginine mutations (EC₅₀: >10 mM at all three sites) but was partially preserved by charge-preserving aspartate or glutamate mutations (EC₅₀: 70 ± 20 μM, 90 ± 10 μM, 270 ± 30 μM, respectively) (Figures 3.5C, D, F, and G), confirming the importance of side chain charge in divalent cation coordination at these three sites. Although we were not able to accurately estimate the true EC₅₀ of alanine, cysteine, and arginine mutations at D734 because channel activity was too low to properly normalize current amplitude even at 10 mM Sr²⁺, it is clear that these mutants form functional channels because they can still be activated by intracellular cadmium (see Figure 3.6). Consistent with our recordings of channels activated by calcium ions (Figure 3.4E), it appears that although glutamate is able to partially substitute for aspartate at this site, the side chain length as well as charge of D734 is important for channel activation by hard divalent cation ligands (Figure 3.5F).

As we observed earlier (Figure 3.4D), TMEM16A's apparent EC_{50} seems to depend more on the physical conformation of E730 than the presence of a carboxylate moiety at this site. Channels containing a charge-preserving aspartate (EC_{50} : 0.27 ± 0.03 mM) mutation at E730 are not much more sensitive to strontium than channels containing a charge-neutralizing alanine mutation (EC_{50} : 0.44 ± 0.10 mM) (Figure 3.5E). Channels containing the aspartate substitution had the highest sensitivity for strontium out of the five mutations tested (Figure 3.5G) even though E730D had the lowest affinity for calcium (Figure 3.4F). It is conceivable that the smaller aspartate side chain at this position can accommodate the larger strontium ion more easily.

In addition to strontium, we also tested how these mutations affected the ability of cadmium to activate TMEM16A. Cadmium, like strontium, is a divalent cation that is able to substitute for calcium and activate wildtype TMEM16A channels (Figures 3.6A and B). Unlike calcium and strontium ions, however, cadmium is a "soft" ligand typically coordinated by only four residues (Dudev et al., 2006), and it prefers coordination by moieties containing nitrogen and sulfur atoms (Andersen, 1984, Sóvágó and Várnagy, 2013). Reasoning that the TMEM16A calcium-binding site is evolutionarily optimized for "hard" ions like calcium, we hypothesized that TMEM16A sensitivity for cadmium ions would be low and would not be greatly impacted by mutations that alter the charge of only one acidic residue in the calcium sensor.

Indeed, although mutations at all four putative calcium-coordination sites shifted the EC_{50} of cadmium activation, the differences in EC_{50} between different mutants were smaller than those observed with calcium and strontium (Figures 3.6C–F). The EC_{50} s of TMEM16A channels containing charge-reversing or charge-neutralizing mutations were all

in the millimolar range, similar to those of wildtype channels and those with charge-preserving mutations (Figure 3.6G). These observations are consistent with the notion that cadmium may coordinate fewer chemical moieties in the binding pocket than calcium.

Since calcium, strontium, and cadmium activation of TMEM16A-CaCC are all affected by mutations of E698, E701, E730, and D734, it appears that all three divalent cations can interact with the same TMEM16A calcium sensor. Because the effects of each mutation are contingent on the divalent cation species used to activate the channel, it is likely that these sites directly alter the metal ion-binding pocket. In addition, because all of our mutations targeted residues on TMEM16A, our results lend further support to the notion that the TMEM16A polypeptide itself encodes the calcium sensor responsible for channel activation.

E698, E701, E730, and D734 are spatially clustered and exposed to the intracellular solution

Our results implicating E698, E701, E730, and D734 as divalent cation coordinating residues in the TMEM16A calcium-sensing domain suggest that these acidic residues are exposed to the cytoplasm. However, due to the high hydrophobicity of the residues in the region between the putative transmembrane segments 5 and 7, current models of TMEM16A topology (Model A and Model B in Figure 3.7C) do not clearly predict their solvent-accessibility (Yu et al., 2012, Yang et al., 2008, Das et al., 2008). To confirm that these residues are accessible to internal calcium ions despite their predicted vicinity to the cellular membrane and to demonstrate the spatial proximity of these residues, we tested whether the activity of TMEM16A channels containing double cysteine mutations can be modulated by the redox potential of the internal solution.

In support of a TMEM16A topological model shown as Model C in Figure 7C where E698, E701, E730, and D734 are clustered together and facing the cytoplasm, the perfusion of redox chemicals altered the amplitude of chloride currents through channels containing a E701C/E730C double mutation but not those containing a E701C or a E730C single mutation. Channel activity at 300 μ M internal calcium recorded in oxidizing buffers was significantly smaller than those recorded in reducing buffers, suggesting that a disulfide bridge between E701C and E730C decreases TMEM16A-CaCCs activation by calcium (Figures 3.7A and B). Thus, these residues appear to be spatially clustered at a cytoplasm-accessible site.

DISCUSSION

Calcium is an important second messenger responsible for signaling in many cellular pathways. Although a variety of calcium binding protein motifs responsible for detecting changes in intracellular calcium concentration have been characterized (Yáñez et al., 2012), the primary sequences of proteins in the TMEM16 family show no homology to any of these motifs notwithstanding the robust calcium-dependent activation of several TMEM16 proteins. We performed a comprehensive screen of intracellular acidic residues in the TMEM16A protein and mapped its calcium sensor to a region localized between transmembrane segments 5 and 7. By manipulating the charge, size, and reactivity of these side chains, we showed that four critical acidic residues in this region are situated at a solvent-accessible site that likely interacts with calcium in the cytoplasm during channel activation.

Our study of the TMEM16A calcium-sensing domain demonstrates that calcium-activated chloride channels are gated by the direct coordination of divalent cations with TMEM16A subunits. Because the mutations of E698, E701, E730, and D734 differentially shifted the EC₅₀ of channel activation to different calcium concentrations depending on the identity of the amino acid side chains, it is likely that these residues are involved in binding calcium. Furthermore, the differences in the way these mutations affect channel sensitivity to the hard calcium and strontium ions and the softer cadmium ions suggest that these mutations directly impact channel-ion interactions rather than via an allosteric mechanism.

Although previous studies have also investigated the calcium-dependency of TMEM16A-CaCCs, the types of experimental evidence generated in these studies render it difficult to unambiguously identify sites of TMEM16A-calcium interaction. Studies testing whether calmodulin co-purifies with TMEM16A channel complexes (Vocke et al., 2013, Jung et al., 2013, Terashima et al., 2013) do not provide definitive evidence of calmodulin's role in TMEM16A-CaCC activation. In addition, recent electrophysiological studies of TMEM16A-CaCCs containing mutations of putative calmodulin or calcium interaction sites (Vocke et al., 2013, Jung et al., 2013, Yu et al., 2012) have reported that manipulations disrupting calcium-dependent channel activation also substantially reduce the magnitude of the chloride current. By using current magnitude as the only assay of channel function in these studies, it has been difficult to distinguish mutations that disrupt calcium binding from those that prevent proper channel folding, trafficking, gating, or ion permeation. Furthermore, even if these mutations alter the calcium sensitivity of channel activation, it is unclear whether these mutations directly alter the calcium-binding sites or whether they target the transduction machinery that links the calcium sensor to channel gating.

Our results support the conclusions of Terashima et al. (2013) and Yu et al. (2014), that calmodulin is not involved in the calcium-dependent activation of TMEM16A channels. Similar to these studies, we were unable to detect alterations of TMEM16A channel activity by manipulating calmodulin function. Moreover, our experiments provide evidence in support of the notion that four acidic residues situated between transmembrane segments 5 and 7 are involved in coordinating calcium ions during channel activation (Figure 3.7C).

In addition, we provide evidence for the physical proximity of these four acidic residues. Previous studies (Yu et al., 2012, Yang et al., 2008) have proposed two different models of membrane topology for TMEM16A. The earlier model (Model A in Figure 3.7C) includes a long extracellular or reentrant loop between TM5 and TM6 (Yang et al., 2008) while a subsequent model (Model B in Figure 3.7C) proposes that the sequences between TM5 and TM6 in Model A actually correspond to the sixth transmembrane segment (Yu et al., 2012). Our study provides additional insight into the membrane topology of this region by showing that residues E701, and E730 are accessible to the intracellular solvent. In addition, because disulfide bridges can form between E701C and E730C, acidic residues at positions 698, 701, 730, and 734 are likely to be in physical proximity for calcium coordination. This implies that the hydrophobic region spanning 28 residues between E701 and E730 likely forms a short reentrant loop (Model C in Figure 3.7C).

In summary, our experiments have identified several critical residues that are responsible for the calcium sensitivity of TMEM16A channel activation. These acidic residues are highly conserved among proteins in the TMEM16 family, which are responsible for numerous cellular functions ranging from mucus secretion to blood coagulation in mammals and host defense in *Drosophila*. By clarifying the mechanism

underlying this signaling, our studies involving a comprehensive survey of evolutionarily conserved acidic residues to identify those likely to coordinate calcium contribute towards an understanding of how these physiological processes are regulated.

METHODS

Molecular biology and cell culture

cDNAs (Open Biosystems cDNA clones number 30547439, Uniprot identification number Q8BHY3-2) derived from mouse TMEM16A (mTMEM16A) were subcloned into the pEGFP-N1 vector (Clontech) via standard molecular biology techniques. Our clone corresponds to the 'a' splice form identified in Caputo et al. (2008) and lacks alternative exons b, c, and d. Site-directed mutations were generated by PCR with Pfu Turbo DNA polymerase following the Quikchange protocol from Agilent. All mutants were verified by sequencing.

HEK 293 cells were cultured in Dulbecco's Modified Eagle Medium (DMEM) supplemented with 4.5 g/L D-glucose, 110 mg/L sodium pyruvate, 584 mg/L L-glutamine, and 10% fetal bovine serum (FBS) and were transfected with Lipofectamine 2000 (Invitrogen), FuGENE 6 (Promega), or X-tremeGENE (Roche) and cultured for 1-2 days before recording.

For some experiments testing the effects of calmodulin on channel function, endogenous CaCC currents were recorded from *Xenopus* oocytes without exogenously introducing TMEM16A. Female *Xenopus laevis* were purchased from Nasco. The procedures for harvesting oocytes and housing animals were approved by the UCSF Institutional Animal Care and Use Committee. The loss-of function calmodulin mutants were kindly

provided by Dr. John Adelman (Xia et al., 1998). Defolliculated oocytes were injected with 5–100 ng cRNA and maintained at 17°C in ND96 (96mM NaCl, 10mM HEPES, 2mM KCl, 1mM MgCl₂, pH 7.4) solution for 2–7 days before recording. The monoclonal anti-CaM antibody (CaM85) and the CaM antagonist W7 (*N*-(6-Aminoethyl)-5-chloro-1-naphthalenesulfonamide hydrochloride) were purchased from Invitrogen and Santa Cruz Biotech, respectively. For chronic treatments of W7, *Xenopus* oocytes were incubated in ND96 supplemented with 50 μM W7 for 2–6 days before patch recording.

Electrophysiology

Twenty-four hours following transfection, cells were transferred to our standard recording bath solution (described below) for inside-out patch clamp recording. Macroscopic currents were recorded from inside-out patches formed with borosilicate pipettes of 1-5 MΩ resistance. Data were acquired using Axopatch 200-B and Axopatch 700-B patch-clamp amplifiers and pClamp10 software (Molecular Devices). All experiments were performed at room temperature (22–24°C).

Unless otherwise stated, all solutions used in this study were based on isotonic 140 mM NaCl. Both the basal extracellular solution and the zero calcium intracellular solution contained 140 mM NaCl, 5 mM EGTA, and 10 mM HEPES. Pipette (extracellular) solutions were supplemented with 1mM MgCl₂. Internal solutions with various calcium concentrations (< 100 μM) were prepared with the pH-metric method (Tsien and Pozzan, 1989). Briefly, a “high calcium” solution (140 mM NaCl, 5 mM Ca-EGTA, 10 mM HEPES) and a zero calcium intracellular solution were mixed in different ratios to give various calcium concentrations. The basal internal solution (without calcium buffer) contained 140 mM NaCl, and 10 mM HEPES. For solutions with [Ca²⁺]_i ≥ 100 μM, CaCl₂ was directly added

to the basal internal solutions (without EGTA) and the free $[Ca^{2+}]_i$ was measured with a Ca^{2+} -sensitive electrode (Thermo Scientific). The pH of all solutions was titrated with N-methyl-D-glucamine (NMDG) or NaOH to 7.2.

To test channel activation by Sr^{2+} or Cd^{2+} , inside out patches were exposed to a series of Sr^{2+} or Cd^{2+} -containing solutions prepared by serial dilution of a base solution containing 140 mM NaCl, 10 mM HEPES, and 10 mM $SrCl_2$ or $CdCl_2$ for a range of divalent concentrations from 10 μ M to 10 mM. While most constructs required greater than 10 μ M of either divalent to be activated, wildtype TMEM16A required solutions with lower $[Sr^{2+}]$. As Sr^{2+} concentration cannot be accurately diluted below 10 μ M, Sr^{2+} -EDTA solutions were prepared based on the CaBuf divalent buffering prediction software created by Dr. G. Droogmans (Department of Physiology, KU Leuven, Leuven, Belgium). For some constructs, 10 mM cation was insufficient to fully activate the channel, and the EC_{50} could not be calculated with confidence and is not reported.

For experiments manipulating the redox potential of the internal solution, 10mM H_2O_2 or 10mM DTT (dithiothreitol) from Sigma was freshly added (\leq one hour prior to use) to internal solutions containing either 0 μ M or 300 μ M free calcium.

Data Analysis

Data analysis was performed with Clampfit 10 (Molecular Devices) and Origin 7.5 (OriginLab). Concentration dose-response curves were fit to an equation of the form:

$$I/I_{MAX} = \frac{Amp}{1 + \left(\frac{K_D}{[Ca]}\right)^H}$$

where I denotes current, I_{MAX} is the maximum current elicited by the highest concentration of divalent cation, Amp is the maximum value of I/I_{MAX} at a given voltage, K_D is the apparent dissociation constant, and H is the Hill coefficient. EC_{50} values were log-transformed for one-way ANOVA and were compared to wildtype values using Tukey's post-hoc test for significance. Values were considered significantly different if $p < 0.05$.

ACKNOWLEDGMENTS

We thank Dr. John Adelman for providing the loss-of-function calmodulin mutants and Dr. Jianmin Cui for advice on the project. J.T. is supported by a NIH Ruth L. Kirschstein National Research Service Award under grant number 5F31NS076180. C.J.P. is supported by a Junior Personnel Research Fellowship from the Heart & Stroke Foundation of BC and the Yukon. Research reported in this publication was supported by NIH grant R01NS069229 to L.Y.J. The content is solely the responsibility of the authors and does not necessarily represent the official views of the National Institutes of Health. Y.N.J. and L.Y.J. are investigators of the Howard Hughes Medical Institute.

AUTHOR CONTRIBUTIONS

Jason Tien, Christian J. Peters, Xiu Ming Wong, Tong Cheng, Yuh Nung Jan, Lily Yeh Jan, and Huanghe Yang contributed to this work. J.T. and C.J.P. contributed equally to this work.

H.Y., Y.N.J. and L.Y.J. conceived and designed the study. H.Y. and X.M.W. tested calmodulin effects. H.Y. conducted the screen with alanine mutations and identified/verified the key residues for calcium binding. C.J.P. and J.T. tested the divalent cation effects on these residues. J.T. performed the crosslinking experiment. H.Y., J.T. and

C.J.P. analyzed the data. J.T. and T.C. made all the mutations. J.T., H.Y., C.J.P. and L.Y.J. wrote the manuscript.

Figure Legends

Figure 1.1. Examples of ion channel pores from various potassium channels. (A) A water-filled cavity is formed from four protein subunits, two of which are shown in the bacterial potassium channel, KcsA. The cavity creates a passageway through which ions can flow across the membrane, into or out of the cell. (B) The unique amino acid sequence of each family of channels allows it to selectively filter out particular ions. In the case of KcsA, K⁺ but not Na⁺ ions are allowed to pass through the selectivity filter, even though K⁺ ions are bigger than Na⁺ ions are. S1-4 refer to the four K⁺ ion-binding sites in the selectivity filter, each composed of 8 oxygen atoms from the TVGYG signature motif. (C) Pore-region sequence alignments of five structurally known potassium channels are shown with the GYG signature motif boxed in magenta and other highly conserved regions labeled in black. (D) Structural comparison of the pore regions from the same five potassium channels. (A) and (B) adapted from Lockless et al. (PloS 2007, p. e121); (C) and (D) from Shrivastava et al. (Biophys J 2006, pp. 3929-3940).

Figure 1.2: Several major families of ion channels use similar designs. (A) The 6-TM family includes voltage-gated sodium, calcium, and potassium channels, the calcium-gated potassium channels, the cyclic nucleotide-gated cation channels, and the transient receptor potential channels. (B) The 2-TM family includes inwardly rectifying potassium channels and the bacterial potassium channel KcsA. (C) Two-pore potassium channels contain four transmembrane segments. (D) The voltage-gated proton channel contains just the voltage sensor domain from the 6-TM channels. (E) Ionotropic glutamate receptors contain pore-lining domains that appear to be upside down relative to other channels in this figure. Glutamate receptors in the animal kingdom (left) are cation channels whereas a

prokaryotic glutamate receptor (right) is selective for potassium ions. (F) The cys-loop receptors are composed of five subunits, each with four transmembrane segments. The M2 segment lines the pore and rotates to open the channel upon acetylcholine binding. (G) IP_3 is a major second messenger that leads to Ca^{2+} ion influx from internal stores by binding intracellular calcium channels, such as $InsP_3R$ Ca^{2+} release channels. The NH_2 -terminal region includes an IP_3 binding domain. (H) The epithelia sodium channels have two transmembrane segments and a large extracellular domain between them. The extracellular domain respond to environmental stimuli to regulate channel function. (I) The P2X ionotropic purinergic cation channels also have two membrane spanning segments with a large extracellular domain that bind ligands. (J) Each subunit of the ClC channel has eighteen membrane segments, not all of which completely cross the membrane. Each subunit is arranged with approximate two-fold symmetry around a central pore. (K) The pivotal role of the chloride Cystic Fibrosis Transmembrane Regulator channel becomes clear when mutations in the channel lead to a deficiency in movement of salt and water out of cells, blocking passageways and ultimately leading to increased morbidity and mortality in human patients. It is a member of the ABC family and contains both transmembrane domains and nucleotide binding domains on the same polypeptide. (L) The topology of TMEM16 family of ion channels have not been fully characterized. There are approximately eight transmembrane domains per subunit and two subunits assemble to form a pore.

Figure 1.3: Voltage-gated Ca^{2+} and K^+ channels share a 6-TM architecture. (A) As with many other channels, Ca_v channels consist of many protein domains that allow the channel to be regulated by a variety of extra- and intracellular signals in addition to voltage

sensitivity through the α_1 subunit. (B) Voltage-gated K^+ channels consist of four α subunits that together form a pore for the passage of ions, as well as a cytoplasmic β subunit. (C) BK_{Ca} is an example of a K^+ channel that has an additional domain sensitive to Ca^{2+} . (A) from Arrikath and Campbell (Curr Op Neurobio 2003, pp. 298-307); (B) and (C) from Torres et al. (JBC 2007, pp. 24485-24489).

Figure 1.4: Voltage dependent block of K_{ir} channels. (A) At hyperpolarized voltages, potassium ions flow freely into the cell. (B) At depolarized voltages, movement of large divalent cations into the channel block potassium ion exit.

Figure 2.1. TMEM16 family proteins form dimeric protein complexes. (A) GFP (V), mTMEM16A-GFP, mTMEM16B-GFP, or mTMEM16F-GFP was co-expressed in HEK 293 cells with mTMEM16A-mCherry, mTMEM16B-mCherry, or mTMEM16F-mCherry. Proteins were immunoprecipitated from HEK 293 cell lysates with an anti-GFP antibody. Immunoprecipitated proteins were separated by SDS-PAGE and identified by Western blot analysis with anti-dsRed and anti-GFP antibodies. (B) Lysates from HEK 293 cells transfected with mTMEM16A-GFP, mTMEM16B-GFP, or mTMEM16F-GFP were treated with increasing concentrations of SDS. Proteins in the lysate were separated by native gel electrophoresis and identified by Western blot analysis with an anti-GFP antibody. (C) HEK 293 cells transfected with mTMEM16A-GFP, mTMEM16B-GFP, or mTMEM16F-GFP were incubated with increasing concentrations of either DTSSP or DSP. Proteins in HEK 293 cell lysates were separated by SDS-PAGE and identified by Western blot analysis with an anti-GFP antibody. (D-F) GFP (Vector), mTMEM16A-GFP, mTMEM16B-GFP, or mTMEM16F-GFP was co-expressed in HEK 293 cells with mTMEM16A-mCherry (D), mTMEM16B-mCherry (E), or mTMEM16F-mCherry (F). Proteins were immunoprecipitated from HEK 293 cell

lysates with an anti-GFP antibody. Immunoprecipitated proteins were separated by SDS-PAGE and identified by Western blot analysis with anti-dsRed and anti-GFP antibodies. (G) mCherry (Vector), mTMEM16A-mCherry, or mTMEM16B-mCherry was co-expressed in HEK 293 cells with xTMEM16A-HA. Proteins were immunoprecipitated from HEK 293 cell lysates with an anti-HA antibody. Immunoprecipitated proteins were separated by SDS-PAGE and identified by Western blot analysis with anti-HA and anti-dsRed antibodies.

Figure 2.2. The TMEM16A N-terminal domain is sufficient for subunit interaction. (A) Hypothetical topology indicating cytosolic regions used in our experiments. (B) GST-tagged cytosolic fragments of TMEM16A were purified on glutathione-conjugated beads and used to affinity capture interacting proteins in cell lysates from HEK 293 cells expressing TMEM16A-GFP. Proteins co-purifying with the GST tag were separated by SDS-PAGE, stained with Ponceau S, and identified by Western blot analysis with an anti-GFP antibody. (C) HEK 293 cells stably expressing full length (FL) TMEM16A-mCherry were transfected with different amounts of a GFP-tagged truncation mutant containing residues 1–366 of TMEM16A. Surface proteins were labeled with a membrane-impermeable biotinylation reagent. Proteins enriched from HEK 293 cell lysates on avidin-conjugated beads were separated by SDS-PAGE and identified by Western blot analysis with anti-dsRed, anti-GFP, and anti-actin antibodies. (D) Either mCherry (Vector) or a mCherry-tagged truncation mutant containing residues 1–366 of TMEM16A was co-expressed in HEK 293 cells with wildtype TMEM16A-GFP. Average steady-state whole-cell currents were measured at +100 mV with 300 nM internal free calcium and symmetric chloride. Each bar represents five to seven cells and ** indicates $p < 0.01$ in unpaired *t*-tests as compared to cells co-expressing full length TMEM16A with only mCherry. Error bars are

\pm SEM. (E) I-V curve of the cells in (D). Plots represent steady-state whole-cell currents recorded with 300 nM internal free calcium and symmetric chloride from -60 mV to $+100$ mV in $+20$ mV steps lasting 500 ms. (F) Representative traces of cells illustrated in (D) and (E).

Figure 2.3. A region in the cytoplasmic N-terminus is responsible for subunit dimerization. (A) Schematic depiction of TMEM16A N-terminal fragments used in our experiments. (B) GFP (Vector), full-length TMEM16A-GFP, or GFP fused to residues 1–366 or 1–321 was co-expressed in HEK 293 cells with mTMEM16A-mCherry. (C–D) GFP or GFP fused to residues 1–321 or 117–321 was co-expressed in HEK 293 cells with TMEM16A-mCherry (C) or mCherry fused to residues 1–321 (D) or 117–321 (D). (E–F) GFP or GFP fused to TMEM16A truncation mutants containing indicated residues was co-expressed in HEK 293 cells with TMEM16A-mCherry (E) or mCherry fused to residues 117–321 (F). (G) GFP or GFP fused to residues 152–231 was co-expressed in HEK 293 cells with mCherry fused to residues 152–231. (B–G) Proteins were immunoprecipitated from HEK 293 cell lysates with an anti-GFP antibody. Immunoprecipitated proteins were separated by SDS-PAGE and identified by Western blot analysis with anti-dsRed and anti-GFP antibodies.

Figure 2.4. Residues 117–179 are sufficient for a homotypic dimer interaction (A) Schematic depiction of TMEM16A N-terminal fragments used in our experiments. (B) GFP (Vector) or GFP fused to TMEM16A truncation mutants containing indicated residues was co-expressed in HEK 293 cells with TMEM16A-mCherry. (C) GFP fused to TMEM16A truncation mutants was co-expressed in HEK 293 cells with mCherry fused to residues 117–179. (D) GFP-tagged TMEM16A truncation mutants was co-expressed in HEK 293 cells with mCherry-tagged versions of the same mutants. (B–D) Proteins were

immunoprecipitated from HEK 293 cell lysates with an anti-GFP antibody.

Immunoprecipitated proteins were separated by SDS-PAGE and identified by Western blot analysis with anti-dsRed and anti-GFP antibodies. (E) Either mCherry (Vector) or mCherry fused to residues 117–179 was co-expressed in HEK 293 cells with wildtype TMEM16A-GFP. Average steady-state whole-cell currents were measured at +100 mV with 300 nM internal free calcium, and symmetric chloride. Each bar represents five to seven cells and ** indicates $p < 0.01$ in unpaired *t*-tests as compared to cells co-expressing full length TMEM16A with only mCherry. Error bars are \pm SEM. (F) I-V curve of the cells in (E). Plots represent steady-state whole-cell currents recorded with 300 nM internal free calcium and symmetric chloride from -60 mV to +100 mV in +20 mV steps lasting 500 ms. (G) Representative traces of cells illustrated in (E) and (F).

Figure 2.5. Replacement of the TMEM16A dimerization domain with that of TMEM16F yields functional channels. (A) GFP-tagged wildtype TMEM16A, A/F chimera 117–179, or A/F chimera 152–179 was expressed in HEK 293 cells. Average steady-state whole-cell currents were measured at +100 mV with 300 nM internal free calcium and symmetric chloride. Each bar represents five to six cells and * indicates $p < 0.05$ in Dunn's test as compared with cells expressing only wildtype TMEM16A. Error bars are \pm SEM. (B) I-V curve of the cells in (A). Plots represent steady-state whole-cell currents recorded with 300 nM internal free calcium and symmetric chloride from -60 mV to +100 mV in +20 mV steps lasting 500 ms. (C) Representative traces of cells illustrated in (A) and (B). (D–E) GFP (Vector) or GFP-tagged wildtype TMEM16A, A/F chimera 117–179, or A/F chimera 152–179 was co-expressed in HEK 293 cells with TMEM16A-mCherry (D) or TMEM16B-mCherry (E). Proteins were immunoprecipitated from HEK 293 cell lysates with an anti-

GFP antibody. Immunoprecipitating proteins were separated by SDS-PAGE and identified by Western blot analysis with anti-dsRed and anti-GFP antibodies.

Figure 2.6. A Segment of 19 Residues is necessary for TMEM16A function (A) GFP (Vector), wildtype TMEM16A-GFP, or GFP-tagged TMEM16A mutants was expressed in HEK 293 cells as indicated. Average steady-state whole-cell currents were measured at +100 mV with 300 nM internal free calcium and symmetric chloride. Each bar represents eight to ten cells and *** indicates $p < 0.001$ in Dunn's tests as compared with cells expressing wildtype TMEM16A-GFP. Error bars are \pm SEM. (B) I-V curve of the cells in (A). Plots represent steady-state whole-cell currents recorded with 300 nM internal free calcium and symmetric chloride from -100 mV to +100 mV in +50 mV steps lasting 300 ms. (C) Representative traces of cells illustrated in (A) and (B). (D) GFP, wildtype TMEM16A-GFP, or GFP-tagged TMEM16A mutants was co-expressed in HEK 293 cells with TMEM16A-mCherry. Proteins were immunoprecipitated from HEK 293 cell lysates with an anti-GFP antibody. Immunoprecipitating proteins were separated by SDS-PAGE and identified by Western blot analysis with anti-dsRed and anti-GFP antibodies. (E) Wildtype TMEM16A-mCherry or mCherry-tagged TMEM16A mutants was expressed in HEK 293 cells. Surface proteins were labeled with a membrane-impermeable biotinylation reagent. Immunostaining was performed using a ds-Red antibody (magenta, top) and biotin was detected with an avidin-conjugated Alexa-fluor (green, middle). Colocalization of dsRed and membrane biotin shown in white (bottom). Scale bar is 20 μ m.

Figure 2.S1. Dendrogram showing sequence conservation between TMEM16 homologues in mouse (m) and Xenopus (x). Sequence alignment was calculated using ClustalW2 (Goujon et al., 2010). Schematic was generated with Jalview (Waterhouse et al.,

2009). Pairwise sequence identity was calculated with http://www.ch.embnet.org/software/LALIGN_form.html. Numbers indicate percent amino acid identity and length of branches are inversely proportional to homology.

Figure 2.S2. Sequence alignment between mTMEM16A, xTMEM16A, mTMEM16B and mTMEM16F calculated using ClustalW2 (Goujon et al., 2010). Schematic was generated with Jalview (Waterhouse et al., 2009). Yellow box indicates mTMEM16A residues 117-321 used in truncation mutant experiments.

Figure 2.S3. Cysteine residue in the TMEM16A dimerization domain is dispensable for subunit dimerization. (A) Schematic diagram of alanine substitution mutations. (B-C) GFP (Vector) or GFP-fused to wildtype TMEM16A fragments containing residues 117-204, 164AAA, 165AAA, or 166AAA was co-expressed in HEK 293 cells with TMEM16A-mCherry (B) or mCherry fused to wildtype or mutant TMEM16A truncation residues 117-204 (C). Proteins were immunoprecipitated from HEK 293 cell lysates with an anti-GFP antibody. Immunoprecipitating proteins were separated by SDS-PAGE and identified by Western blot analysis with anti-dsRed and anti-GFP antibodies.

Figure 2.S4. Alignment from Figure S2 of region replaced in chimera mutants between mTMEM16A and mTMEM16F. Residues 117-179 correspond to the shortest fragment of TMEM16A sufficient for co-immunoprecipitation in Figure 4D while residues 152-179 correspond to the region of overlap between two homomeric fragments spanning residues 117-179 and residues 152-231 in Figure 4D.

Figure 2.S5. Same cells from Figure 6 with ER-specific label shown. TMEM16A-mCherry, Δ 161-179-mCherry, A169P-mCherry, A169G-mCherry, V164G/A179G/L174G-mCherry or C166S-mCherry was co-expressed in HEK 293 cells with CD4-KKXX-GFP

(green). Immunostaining was performed using a dsRed antibody (magenta). Scale bar is 20 μ m.

Figure 3.1. Calmodulin (CaM) is not responsible for the calcium-dependent activation of TMEM16A calcium-activated chloride channels (CaCC). A) Two competing models to explain TMEM16A calcium sensitivity have been proposed. It is unclear whether calcium directly binds to TMEM16A-CaCCs (upper panel) or whether CaM is required to mediate the calcium sensitivity of the channel (lower panel). B) Representative current traces of wildtype mouse TMEM16A-CaCC (mTMEM16A) recorded at ± 60 mV in response to various intracellular calcium concentrations using an inside-out patch clamp configuration. Table indicates the concentration of calcium used. C) Calcium dose-response of mTMEM16A channel at ± 60 mV. The smooth curves represent fits to the Hill equation (see Methods). D) Loss-of-function CaM mutants (CaM₁₂, CaM₃₄, CaM₁₂₃₄) did not reduce the apparent calcium sensitivity of the endogenous TMEM16A (x16A) channel in *Xenopus* oocytes. n.s.: non-significant. E) Application of monoclonal anti-CaM antibody CaM85 (2 μ g/mL) to the cytosolic face of inside-out patches had no effect on the calcium sensitivity of endogenous *Xenopus* TMEM16A CaCC. F) Mutating residues reported by Vocke et al. (2013) to be in the CaM binding domain of mTMEM16A did not affect apparent TMEM16A-CaCC calcium sensitivity.

Figure 3.2. Screen for potential calcium-binding residues in TMEM16A-CaCC. A-B) Quantification of the apparent calcium sensitivity of E698Q and E701Q (Yu et al., 2012) mutant TMEM16A channels. A) Representative current traces of E698Q and E701Q mutants in response to intracellular solutions with different calcium concentrations recorded at +60mV. Table indicates the concentration of calcium used. B) Calcium dose-

response curves of the mTMEM16A channels at +60mV. Smooth curves represent fits to the Hill equation. C) Sequence alignment of the calcium-activated TMEM16 channels. h16A, m16A, x16A, m16B, m16F and Fly16 are the human TMEM16A (Uniprot ID #Q5XXA6), mouse TMEM16A (Uniprot ID #Q8BHY3-2), *Xenopus* TMEM16A (Uniprot ID # B5SVV6), mouse TMEM16B (Uniprot ID #Q8CFW1), mouse TMEM16F (Uniprot ID #Q6P9J9) and *Drosophila* TMEM16 channels (Uniprot ID #Q86P24), respectively. Highly conserved acidic residues that are potentially exposed to the cytoplasm are highlighted in red. Some residues with conserved oxygen-containing side chains in m16F and Fly16 are highlighted in green. Putative transmembrane (TM) segments are highlighted in cyan. The controversial TM6 segments are highlighted in gray and labeled as TM6' and TM6'', respectively. "In" and "Out" indicate the intracellular and extracellular side of the membrane.

Figure 3.3. Systematic alanine scan of highly conserved intracellular acidic residues identified five mutations that dramatically reduced the apparent calcium sensitivity of TMEM16A-CaCC. A) Representative current traces of the E650A, E698A, E701A, E730A and D734A mutant channels in response to different intracellular calcium solutions recorded at +60 mV. Table indicates the concentration of calcium used. B) Calcium dose-response curves of these mutant mTMEM16A channels at +60 mV. Smooth curves represent fits to the Hill equation. C) Summary of apparent calcium sensitivity (EC_{50} s) of all alanine mutants tested. Dotted line indicates a 10-fold increase in EC_{50} compared to wildtype channels.

Figure 3.4. The effects of different amino acid side chains on the calcium sensitivity of mutant TMEM16A-CaCC channels indicate that E698, E701, E730 and D734 might be directly involved in binding calcium. A-E) Calcium dose-response curves of A) E650, B)

E698, C) E701, D), E730, and E) D734 mutant mTMEM16A channels at +60 mV. Smooth curves represent fits to the Hill equation. F) Summary of apparent calcium sensitivity (EC_{50} s) of mTMEM16A mutants. N.C.: no obvious CaCC current recorded. ***: $p < 0.001$.

Figure 3.5. TMEM16A channel sensitivity to strontium ions is disrupted by mutations of the identified calcium-binding sites. A) Representative current trace of wildtype mTMEM16A in response to different intracellular strontium solutions recorded at +60 mV. Table indicates the concentration of strontium used. B) Strontium dose-response curve of wildtype mTMEM16A channels at +60 mV. C-F) Strontium dose-response curves of the C) E698, D) E701, E) E730, and F) D734 mutant mTMEM16A channels at +60 mV. Smooth curves represent fits to the Hill equation. G) Summary of apparent strontium sensitivity (EC_{50} s) of mTMEM16A mutants. N.C.: no obvious CaCC current recorded. Upward arrows: estimated strontium $EC_{50} > 10$ mM and cannot be reported with confidence. ***: $p < 0.001$.

Figure 3.6. TMEM16A channel sensitivity to cadmium ions is disrupted by mutations at the identified calcium-binding sites. A) Representative current trace of wildtype mTMEM16A in response to different intracellular cadmium solutions recorded at +60 mV. Table indicates the concentration of cadmium used. B) Cadmium dose-response curve of wildtype mTMEM16A channels at +60 mV. C-F) Cadmium dose-response curves of the C) E698, D) E701, E) E730, and F) D734 mutant mTMEM16A channels at +60 mV. Smooth curves represent fits to the Hill equation. G) Summary of apparent cadmium sensitivity (EC_{50} s) of mTMEM16A mutants. Upward arrows: estimated cadmium $EC_{50} > 10$ mM and cannot be reported with confidence. *: $p < 0.05$; **: $p < 0.01$; ***: $p < 0.001$.

Figure 3.7. Cysteine crosslinking suggests that the calcium-binding residues in TMEM16A-CaCC form a metal ion binding pocket that is exposed to the cytoplasm. A Representative traces of E701C/E730C, E701C, and E730C mTMEM16A mutants recorded under reducing (DTT) and oxidizing (H₂O₂) conditions. B) Comparison of currents recorded in oxidizing conditions of mutants shown in A. Amplitudes are normalized to currents recorded in reducing conditions. ***: $p < 0.001$. C) Schematic illustrating the position of the putative calcium binding residues (E698, E701, E730 and D734) based on two previous membrane topological models (Model A and B) (Yu et al., 2012, Yang et al., 2008) and our experimental data (Model C).

Figure 3.S1. Calmodulin (CaM) is not involved in the calcium-dependent activation of TMEM16A-CaCC. A) Acute application of 50 μ M W7, a CaM antagonist, to the cytosolic face of the inside-out patches failed to inhibit endogenous *Xenopus* TMEM16A-CaCC currents. B) Chronic incubation of *Xenopus* oocytes with W7 did not reduce the apparent calcium sensitivity of endogenous *Xenopus* TMEM16A-CaCC. C-D) Barium, a divalent cation that is incapable of binding CaM, can robustly activate mouse TMEM16A-CaCC. C) CaCC currents were recorded with voltage steps in +20 mV increments from -80 mV to +120 mV in isotonic 140 mM NaCl solutions. Both holding and repolarizing potentials were -80 mV. Dotted lines indicate the zero current level. D) Barium dose-response curves of wildtype mTMEM16A channel at ± 60 mV. Smooth curve represent fits to the Hill equation.

References

- ADAM, G. & DELBRUCK, M. 1968. Reduction of Dimensionality In Biological Diffusion Processes. *In: RICH, A. & DAVIDSON, N. (eds.) Structural Chemistry and Molecular Biology*. San Francisco: W. H. Freeman and Company.
- ASHCROFT, F. M. & GRIBBLE, F. M. 1998. Correlating structure and function in ATP-sensitive K⁺ channels. *Trends Neurosci*, 21, 288-94.
- ASHCROFT, S. J. 2000. The beta-cell K(ATP) channel. *J Membr Biol*, 176, 187-206.
- ATKINSON, N. S., ROBERTSON, G. A. & GANETZKY, B. 1991. A component of calcium-activated potassium channels encoded by the *Drosophila slo* locus. *Science*, 253, 551-5.
- AYALON, G. & STERN-BACH, Y. 2001. Functional assembly of AMPA and kainate receptors is mediated by several discrete protein-protein interactions. *Neuron*, 31, 103-13.
- BABENKO, A. P., AGUILAR-BRYAN, L. & BRYAN, J. 1998. A view of sur/KIR6.X, KATP channels. *Annu Rev Physiol*, 60, 667-87.
- BAUER, C. K. & SCHWARZ, J. R. 2001. Physiology of EAG K⁺ channels. *J Membr Biol*, 182, 1-15.
- BEN-SHAHAR, Y. 2011. Sensory functions for degenerin/epithelial sodium channels (DEG/ENaC). *Adv Genet*, 76, 1-26.
- BERG, J., YANG, H. & JAN, L. Y. 2012. Ca²⁺-activated Cl⁻ channels at a glance. *J Cell Sci*, 125, 1367-71.
- BERGER, A. L., IKUMA, M. & WELSH, M. J. 2005. Normal gating of CFTR requires ATP binding to both nucleotide-binding domains and hydrolysis at the second nucleotide-binding domain. *Proc Natl Acad Sci U S A*, 102, 455-60.

- BERGER, T. K. & ISACOFF, E. Y. 2011. The pore of the voltage-gated proton channel. *Neuron*, 72, 991-1000.
- BERKEFELD, H., FAKLER, B. & SCHULTE, U. 2010. Ca²⁺-activated K⁺ channels: from protein complexes to function. *Physiol Rev*, 90, 1437-59.
- BIEL, M. & MICHALAKIS, S. 2009. Cyclic nucleotide-gated channels. *Handb Exp Pharmacol*, 111-36.
- BILLIG, G. M., PÁL, B., FIDZINSKI, P. & JENTSCH, T. J. 2011. Ca²⁺-activated Cl⁻ currents are dispensable for olfaction. *Nat Neurosci*, 14, 763-9.
- BOLDUC, V., MARLOW, G., BOYCOTT, K., SALEKI, K., INOUE, H., KROON, J., ITAKURA, M., ROBITAILLE, Y., PARENT, L., BAAS, F., MIZUTA, K., KAMATA, N., RICHARD, I., LINSSEN, W., MAHJNEH, I., DE VISSER, M., BASHIR, R. & BRAIS, B. 2010. Recessive mutations in the putative calcium-activated chloride channel Anoctamin 5 cause proximal LGMD2L and distal MMD3 muscular dystrophies. *Am J Hum Genet*, 86, 213-21.
- BRAUCHI, S., ORTA, G., SALAZAR, M., ROSENMANN, E. & LATORRE, R. 2006. A hot-sensing cold receptor: C-terminal domain determines thermosensation in transient receptor potential channels. *J Neurosci*, 26, 4835-40.
- BRITSCHGI, A., BILL, A., BRINKHAUS, H., ROTHWELL, C., CLAY, I., DUSS, S., REBHAN, M., RAMAN, P., GUY, C. T., WETZEL, K., GEORGE, E., POPA, M. O., LILLEY, S., CHOUDHURY, H., GOSLING, M., WANG, L., FITZGERALD, S., BORAWSKI, J., BAFFOE, J., LABOW, M., GAITHER, L. A. & BENTIREN-ALJ, M. 2013. Calcium-activated chloride channel ANO1 promotes breast cancer progression by activating EGFR and CAMK signaling. *Proc Natl Acad Sci U S A*, 110, E1026-34.

- BROHAWN, S. G., DEL MÁRMOL, J. & MACKINNON, R. 2012. Crystal structure of the human K2P TRAAK, a lipid- and mechano-sensitive K⁺ ion channel. *Science*, 335, 436-41.
- BURNSTOCK, G. 2007. Purine and pyrimidine receptors. *Cell Mol Life Sci*, 64, 1471-83.
- CAPUTO, A., CACI, E., FERRERA, L., PEDEMONTE, N., BARSANTI, C., SONDO, E., PFEFFER, U., RAVAZZOLO, R., ZEGARRA-MORAN, O. & GALIETTA, L. 2008. TMEM16A, a membrane protein associated with calcium-dependent chloride channel activity. *Science*, 322, 590-4.
- CASTOLDI, E., COLLINS, P. W., WILLIAMSON, P. L. & BEVERS, E. M. 2011. Compound heterozygosity for 2 novel TMEM16F mutations in a patient with Scott syndrome. *Blood*, 117, 4399-400.
- CATTERALL, W. A. 1998. Structure and function of neuronal Ca²⁺ channels and their role in neurotransmitter release. *Cell Calcium*, 24, 307-23.
- CATTERALL, W. A. 2000. From ionic currents to molecular mechanisms: the structure and function of voltage-gated sodium channels. *Neuron*, 26, 13-25.
- CENEDESE, V., BETTO, G., CELSI, F., CHERIAN, O. L., PIFFERI, S. & MENINI, A. 2012. The voltage dependence of the TMEM16B/anoctamin2 calcium-activated chloride channel is modified by mutations in the first putative intracellular loop. *J Gen Physiol*, 139, 285-94.
- CHAMOVA, T., FLOREZ, L., GUERGUELTCHEVA, V., RAYCHEVA, M., KANEVA, R., LOCHMÜLLER, H., KALAYDJIEVA, L. & TOURNEV, I. 2012. ANO10 c.1150_1151del is a founder mutation causing autosomal recessive cerebellar ataxia in Roma/Gypsies. *J Neurol*, 259, 906-11.

- CHANDRASHEKAR, J., KUHN, C., OKA, Y., YARMOLINSKY, D. A., HUMMLER, E., RYBA, N. J. & ZUKER, C. S. 2010. The cells and peripheral representation of sodium taste in mice. *Nature*, 464, 297-301.
- CHARLESWORTH, G., PLAGNOL, V., HOLMSTRÖM, K. M., BRAS, J., SHEERIN, U. M., PREZA, E., RUBIO-AGUSTI, I., RYTEN, M., SCHNEIDER, S. A., STAMELOU, M., TRABZUNI, D., ABRAMOV, A. Y., BHATIA, K. P. & WOOD, N. W. 2012. Mutations in ANO3 cause dominant craniocervical dystonia: ion channel implicated in pathogenesis. *Am J Hum Genet*, 91, 1041-50.
- CHEN, G. Q., CUI, C., MAYER, M. L. & GOUAUX, E. 1999. Functional characterization of a potassium-selective prokaryotic glutamate receptor. *Nature*, 402, 817-21.
- CHENG, J., RANDALL, A. Z., SWEREDOSKI, M. J. & BALDI, P. 2005. SCRATCH: a protein structure and structural feature prediction server. *Nucleic Acids Res*, 33, W72-6.
- CHENG, S. H., RICH, D. P., MARSHALL, J., GREGORY, R. J., WELSH, M. J. & SMITH, A. E. 1991. Phosphorylation of the R domain by cAMP-dependent protein kinase regulates the CFTR chloride channel. *Cell*, 66, 1027-36.
- CHO, H., YANG, Y. D., LEE, J., LEE, B., KIM, T., JANG, Y., BACK, S. K., NA, H. S., HARFE, B. D., WANG, F., RAOUF, R., WOOD, J. N. & OH, U. 2012. The calcium-activated chloride channel anoctamin 1 acts as a heat sensor in nociceptive neurons. *Nat Neurosci*, 15, 1015-21.
- COLE, C., BARBER, J. D. & BARTON, G. J. 2008. The Jpred 3 secondary structure prediction server. *Nucleic Acids Res*, 36, W197-201.
- COMBET, C., BLANCHET, C., GEOURJON, C. & DELÉAGE, G. 2000. NPS@: network protein sequence analysis. *Trends Biochem Sci*, 25, 147-50.

- CORDERO-MORALES, J. F., GRACHEVA, E. O. & JULIUS, D. 2011. Cytoplasmic ankyrin repeats of transient receptor potential A1 (TRPA1) dictate sensitivity to thermal and chemical stimuli. *Proc Natl Acad Sci U S A*, 108, E1184-91.
- COSCOY, S., LINGUEGLIA, E., LAZDUNSKI, M. & BARBRY, P. 1998. The Phe-Met-Arg-Phe-amide-activated sodium channel is a tetramer. *J Biol Chem*, 273, 8317-22.
- CULL-CANDY, S. & LESZKIEWICZ, D. 2004. Role of distinct NMDA receptor subtypes at central synapses. *Sci STKE*, 2004, re16.
- DAS, S., HAHN, Y., NAGATA, S., WILLINGHAM, M., BERA, T., LEE, B. & PASTAN, I. 2007. NGEF, a prostate-specific plasma membrane protein that promotes the association of LNCaP cells. *Cancer Res*, 67, 1594-601.
- DAUNER, K., LISSMANN, J., JERIDI, S., FRINGS, S. & MÖHRLLEN, F. 2012. Expression patterns of anoctamin 1 and anoctamin 2 chloride channels in the mammalian nose. *Cell Tissue Res*, 347, 327-41.
- DAUNER, K., MÖBUS, C., FRINGS, S. & MÖHRLLEN, F. 2013. Targeted expression of anoctamin calcium-activated chloride channels in rod photoreceptor terminals of the rodent retina. *Invest Ophthalmol Vis Sci*, 54, 3126-36.
- DECOURSEY, T. E. 2003. Voltage-gated proton channels and other proton transfer pathways. *Physiol Rev*, 83, 475-579.
- DIBATTISTA, M., AMJAD, A., MAURYA, D. K., SAGHEDDU, C., MONTANI, G., TIRINDELLI, R. & MENINI, A. 2012. Calcium-activated chloride channels in the apical region of mouse vomeronasal sensory neurons. *J Gen Physiol*, 140, 3-15.
- DIXON, R. E., HENNIG, G. W., BAKER, S. A., BRITTON, F. C., HARFE, B. D., ROCK, J. R., SANDERS, K. M. & WARD, S. M. 2011. Electrical Slow Waves in the Mouse Oviduct

Are Dependent upon a Calcium Activated Chloride Conductance Encoded by
Tmem16a. *Biol Reprod*.

DOYLE, D. A., MORAIS CABRAL, J., PFUETZNER, R. A., KUO, A., GULBIS, J. M., COHEN, S. L.,
CHAIT, B. T. & MACKINNON, R. 1998. The structure of the potassium channel:
molecular basis of K⁺ conduction and selectivity. *Science*, 280, 69-77.

DURAN, C. & HARTZELL, H. C. 2011. Physiological roles and diseases of
Tmem16/Anoctamin proteins: are they all chloride channels? *Acta Pharmacol Sin*,
32, 685-92.

DUTTA, A. K., KHIMJI, A. K., KRESGE, C., BUGDE, A., DOUGHERTY, M., ESSER, V., UENO, Y.,
GLASER, S. S., ALPINI, G., ROCKEY, D. C. & FERANCHAK, A. P. 2011. Identification and
functional characterization of TMEM16A, a Ca²⁺-activated Cl⁻ channel activated by
extracellular nucleotides, in biliary epithelium. *J Biol Chem*, 286, 766-76.

DUTZLER, R., CAMPBELL, E. B., CADENE, M., CHAIT, B. T. & MACKINNON, R. 2002. X-ray
structure of a ClC chloride channel at 3.0 Å reveals the molecular basis of anion
selectivity. *Nature*, 415, 287-94.

DUTZLER, R., CAMPBELL, E. B. & MACKINNON, R. 2003. Gating the selectivity filter in ClC
chloride channels. *Science*, 300, 108-12.

DUVVURI, U., SHIWARSKI, D. J., XIAO, D., BERTRAND, C., HUANG, X., EDINGER, R. S., ROCK, J.
R., HARFE, B. D., HENSON, B. J., KUNZELMANN, K., SCHREIBER, R., SEETHALA, R. S.,
EGLOFF, A. M., CHEN, X., LUI, V. W., GRANDIS, J. R. & GOLLIN, S. M. 2012. TMEM16A
induces MAPK and contributes directly to tumorigenesis and cancer progression.
Cancer Res, 72, 3270-81.

- EL HIANI, Y. & LINSDELL, P. 2012. Tuning of CFTR chloride channel function by location of positive charges within the pore. *Biophys J*, 103, 1719-26.
- ELLGAARD, L. & HELENIUS, A. 2003. Quality control in the endoplasmic reticulum. *Nat Rev Mol Cell Biol*, 4, 181-91.
- ENYEDI, P. & CZIRJÁK, G. 2010. Molecular background of leak K⁺ currents: two-pore domain potassium channels. *Physiol Rev*, 90, 559-605.
- FALLAH, G., RÖMER, T., DETRO-DASSEN, S., BRAAM, U., MARKWARDT, F. & SCHMALZING, G. 2011. TMEM16A(a)/anoctamin-1 shares a homodimeric architecture with CLC chloride channels. *Mol Cell Proteomics*, 10, M110.004697.
- FEI, B. Y., YANG, J. M. & ZHAO, Z. S. 2014. Differential clinical and pathological characteristics of esophageal stromal tumors and leiomyomata. *Dis Esophagus*, 27, 30-5.
- FERRERA, L., CAPUTO, A., UBBY, I., BUSSANI, E., ZEGARRA-MORAN, O., RAVAZZOLO, R., PAGANI, F. & GALIETTA, L. 2009. Regulation of TMEM16A chloride channel properties by alternative splicing. *J Biol Chem*, 284, 33360-8.
- FERRERA, L., SCUDIERI, P., SONDO, E., CAPUTO, A., CACI, E., ZEGARRA-MORAN, O., RAVAZZOLO, R. & GALIETTA, L. J. 2011. A minimal isoform of the TMEM16A protein associated with chloride channel activity. *Biochim Biophys Acta*, 1808, 2214-23.
- FORREST, A., ANGERMANN, J., RAGHUNATHAN, R., LACHENDRO, C., GREENWOOD, I. & LEBLANC, N. 2010. Intricate interaction between store-operated calcium entry and calcium-activated chloride channels in pulmonary artery smooth muscle cells. *Adv Exp Med Biol*, 661, 31-55.

- FOSKETT, J. K., WHITE, C., CHEUNG, K. H. & MAK, D. O. 2007. Inositol trisphosphate receptor Ca²⁺ release channels. *Physiol Rev*, 87, 593-658.
- GADSBY, D. C., VERGANI, P. & CSANÁDY, L. 2006. The ABC protein turned chloride channel whose failure causes cystic fibrosis. *Nature*, 440, 477-83.
- GALZI, J. L., DEVILLERS-THIÉRY, A., HUSSY, N., BERTRAND, S., CHANGEUX, J. P. & BERTRAND, D. 1992. Mutations in the channel domain of a neuronal nicotinic receptor convert ion selectivity from cationic to anionic. *Nature*, 359, 500-5.
- GAYMARD, F., CERUTTI, M., HOREAU, C., LEMAILLET, G., URBACH, S., RAVALLEC, M., DEVAUCHELLE, G., SENTENAC, H. & THIBAUD, J. B. 1996. The baculovirus/insect cell system as an alternative to *Xenopus* oocytes. First characterization of the AKT1 K⁺ channel from *Arabidopsis thaliana*. *J Biol Chem*, 271, 22863-70.
- GEORGE, C. H., JUNDI, H., THOMAS, N. L., SCOOTE, M., WALTERS, N., WILLIAMS, A. J. & LAI, F. A. 2004. Ryanodine receptor regulation by intramolecular interaction between cytoplasmic and transmembrane domains. *Mol Biol Cell*, 15, 2627-38.
- GOUJON, M., MCWILLIAM, H., LI, W., VALENTIN, F., SQUIZZATO, S., PAERN, J. & LOPEZ, R. 2010. A new bioinformatics analysis tools framework at EMBL-EBI. *Nucleic Acids Res*, 38, W695-9.
- GUNDERSON, K. L. & KOPITO, R. R. 1995. Conformational states of CFTR associated with channel gating: the role ATP binding and hydrolysis. *Cell*, 82, 231-9.
- HARTZELL, C., PUTZIER, I. & ARREOLA, J. 2005. Calcium-activated chloride channels. *Annu Rev Physiol*, 67, 719-58.
- HATTORI, M. & GOUAUX, E. 2012. Molecular mechanism of ATP binding and ion channel activation in P2X receptors. *Nature*, 485, 207-12.

- HEINEMANN, S. H., TERLAU, H., STÜHMER, W., IMOTO, K. & NUMA, S. 1992. Calcium channel characteristics conferred on the sodium channel by single mutations. *Nature*, 356, 441-3.
- HIBINO, H., INANOBE, A., FURUTANI, K., MURAKAMI, S., FINDLAY, I. & KURACHI, Y. 2010. Inwardly rectifying potassium channels: their structure, function, and physiological roles. *Physiol Rev*, 90, 291-366.
- HILLE, B. 2001. *Ion channels of excitable membranes*, Sunderland, Mass., Sinauer.
- HOWARD, R. J., CLARK, K. A., HOLTON, J. M. & MINOR, D. L. 2007. Structural insight into KCNQ (Kv7) channel assembly and channelopathy. *Neuron*, 53, 663-75.
- HUANG, F., WANG, X., OSTERTAG, E. M., NUWAL, T., HUANG, B., JAN, Y. N., BASBAUM, A. I. & JAN, L. Y. 2013. TMEM16C facilitates Na(+)-activated K⁺ currents in rat sensory neurons and regulates pain processing. *Nat Neurosci*, 16, 1284-90.
- HUANG, F., WONG, X. & JAN, L. Y. 2012a. International Union of Basic and Clinical Pharmacology. LXXXV: calcium-activated chloride channels. *Pharmacol Rev*, 64, 1-15.
- HUANG, F., ZHANG, H., WU, M., YANG, H., KUDO, M., PETERS, C. J., WOODRUFF, P. G., SOLBERG, O. D., DONNE, M. L., HUANG, X., SHEPPARD, D., FAHY, J. V., WOLTERS, P. J., HOGAN, B. L., FINKBEINER, W. E., LI, M., JAN, Y. N., JAN, L. Y. & ROCK, J. R. 2012b. Calcium-activated chloride channel TMEM16A modulates mucin secretion and airway smooth muscle contraction. *Proc Natl Acad Sci U S A*, 109, 16354-9.
- HUANG, W. C., XIAO, S., HUANG, F., HARFE, B. D., JAN, Y. N. & JAN, L. Y. 2012c. Calcium-activated chloride channels (CaCCs) regulate action potential and synaptic response in hippocampal neurons. *Neuron*, 74, 179-92.

- IMOTO, K., BUSCH, C., SAKMANN, B., MISHINA, M., KONNO, T., NAKAI, J., BUJO, H., MORI, Y., FUKUDA, K. & NUMA, S. 1988. Rings of negatively charged amino acids determine the acetylcholine receptor channel conductance. *Nature*, 335, 645-8.
- IQBAL, J., TONTA, M. A., MITSUI, R., LI, Q., KETT, M., LI, J., PARKINGTON, H. C., HASHITANI, H. & LANG, R. J. 2012. Potassium and ANO1/ TMEM16A chloride channel profiles distinguish atypical and typical smooth muscle cells from interstitial cells in the mouse renal pelvis. *Br J Pharmacol*, 165, 2389-408.
- JACOBSEN, K. S., ZEEBERG, K., SAUTER, D. R., POULSEN, K. A., HOFFMANN, E. K. & SCHWAB, A. 2013. The role of TMEM16A (ANO1) and TMEM16F (ANO6) in cell migration. *Pflugers Arch*, 465, 1753-62.
- JAN, L. Y. & JAN, Y. N. 1997. Cloned potassium channels from eukaryotes and prokaryotes. *Annu Rev Neurosci*, 20, 91-123.
- JANG, Y. & OH, U. 2014. Anoctamin 1 in secretory epithelia. *Cell Calcium*.
- JASTI, J., FURUKAWA, H., GONZALES, E. B. & GOUAUX, E. 2007. Structure of acid-sensing ion channel 1 at 1.9 Å resolution and low pH. *Nature*, 449, 316-23.
- JENTSCH, T. J., NEAGOE, I. & SCHEEL, O. 2005. CLC chloride channels and transporters. *Curr Opin Neurobiol*, 15, 319-25.
- JEON, J. H., PAIK, S. S., CHUN, M. H., OH, U. & KIM, I. B. 2013. Presynaptic Localization and Possible Function of Calcium-Activated Chloride Channel Anoctamin 1 in the Mammalian Retina. *PLoS One*, 8, e67989.
- JEON, J. H., PARK, J. W., LEE, J. W., JEONG, S. W., YEO, S. W. & KIM, I. B. 2011. Expression and immunohistochemical localization of TMEM16A/noctamin 1, a calcium-activated chloride channel in the mouse cochlea. *Cell Tissue Res*, 345, 223-30.

- JUNG, J., NAM, J. H., PARK, H. W., OH, U., YOON, J. H. & LEE, M. G. 2013. Dynamic modulation of ANO1/TMEM16A HCO₃⁻ permeability by Ca²⁺/calmodulin. *Proc Natl Acad Sci U S A*, 110, 360-5.
- JUUL, C. A., GRUBB, S., POULSEN, K. A., KYED, T., HASHEM, N., LAMBERT, I. H., LARSEN, E. H. & HOFFMANN, E. K. 2014. Anoctamin 6 differs from VRAC and VSOAC but is involved in apoptosis and supports volume regulation in the presence of Ca(2+). *Pflugers Arch*.
- KANAZAWA, T. & MATSUMOTO, S. 2014. Expression of transient receptor potential vanilloid 1 and anoctamin 1 in rat trigeminal ganglion neurons innervating the tongue. *Brain Res Bull*, 106C, 17-20.
- KANDEL, E. R. 2012. *Principles of neural science*, New York, McGraw-Hill.
- KARLIN, A. 2002. Emerging structure of the nicotinic acetylcholine receptors. *Nat Rev Neurosci*, 3, 102-14.
- KASHLAN, O. B. & KLEYMAN, T. R. 2011. ENaC structure and function in the wake of a resolved structure of a family member. *Am J Physiol Renal Physiol*, 301, F684-96.
- KAWATE, T., MICHEL, J. C., BIRDSONG, W. T. & GOUAUX, E. 2009. Crystal structure of the ATP-gated P2X(4) ion channel in the closed state. *Nature*, 460, 592-8.
- KERCHNER, G. A. & NICOLL, R. A. 2008. Silent synapses and the emergence of a postsynaptic mechanism for LTP. *Nat Rev Neurosci*, 9, 813-25.
- KHAKH, B. S. & NORTH, R. A. 2012. Neuromodulation by extracellular ATP and P2X receptors in the CNS. *Neuron*, 76, 51-69.
- KONNO, T., BUSCH, C., VON KITZING, E., IMOTO, K., WANG, F., NAKAI, J., MISHINA, M., NUMA, S. & SAKMANN, B. 1991. Rings of anionic amino acids as structural

- determinants of ion selectivity in the acetylcholine receptor channel. *Proc Biol Sci*, 244, 69-79.
- KREUSCH, A., PFAFFINGER, P. J., STEVENS, C. F. & CHOE, S. 1998. Crystal structure of the tetramerization domain of the Shaker potassium channel. *Nature*, 392, 945-8.
- KUNER, T., BECK, C., SAKMANN, B. & SEEBURG, P. H. 2001. Channel-lining residues of the AMPA receptor M2 segment: structural environment of the Q/R site and identification of the selectivity filter. *J Neurosci*, 21, 4162-72.
- KÖHLER, M., HIRSCHBERG, B., BOND, C. T., KINZIE, J. M., MARRION, N. V., MAYLIE, J. & ADELMAN, J. P. 1996. Small-conductance, calcium-activated potassium channels from mammalian brain. *Science*, 273, 1709-14.
- LAEMMLI, U. K. 1970. Cleavage of structural proteins during the assembly of the head of bacteriophage T4. *Nature*, 227, 680-5.
- LAGREE, V., BRUNSCHWIG, K., LOPEZ, P., GILULA, N. B., RICHARD, G. & FALK, M. M. 2003. Specific amino-acid residues in the N-terminus and TM3 implicated in channel function and oligomerization compatibility of connexin43. *J Cell Sci*, 116, 3189-201.
- LANNER, J. T., GEORGIU, D. K., JOSHI, A. D. & HAMILTON, S. L. 2010. Ryanodine receptors: structure, expression, molecular details, and function in calcium release. *Cold Spring Harb Perspect Biol*, 2, a003996.
- LEE, B., CHO, H., JUNG, J., YANG, Y. D., YANG, D. J. & OH, U. 2014. Anoctamin 1 contributes to inflammatory and nerve-injury induced hypersensitivity. *Mol Pain*, 10, 5.
- LEE, U. S. & CUI, J. 2010. BK channel activation: structural and functional insights. *Trends Neurosci*, 33, 415-23.

- LESAGE, F. & LAZDUNSKI, M. 2000. Molecular and functional properties of two-pore-domain potassium channels. *Am J Physiol Renal Physiol*, 279, F793-801.
- LI, M., JAN, Y. N. & JAN, L. Y. 1992. Specification of subunit assembly by the hydrophilic amino-terminal domain of the Shaker potassium channel. *Science*, 257, 1225-30.
- LIEWLUCK, T., WINDER, T. L., DIMBERG, E. L., CRUM, B. A., HEPPELMANN, C. J., WANG, Y., BERGEN, H. R. & MILONE, M. 2013. ANO5-muscular dystrophy: clinical, pathological and molecular findings. *Eur J Neurol*, 20, 1383-9.
- LIU, B., LINLEY, J., DU, X., ZHANG, X., OOI, L., ZHANG, H. & GAMPER, N. 2010. The acute nociceptive signals induced by bradykinin in rat sensory neurons are mediated by inhibition of M-type K⁺ channels and activation of Ca²⁺-activated Cl⁻ channels. *J Clin Invest*, 120, 1240-52.
- LIU, J., LIU, Y., REN, Y., KANG, L. & ZHANG, L. 2014. Transmembrane protein with unknown function 16A overexpression promotes glioma formation through the nuclear factor- κ B signaling pathway. *Mol Med Rep*, 9, 1068-74.
- LIU, W., LU, M., LIU, B., HUANG, Y. & WANG, K. 2012. Inhibition of Ca²⁺-activated Cl⁻ channel ANO1/TMEM16A expression suppresses tumor growth and invasiveness in human prostate carcinoma. *Cancer Lett*, 326, 41-51.
- LU, Z., KLEM, A. M. & RAMU, Y. 2001. Ion conduction pore is conserved among potassium channels. *Nature*, 413, 809-13.
- LYNCH, J. W. 2004. Molecular structure and function of the glycine receptor chloride channel. *Physiol Rev*, 84, 1051-95.

- LÜSCHER, C., JAN, L. Y., STOFFEL, M., MALENKA, R. C. & NICOLL, R. A. 1997. G protein-coupled inwardly rectifying K⁺ channels (GIRKs) mediate postsynaptic but not presynaptic transmitter actions in hippocampal neurons. *Neuron*, 19, 687-95.
- LÜTHI, A. & MCCORMICK, D. A. 1998. H-current: properties of a neuronal and network pacemaker. *Neuron*, 21, 9-12.
- MADDEN, D. R. 2002. The structure and function of glutamate receptor ion channels. *Nat Rev Neurosci*, 3, 91-101.
- MANOURY, B., TAMULEVICIUTE, A. & TAMMARO, P. 2010. TMEM16A/anoctamin 1 protein mediates calcium-activated chloride currents in pulmonary arterial smooth muscle cells. *J Physiol*, 588, 2305-14.
- MARICQ, A. V., PETERSON, A. S., BRAKE, A. J., MYERS, R. M. & JULIUS, D. 1991. Primary structure and functional expression of the 5HT₃ receptor, a serotonin-gated ion channel. *Science*, 254, 432-7.
- MARTEN, I., HOTH, S., DEEKEN, R., ACHE, P., KETCHUM, K. A., HOSHI, T. & HEDRICH, R. 1999. AKT3, a phloem-localized K⁺ channel, is blocked by protons. *Proc Natl Acad Sci U S A*, 96, 7581-6.
- MARTÍNEZ, A. D., MARIPILLÁN, J., ACUÑA, R., MINOGUE, P. J., BERTHOUD, V. M. & BEYER, E. C. 2011. Different domains are critical for oligomerization compatibility of different connexins. *Biochem J*, 436, 35-43.
- MAYER, M. L. 2011. Structure and mechanism of glutamate receptor ion channel assembly, activation and modulation. *Curr Opin Neurobiol*, 21, 283-90.
- MAYER, M. L. & ARMSTRONG, N. 2004. Structure and function of glutamate receptor ion channels. *Annu Rev Physiol*, 66, 161-81.

- MAZZOLINI, M., MARCHESI, A., GIORGETTI, A. & TORRE, V. 2010. Gating in CNGA1 channels. *Pflugers Arch*, 459, 547-55.
- MAZZONE, A., BERNARD, C. E., STREGE, P. R., BEYDER, A., GALIETTA, L. J., PASRICHA, P. J., RAE, J. L., PARKMAN, H. P., LINDEN, D. R., SZURSZEWSKI, J. H., ÖRDÖG, T., GIBBONS, S. J. & FARRUGIA, G. 2011. Altered expression of Ano1 variants in human diabetic gastroparesis. *J Biol Chem*, 286, 13393-403.
- MIKOSHIBA, K. 1997. The InsP3 receptor and intracellular Ca²⁺ signaling. *Curr Opin Neurobiol*, 7, 339-45.
- MILENKOVIC, V. M., BROCKMANN, M., STÖHR, H., WEBER, B. H. & STRAUSS, O. 2010. Evolution and functional divergence of the anoctamin family of membrane proteins. *BMC Evol Biol*, 10, 319.
- MILLER, A. N. & LONG, S. B. 2012. Crystal structure of the human two-pore domain potassium channel K2P1. *Science*, 335, 432-6.
- MIYAZAWA, A., FUJIYOSHI, Y. & UNWIN, N. 2003. Structure and gating mechanism of the acetylcholine receptor pore. *Nature*, 423, 949-55.
- MONTELL, C. 2005. The TRP superfamily of cation channels. *Sci STKE*, 2005, re3.
- NICHOLS, C. G. & LOPATIN, A. N. 1997. Inward rectifier potassium channels. *Annu Rev Physiol*, 59, 171-91.
- O'HAGAN, R., CHALFIE, M. & GOODMAN, M. B. 2005. The MEC-4 DEG/ENaC channel of *Caenorhabditis elegans* touch receptor neurons transduces mechanical signals. *Nat Neurosci*, 8, 43-50.
- O'NEIL, K. T. & DEGRADO, W. F. 1990. A thermodynamic scale for the helix-forming tendencies of the commonly occurring amino acids. *Science*, 250, 646-51.

- OHSHIRO, J., YAMAMURA, H., SUZUKI, Y. & IMAIZUMI, Y. 2014. Modulation of TMEM16A-Channel Activity as Ca(2+) Activated Cl(-) Conductance via the Interaction With Actin Cytoskeleton in Murine Portal Vein. *J Pharmacol Sci*, 125, 107-11.
- OLSEN, R. W. & SIEGHART, W. 2009. GABA A receptors: subtypes provide diversity of function and pharmacology. *Neuropharmacology*, 56, 141-8.
- OUSINGSAWAT, J., MARTINS, J. R., SCHREIBER, R., ROCK, J. R., HARFE, B. D. & KUNZELMANN, K. 2009. Loss of TMEM16A causes a defect in epithelial Ca²⁺-dependent chloride transport. *J Biol Chem*, 284, 28698-703.
- OUSINGSAWAT, J., MIRZA, M., TIAN, Y., ROUSSA, E., SCHREIBER, R., COOK, D. I. & KUNZELMANN, K. 2011. Rotavirus toxin NSP4 induces diarrhea by activation of TMEM16A and inhibition of Na⁺ absorption. *Pflugers Arch*, 461, 579-89.
- PATEL, A. J., HONORÉ, E., LESAGE, F., FINK, M., ROMEY, G. & LAZDUNSKI, M. 1999. Inhalational anesthetics activate two-pore-domain background K⁺ channels. *Nat Neurosci*, 2, 422-6.
- PRITCHARD, H. A., LEBLANC, N., ALBERT, A. P. & GREENWOOD, I. A. 2014. Inhibitory role of phosphatidylinositol 4,5 bisphosphate on TMEM16A encoded calcium-activated chloride channels in rat pulmonary artery. *Br J Pharmacol*.
- PUSCH, M. 2004. Structural insights into chloride and proton-mediated gating of CLC chloride channels. *Biochemistry*, 43, 1135-44.
- PUSCH, M., LUDEWIG, U., REHFELDT, A. & JENTSCH, T. J. 1995. Gating of the voltage-dependent chloride channel CIC-0 by the permeant anion. *Nature*, 373, 527-31.
- QUAYLE, J. M., NELSON, M. T. & STANDEN, N. B. 1997. ATP-sensitive and inwardly rectifying potassium channels in smooth muscle. *Physiol Rev*, 77, 1165-232.

- RAMSEY, I. S., MOKRAB, Y., CARVACHO, I., SANDS, Z. A., SANSOM, M. S. & CLAPHAM, D. E. 2010. An aqueous H⁺ permeation pathway in the voltage-gated proton channel Hv1. *Nat Struct Mol Biol*, 17, 869-75.
- RASCHE, S., TOETTER, B., ADLER, J., TSCHAPEK, A., DOERNER, J., KURTENBACH, S., HATT, H., MEYER, H., WARSCHEID, B. & NEUHAUS, E. 2010. Tmem16b is specifically expressed in the cilia of olfactory sensory neurons. *Chem Senses*, 35, 239-45.
- ROCK, J., O'NEAL, W., GABRIEL, S., RANDELL, S., HARFE, B., BOUCHER, R. & GRUBB, B. 2009. Transmembrane protein 16A (TMEM16A) is a Ca²⁺-regulated Cl⁻ secretory channel in mouse airways. *J Biol Chem*, 284, 14875-80.
- ROCK, J. R., FUTTNER, C. R. & HARFE, B. D. 2008. The transmembrane protein TMEM16A is required for normal development of the murine trachea. *Dev Biol*, 321, 141-9.
- ROMANENKO, V., CATALÁN, M., BROWN, D., PUTZIER, I., HARTZELL, H., MARMORSTEIN, A., GONZALEZ-BEGNE, M., ROCK, J., HARFE, B. & MELVIN, J. 2010. Tmem16A encodes the Ca²⁺-activated Cl⁻ channel in mouse submandibular salivary gland acinar cells. *J Biol Chem*, 285, 12990-3001.
- RUIZ, C., MARTINS, J. R., RUDIN, F., SCHNEIDER, S., DIETSCH, T., FISCHER, C. A., TORNILLO, L., TERRACCIANO, L. M., SCHREIBER, R., BUBENDORF, L. & KUNZELMANN, K. 2012. Enhanced expression of ANO1 in head and neck squamous cell carcinoma causes cell migration and correlates with poor prognosis. *PLoS One*, 7, e43265.
- SALAZAR, H., JARA-OSGUERA, A., HERNÁNDEZ-GARCÍA, E., LLORENTE, I., ARIAS-OLGUÍN, I. I., SORIANO-GARCÍA, M., ISLAS, L. D. & ROSENBAUM, T. 2009. Structural determinants of gating in the TRPV1 channel. *Nat Struct Mol Biol*, 16, 704-10.

- SANCHO, M., GARCÍA-PASCUAL, A. & TRIGUERO, D. 2012. Presence of the Ca²⁺-activated chloride channel anoctamin 1 in the urethra and its role in excitatory neurotransmission. *Am J Physiol Renal Physiol*, 302, F390-400.
- SANDERS, K. M., ZHU, M. H., BRITTON, F., KOH, S. D. & WARD, S. M. 2012. Anoctamins and gastrointestinal smooth muscle excitability. *Exp Physiol*, 97, 200-6.
- SCHACHTMAN, D. P., SCHROEDER, J. I., LUCAS, W. J., ANDERSON, J. A. & GABER, R. F. 1992. Expression of an inward-rectifying potassium channel by the Arabidopsis KAT1 cDNA. *Science*, 258, 1654-8.
- SCHROEDER, B., CHENG, T., JAN, Y. & JAN, L. 2008. Expression cloning of TMEM16A as a calcium-activated chloride channel subunit. *Cell*, 134, 1019-29.
- SCHUMACHER, M. A., RIVARD, A. F., BÄCHINGER, H. P. & ADELMAN, J. P. 2001. Structure of the gating domain of a Ca²⁺-activated K⁺ channel complexed with Ca²⁺/calmodulin. *Nature*, 410, 1120-4.
- SHEPPARD, D. N. & WELSH, M. J. 1999. Structure and function of the CFTR chloride channel. *Physiol Rev*, 79, S23-45.
- SHERIDAN, J. T., WORTHINGTON, E. N., YU, K., GABRIEL, S. E., HARTZELL, H. C. & TARRAN, R. 2011. Characterization of the oligomeric structure of the Ca(2+)-activated Cl-channel Ano1/TMEM16A. *J Biol Chem*, 286, 1381-8.
- SINE, S. M. & ENGEL, A. G. 2006. Recent advances in Cys-loop receptor structure and function. *Nature*, 440, 448-55.
- SOBOLEVSKY, A. I., ROSCONI, M. P. & GOUAUX, E. 2009. X-ray structure, symmetry and mechanism of an AMPA-subtype glutamate receptor. *Nature*, 462, 745-56.

- SPERLÁGH, B., VIZI, E. S., WIRKNER, K. & ILLES, P. 2006. P2X7 receptors in the nervous system. *Prog Neurobiol*, 78, 327-46.
- STÖHR, H., HEISIG, J., BENZ, P., SCHÖBERL, S., MILENKOVIC, V., STRAUSS, O., AARTSEN, W., WIJNHOLDS, J., WEBER, B. & SCHULZ, H. 2009. TMEM16B, a novel protein with calcium-dependent chloride channel activity, associates with a presynaptic protein complex in photoreceptor terminals. *J Neurosci*, 29, 6809-18.
- SURPRENANT, A. & NORTH, R. A. 2009. Signaling at purinergic P2X receptors. *Annu Rev Physiol*, 71, 333-59.
- SUZUKI, J., UMEDA, M., SIMS, P. J. & NAGATA, S. 2010. Calcium-dependent phospholipid scrambling by TMEM16F. *Nature*, 468, 834-8.
- SZTEYN, K., SCHMID, E., NURBAEVA, M. K., YANG, W., MÜNZER, P., KUNZELMANN, K., LANG, F. & SHUMILINA, E. 2012. Expression and functional significance of the Ca²⁺-activated Cl⁻ channel ANO6 in dendritic cells. *Cell Physiol Biochem*, 30, 1319-32.
- TANG, C. Y. & PAPAZIAN, D. M. 1997. Transfer of voltage independence from a rat olfactory channel to the Drosophila ether-à-go-go K⁺ channel. *J Gen Physiol*, 109, 301-11.
- TARASKA, J. W. & ZAGOTTA, W. N. 2007. Structural dynamics in the gating ring of cyclic nucleotide-gated ion channels. *Nat Struct Mol Biol*, 14, 854-60.
- TAYLOR, C. W. & TOVEY, S. C. 2010. IP(3) receptors: toward understanding their activation. *Cold Spring Harb Perspect Biol*, 2, a004010.
- TERASHIMA, H., PICOLLO, A. & ACCARDI, A. 2013. Purified TMEM16A is sufficient to form Ca²⁺-activated Cl⁻ channels. *Proc Natl Acad Sci U S A*, 110, 19354-9.

- TIAN, Y., KONGSUPHOL, P., HUG, M., OUSINGSAWAT, J., WITZGALL, R., SCHREIBER, R. & KUNZELMANN, K. 2011. Calmodulin-dependent activation of the epithelial calcium-dependent chloride channel TMEM16A. *FASEB J*, 25, 1058-68.
- TIEN, J., LEE, H. Y., MINOR, D. L., JAN, Y. N. & JAN, L. Y. 2013. Identification of a dimerization domain in the TMEM16A calcium-activated chloride channel (CaCC). *Proc Natl Acad Sci U S A*, 110, 6352-7.
- TOMBOLA, F., ULBRICH, M. H., KOHOUT, S. C. & ISACOFF, E. Y. 2010. The opening of the two pores of the Hv1 voltage-gated proton channel is tuned by cooperativity. *Nat Struct Mol Biol*, 17, 44-50.
- TSIEN, R. & POZZAN, T. 1989. Measurement of cytosolic free Ca²⁺ with quin2. *Methods Enzymol*, 172, 230-62.
- TSUTSUMI, S., KAMATA, N., VOKES, T., MARUOKA, Y., NAKAKUKI, K., ENOMOTO, S., OMURA, K., AMAGASA, T., NAGAYAMA, M., SAITO-OHARA, F., INAZAWA, J., MORITANI, M., YAMAOKA, T., INOUE, H. & ITAKURA, M. 2004. The novel gene encoding a putative transmembrane protein is mutated in gnathodiaphyseal dysplasia (GDD). *Am J Hum Genet*, 74, 1255-61.
- UNWIN, N. 1995. Acetylcholine receptor channel imaged in the open state. *Nature*, 373, 37-43.
- VALERA, S., HUSSY, N., EVANS, R. J., ADAMI, N., NORTH, R. A., SURPRENANT, A. & BUELL, G. 1994. A new class of ligand-gated ion channel defined by P2x receptor for extracellular ATP. *Nature*, 371, 516-9.

- VANSLYKE, J. K., DESCHENES, S. M. & MUSIL, L. S. 2000. Intracellular transport, assembly, and degradation of wild-type and disease-linked mutant gap junction proteins. *Mol Biol Cell*, 11, 1933-46.
- VENKATACHALAM, K. & MONTELL, C. 2007. TRP channels. *Annu Rev Biochem*, 76, 387-417.
- VERGANI, P., LOCKLESS, S. W., NAIRN, A. C. & GADSBY, D. C. 2005. CFTR channel opening by ATP-driven tight dimerization of its nucleotide-binding domains. *Nature*, 433, 876-80.
- VOCKE, K., DAUNER, K., HAHN, A., ULBRICH, A., BROECKER, J., KELLER, S., FRINGS, S. & MÖHRLIN, F. 2013. Calmodulin-dependent activation and inactivation of anoctamin calcium-gated chloride channels. *J Gen Physiol*, 142, 381-404.
- WAHL-SCHOTT, C. & BIEL, M. 2009. HCN channels: structure, cellular regulation and physiological function. *Cell Mol Life Sci*, 66, 470-94.
- WALDMANN, R., CHAMPIGNY, G., BASSILANA, F., HEURTEAUX, C. & LAZDUNSKI, M. 1997. A proton-gated cation channel involved in acid-sensing. *Nature*, 386, 173-7.
- WANG, J., HAANES, K. A. & NOVAK, I. 2013. Purinergic regulation of CFTR and Ca(2+)-activated Cl(-) channels and K(+) channels in human pancreatic duct epithelium. *Am J Physiol Cell Physiol*, 304, C673-84.
- WATERHOUSE, A. M., PROCTER, J. B., MARTIN, D. M., CLAMP, M. & BARTON, G. J. 2009. Jalview Version 2--a multiple sequence alignment editor and analysis workbench. *Bioinformatics*, 25, 1189-91.
- WEATHERALL, K. L., GOODCHILD, S. J., JANE, D. E. & MARRION, N. V. 2010. Small conductance calcium-activated potassium channels: from structure to function. *Prog Neurobiol*, 91, 242-55.

WEST, R., CORLESS, C., CHEN, X., RUBIN, B., SUBRAMANIAN, S., MONTGOMERY, K., ZHU, S., BALL, C., NIELSEN, T., PATEL, R., GOLDBLUM, J., BROWN, P., HEINRICH, M. & VAN DE RIJN, M. 2004. The novel marker, DOG1, is expressed ubiquitously in gastrointestinal stromal tumors irrespective of KIT or PDGFRA mutation status. *Am J Pathol*, 165, 107-13.

WICKMAN, K., NEMEC, J., GENDLER, S. J. & CLAPHAM, D. E. 1998. Abnormal heart rate regulation in GIRK4 knockout mice. *Neuron*, 20, 103-14.

WO, Z. G. & OSWALD, R. E. 1995. Unraveling the modular design of glutamate-gated ion channels. *Trends Neurosci*, 18, 161-8.

XIAO, Q., YU, K., PEREZ-CORNEJO, P., CUI, Y., ARREOLA, J. & HARTZELL, H. C. 2011. Voltage- and calcium-dependent gating of TMEM16A/Ano1 chloride channels are physically coupled by the first intracellular loop. *Proc Natl Acad Sci U S A*, 108, 8891-6.

YAMADA, K., JI, J. J., YUAN, H., MIKI, T., SATO, S., HORIMOTO, N., SHIMIZU, T., SEINO, S. & INAGAKI, N. 2001. Protective role of ATP-sensitive potassium channels in hypoxia-induced generalized seizure. *Science*, 292, 1543-6.

YANG, F., CUI, Y., WANG, K. & ZHENG, J. 2010. Thermosensitive TRP channel pore turret is part of the temperature activation pathway. *Proc Natl Acad Sci U S A*, 107, 7083-8.

YANG, H., KIM, A., DAVID, T., PALMER, D., JIN, T., TIEN, J., HUANG, F., CHENG, T., COUGHLIN, S. R., JAN, Y. N. & JAN, L. Y. 2012a. TMEM16F forms a Ca²⁺-activated cation channel required for lipid scrambling in platelets during blood coagulation. *Cell*, 151, 111-22.

YANG, N., LEI, Z., LI, X., ZHAO, J., LIU, T., NING, N., XIAO, A., XU, L. & LI, J. 2014. Chloroquine stimulates Cl⁻ secretion by Ca²⁺ activated Cl⁻ channels in rat ileum. *PLoS One*, 9, e87627.

- YANG, S. B., TIEN, A. C., BODDUPALLI, G., XU, A. W., JAN, Y. N. & JAN, L. Y. 2012b. Rapamycin ameliorates age-dependent obesity associated with increased mTOR signaling in hypothalamic POMC neurons. *Neuron*, 75, 425-36.
- YANG, Y., CHO, H., KOO, J., TAK, M., CHO, Y., SHIM, W., PARK, S., LEE, J., LEE, B., KIM, B., RAOUF, R., SHIN, Y. & OH, U. 2008. TMEM16A confers receptor-activated calcium-dependent chloride conductance. *Nature*, 455, 1210-5.
- YI, E., LEE, J. & LEE, C. J. 2013. Developmental Role of Anoctamin-1/TMEM16A in Ca(2+)-Dependent Volume Change in Supporting Cells of the Mouse Cochlea. *Exp Neurobiol*, 22, 322-9.
- YU, F. H. & CATTERALL, W. A. 2004. The VGL-chanome: a protein superfamily specialized for electrical signaling and ionic homeostasis. *Sci STKE*, 2004, re15.
- YU, K., DURAN, C., QU, Z., CUI, Y. Y. & HARTZELL, H. C. 2012a. Explaining calcium-dependent gating of anoctamin-1 chloride channels requires a revised topology. *Circ Res*, 110, 990-9.
- YU, K., ZHU, J., QU, Z., CUI, Y. Y. & HARTZELL, H. C. 2014. Activation of the Ano1 (TMEM16A) chloride channel by calcium is not mediated by calmodulin. *J Gen Physiol*.
- YU, W., ZEIDEL, M. L. & HILL, W. G. 2012b. Cellular expression profile for interstitial cells of cajal in bladder - a cell often misidentified as myocyte or myofibroblast. *PLoS One*, 7, e48897.
- YU, X. M. & HALL, Z. W. 1991. Extracellular domains mediating epsilon subunit interactions of muscle acetylcholine receptor. *Nature*, 352, 64-7.

- YUAN, P., LEONETTI, M. D., PICO, A. R., HSIUNG, Y. & MACKINNON, R. 2010. Structure of the human BK channel Ca²⁺-activation apparatus at 3.0 Å resolution. *Science*, 329, 182-6.
- ZECH, M., GROSS, N., JOCHIM, A., CASTROP, F., KAFFE, M., DRESEL, C., LICHTNER, P., PETERS, A., GIEGER, C., MEITINGER, T., HASLINGER, B. & WINKELMANN, J. 2014. Rare sequence variants in ANO3 and GNAL in a primary torsion dystonia series and controls. *Mov Disord*, 29, 143-7.
- ZERANGUE, N., JAN, Y. N. & JAN, L. Y. 2000. An artificial tetramerization domain restores efficient assembly of functional Shaker channels lacking T1. *Proc Natl Acad Sci U S A*, 97, 3591-5.
- ZERANGUE, N., SCHWAPPACH, B., JAN, Y. & JAN, L. 1999. A new ER trafficking signal regulates the subunit stoichiometry of plasma membrane K(ATP) channels. *Neuron*, 22, 537-48.
- ZHANG, C. H., LI, Y., ZHAO, W., LIFSHITZ, L. M., LI, H., HARFE, B. D., ZHU, M. S. & ZHUGE, R. 2013. The transmembrane protein 16A Ca(2+)-activated Cl⁻ channel in airway smooth muscle contributes to airway hyperresponsiveness. *Am J Respir Crit Care Med*, 187, 374-81.
- ZHAO, P., TORCASO, A., MARIANO, A., XU, L., MOHSIN, S., ZHAO, L. & HAN, R. 2014. Anoctamin 6 regulates C2C12 myoblast proliferation. *PLoS One*, 9, e92749.
- ZHU, M., KIM, T., RO, S., YAN, W., WARD, S., KOH, S. & SANDERS, K. 2009. A Ca(2+)-activated Cl(-) conductance in interstitial cells of Cajal linked to slow wave currents and pacemaker activity. *J Physiol*, 587, 4905-18.

Figure 1.1

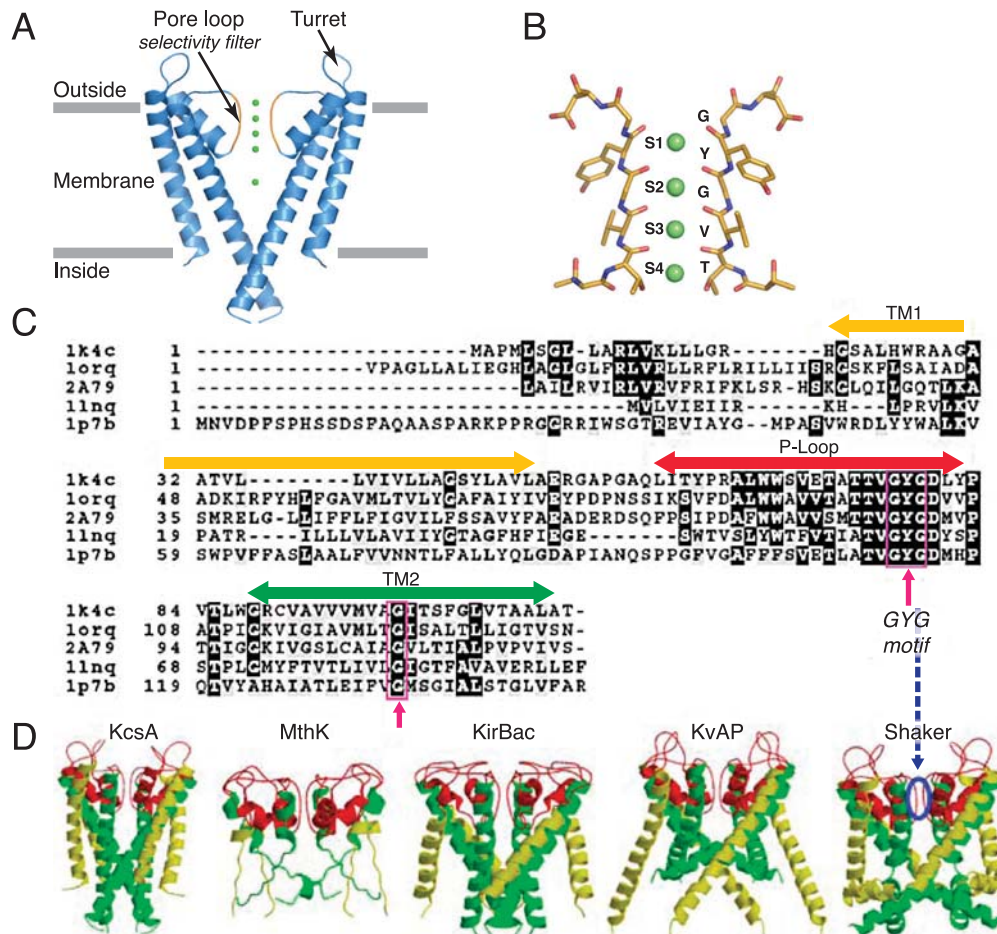
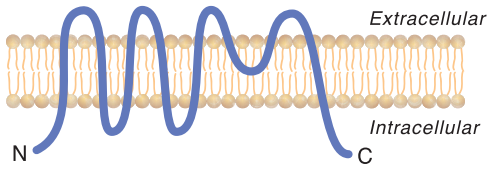
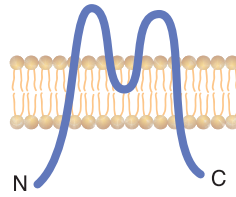


Figure 1.2

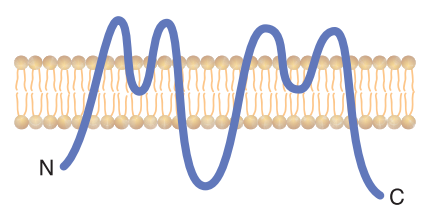
A. 6 TM



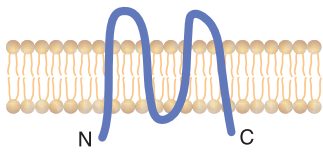
B. 2 TM



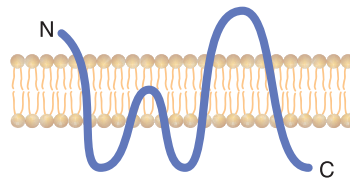
C. Two pore



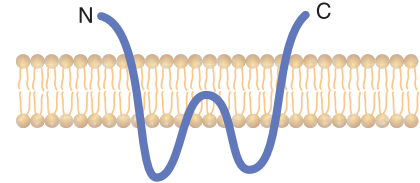
D. Voltage-gated proton channel



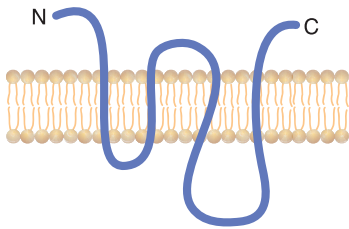
E1. Glutamate receptors



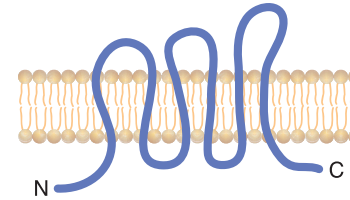
E2. Prokaryotic glutamate receptors



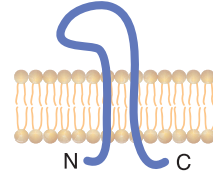
F. Cys-loop receptors



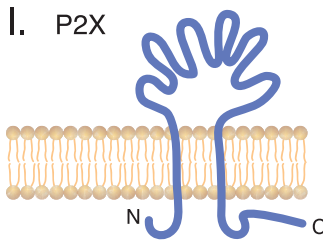
G. IP₃ receptors



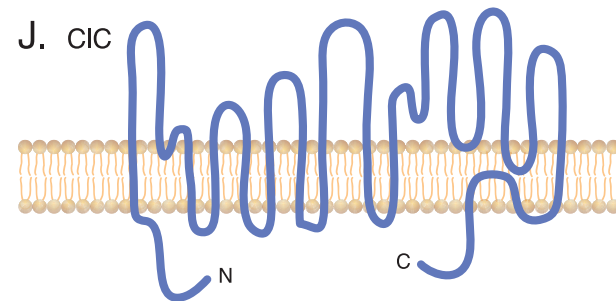
H. ENaC



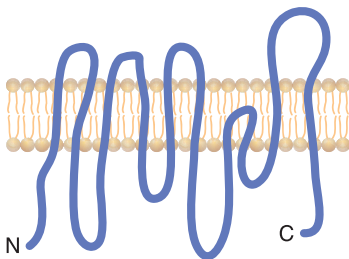
I. P2X



J. CIC



K. TMEM16



L. CFTR

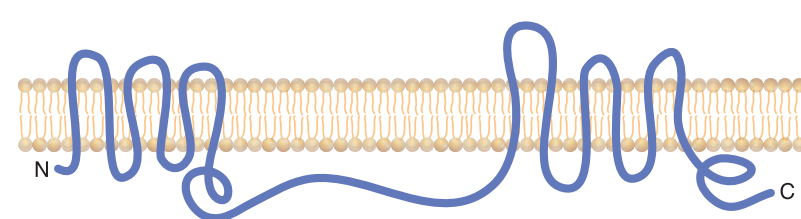


Figure 1.3

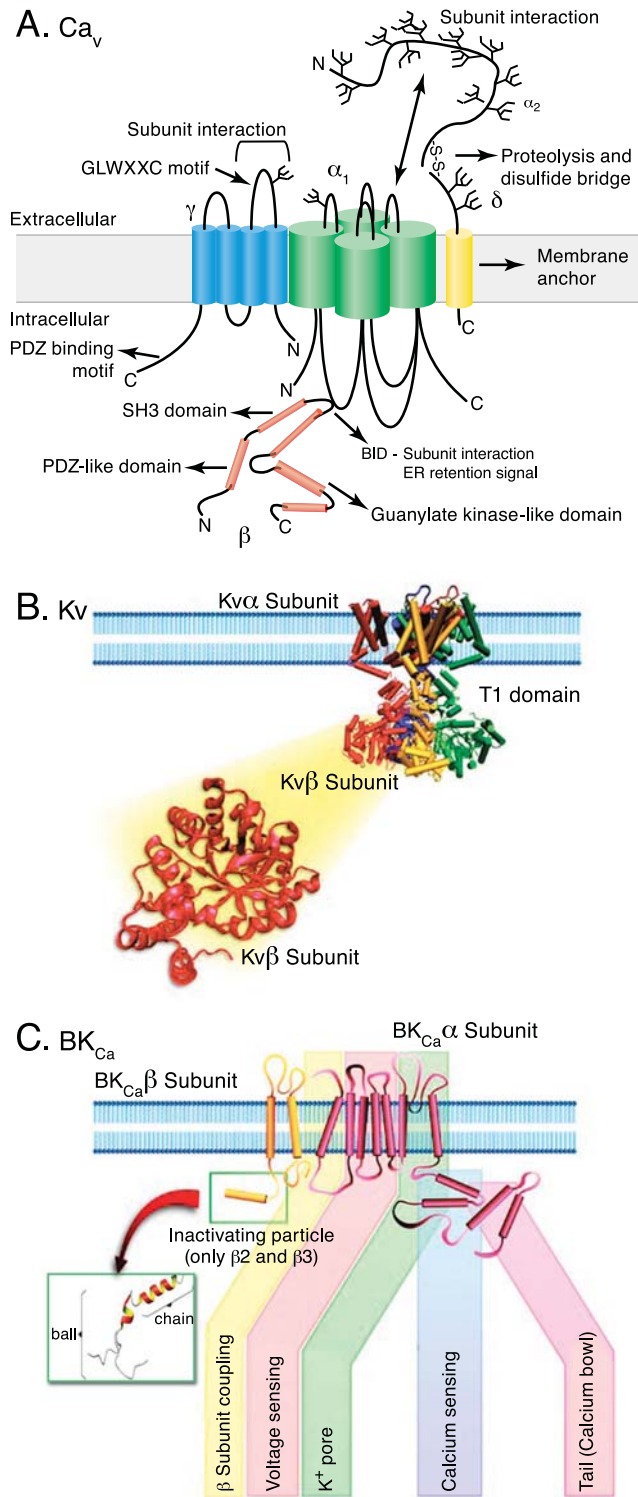


Figure 1.4

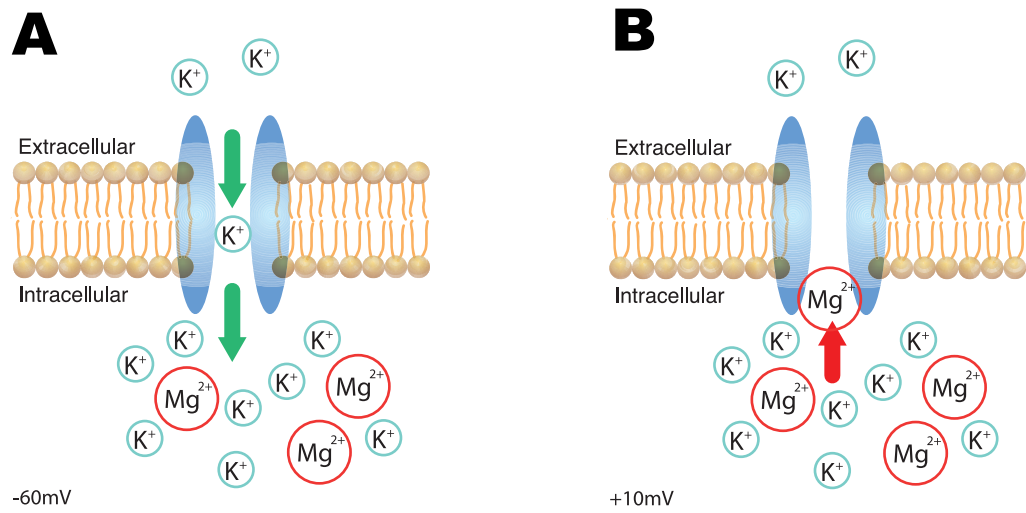


Figure 2.1

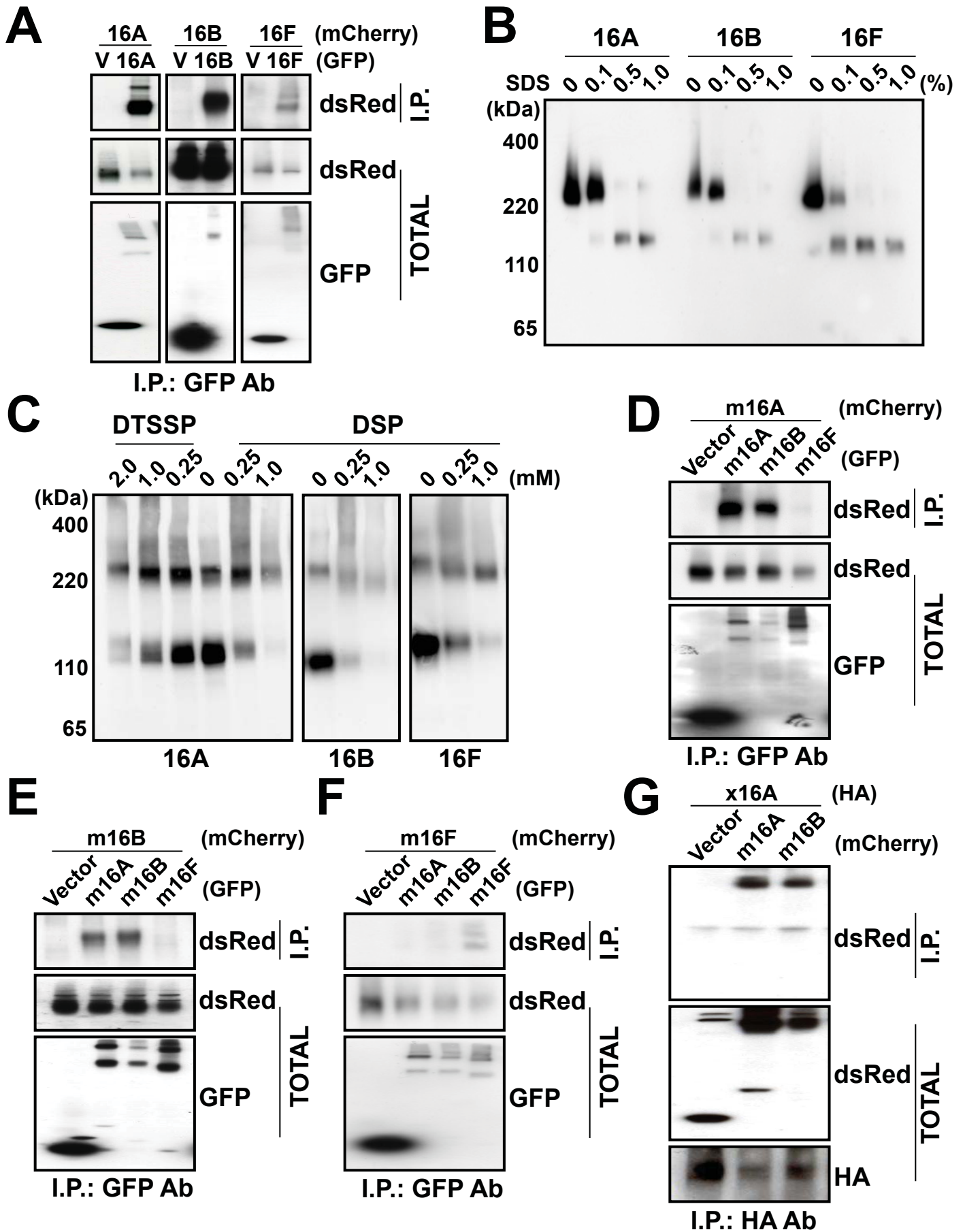
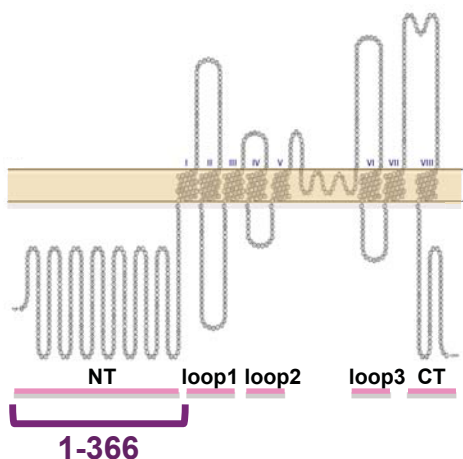
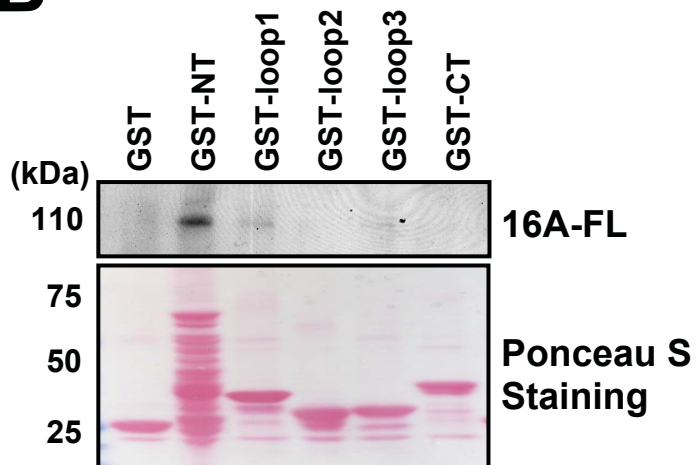


Figure 2.2

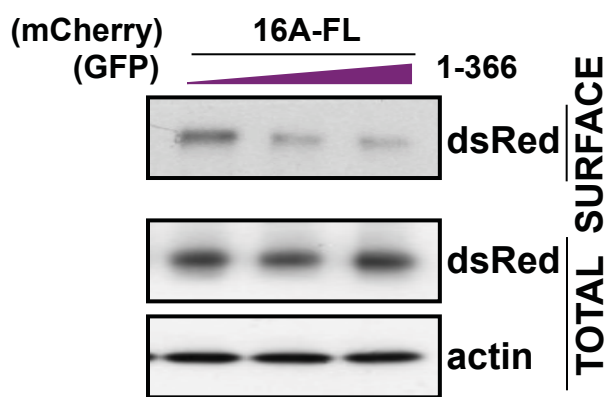
A



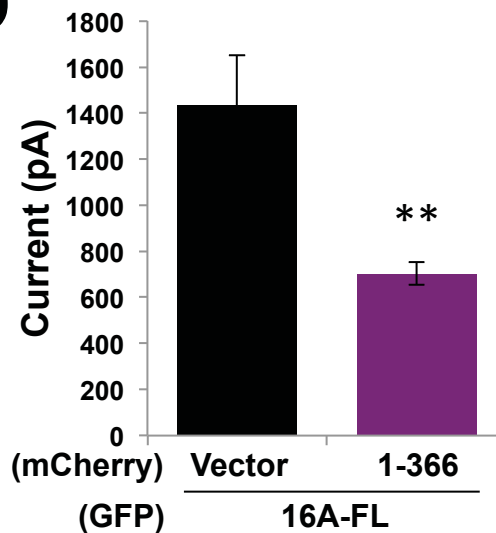
B



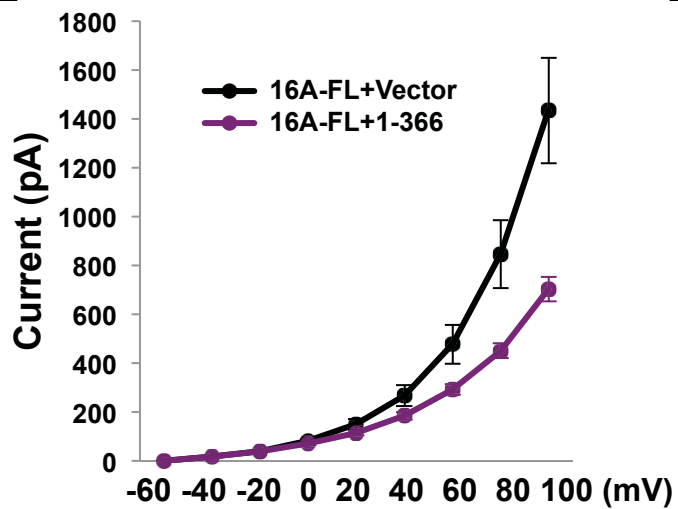
C



D



E



F

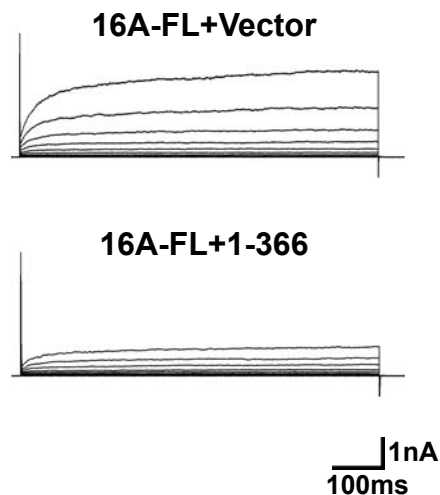
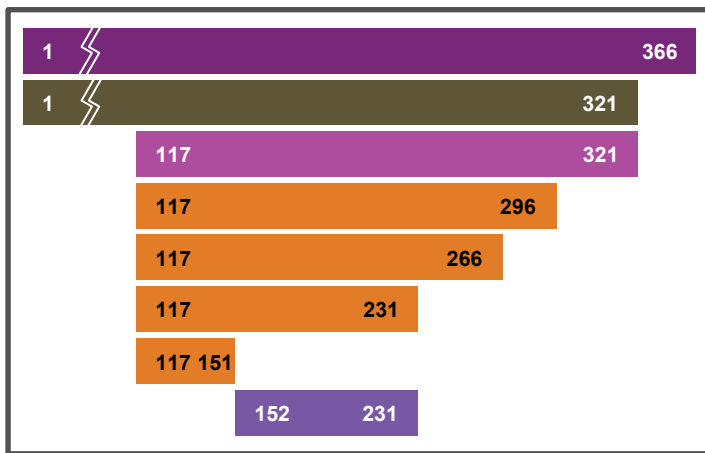
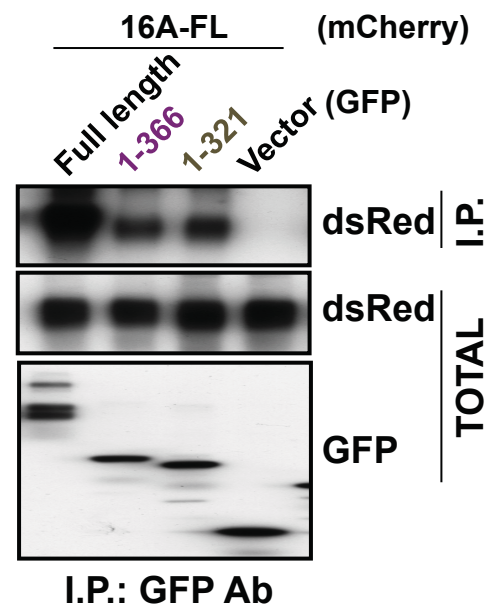


Figure 2.3

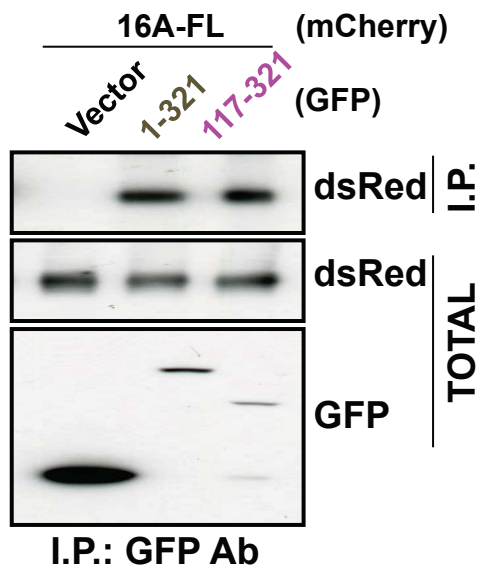
A



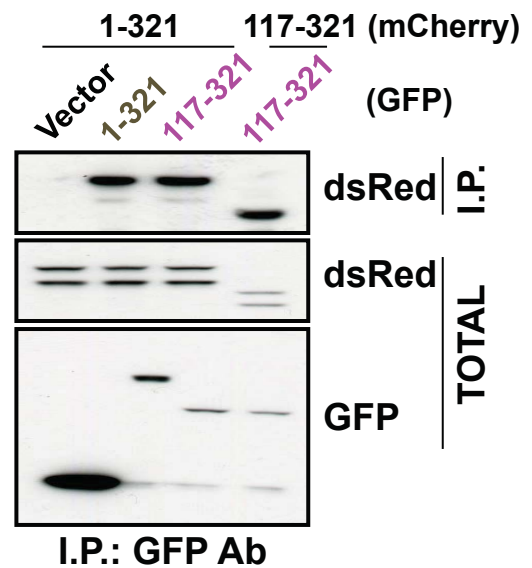
B



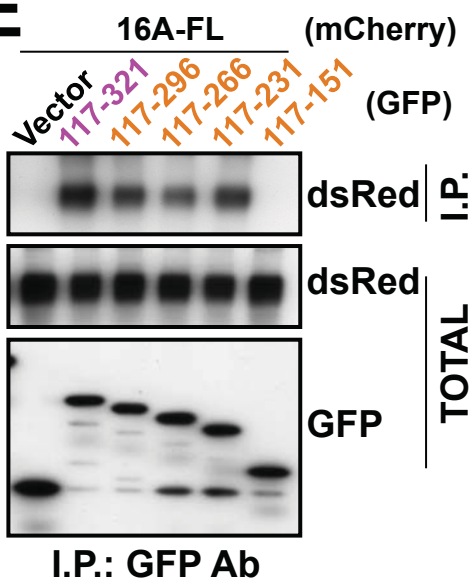
C



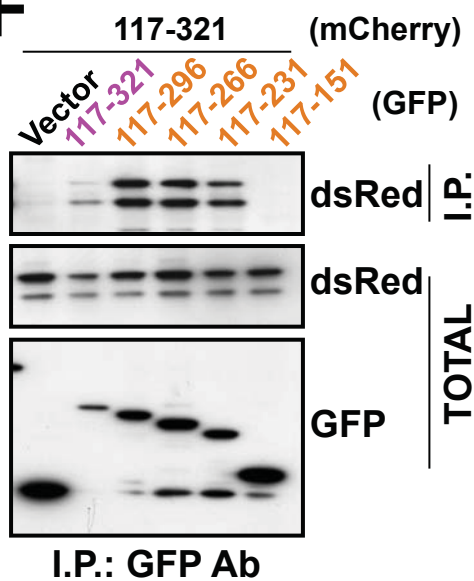
D



E



F



G

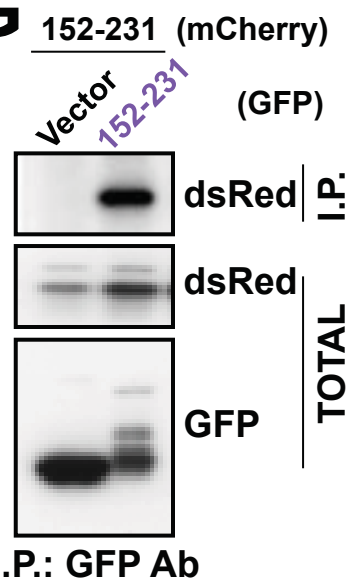


Figure 2.4

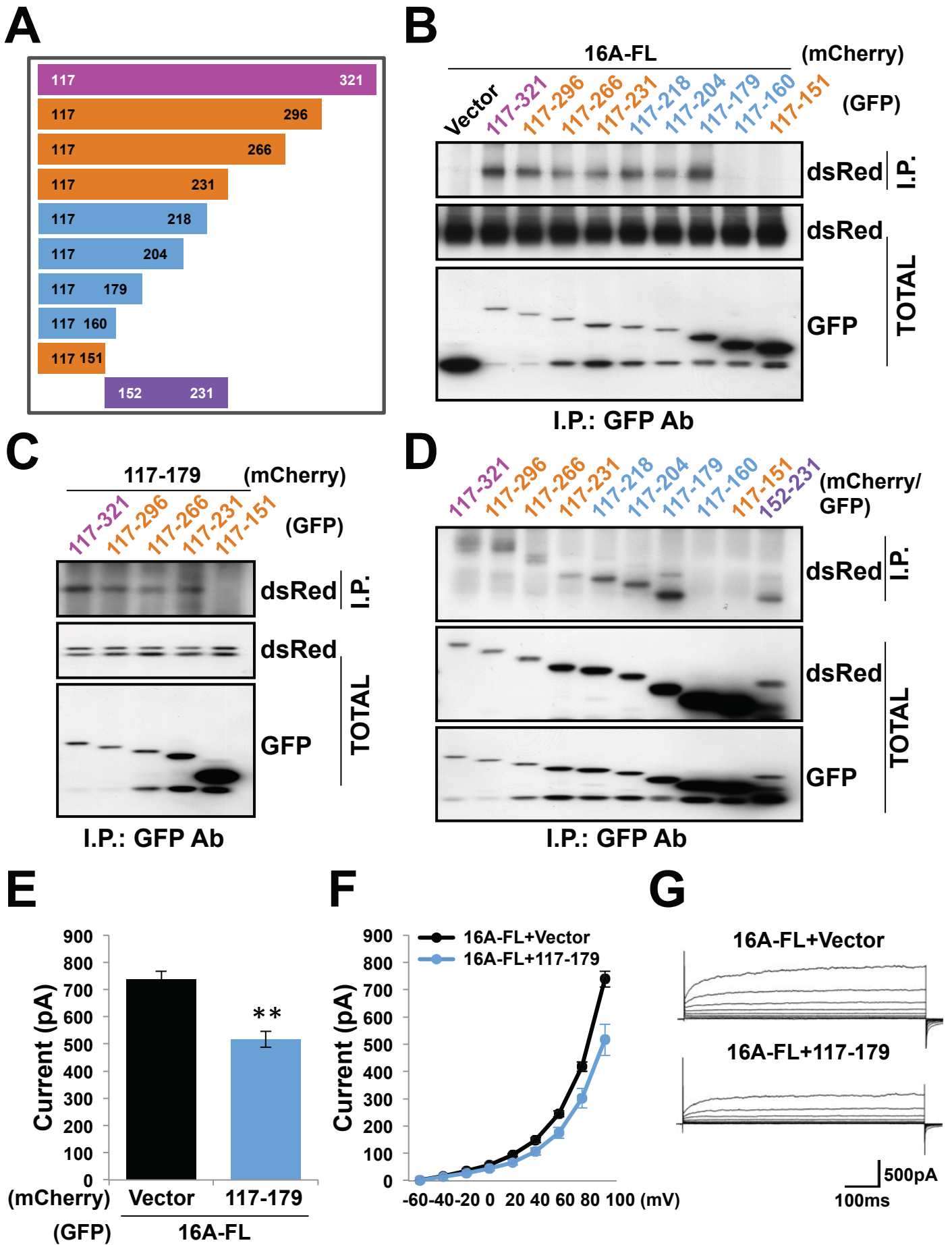


Figure 2.5

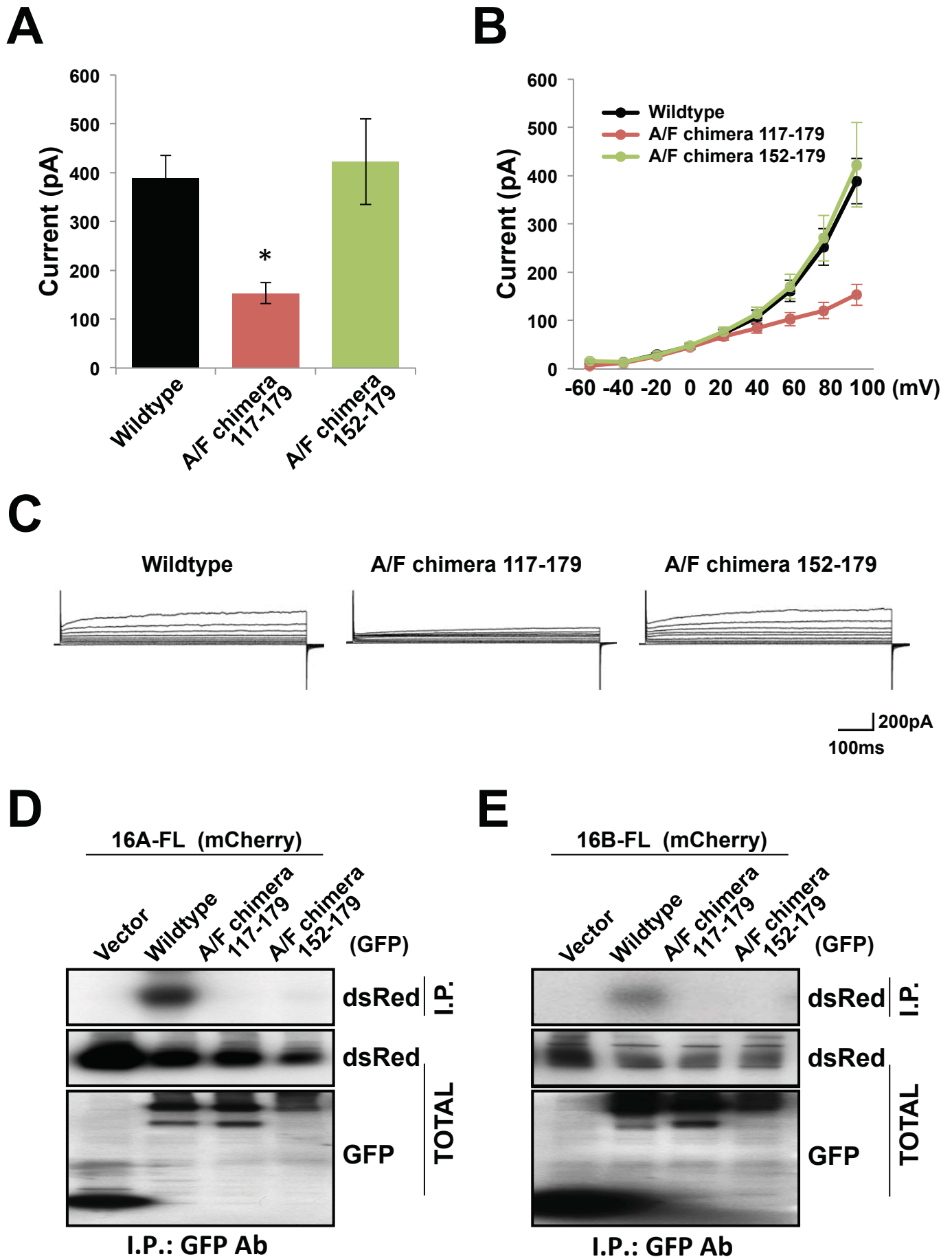


Figure 2.6

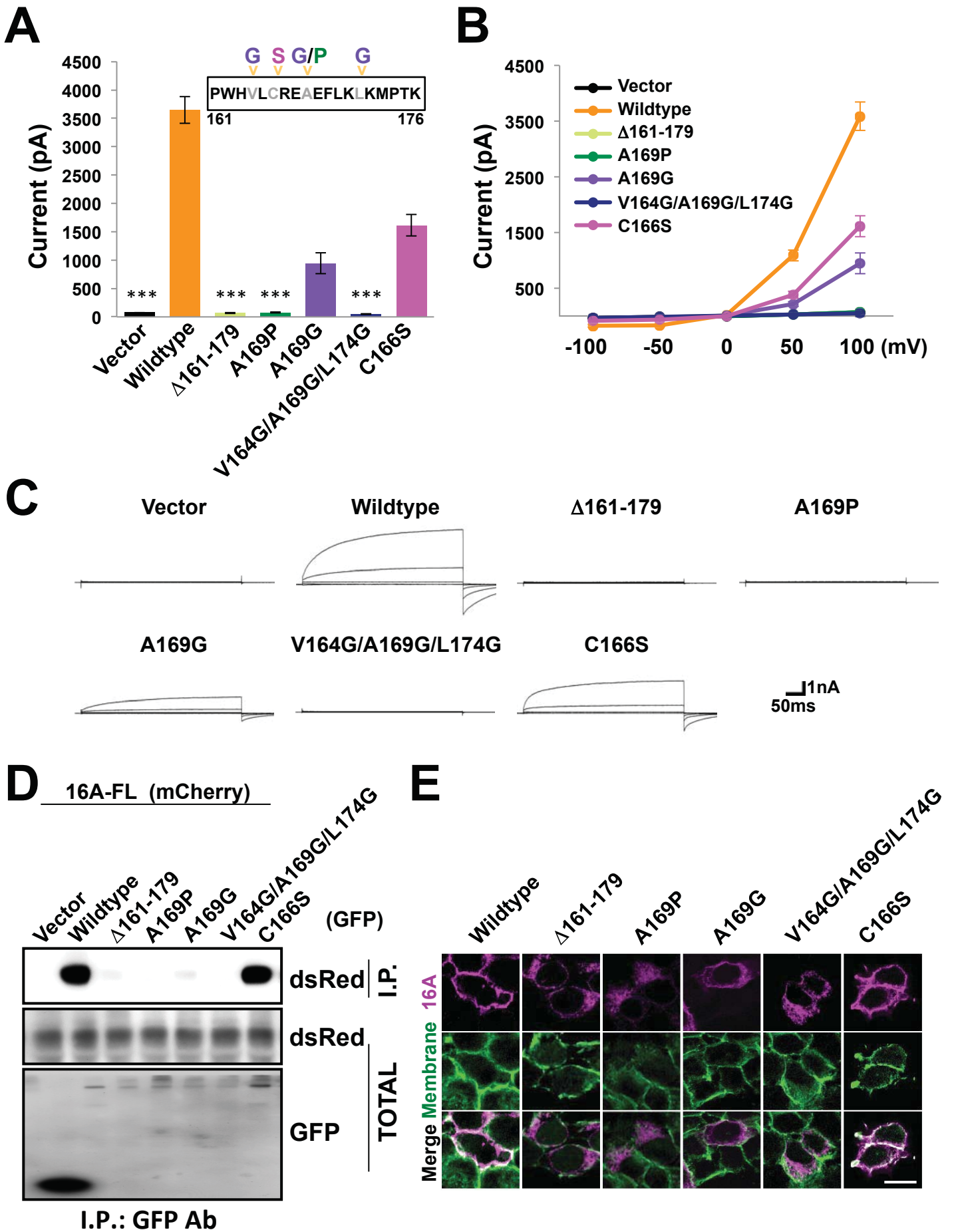


Figure 2.S1

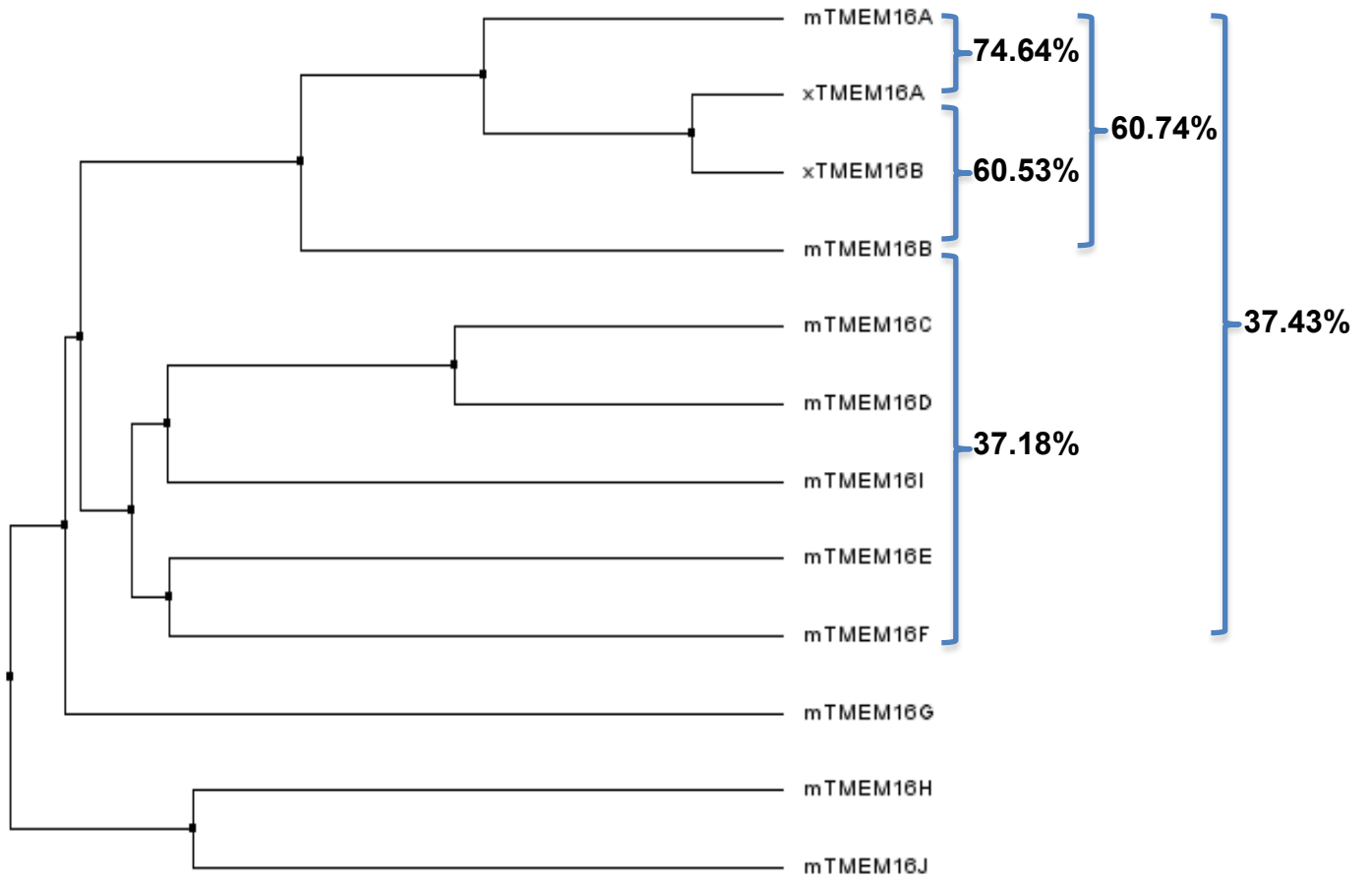


Figure 2.S2

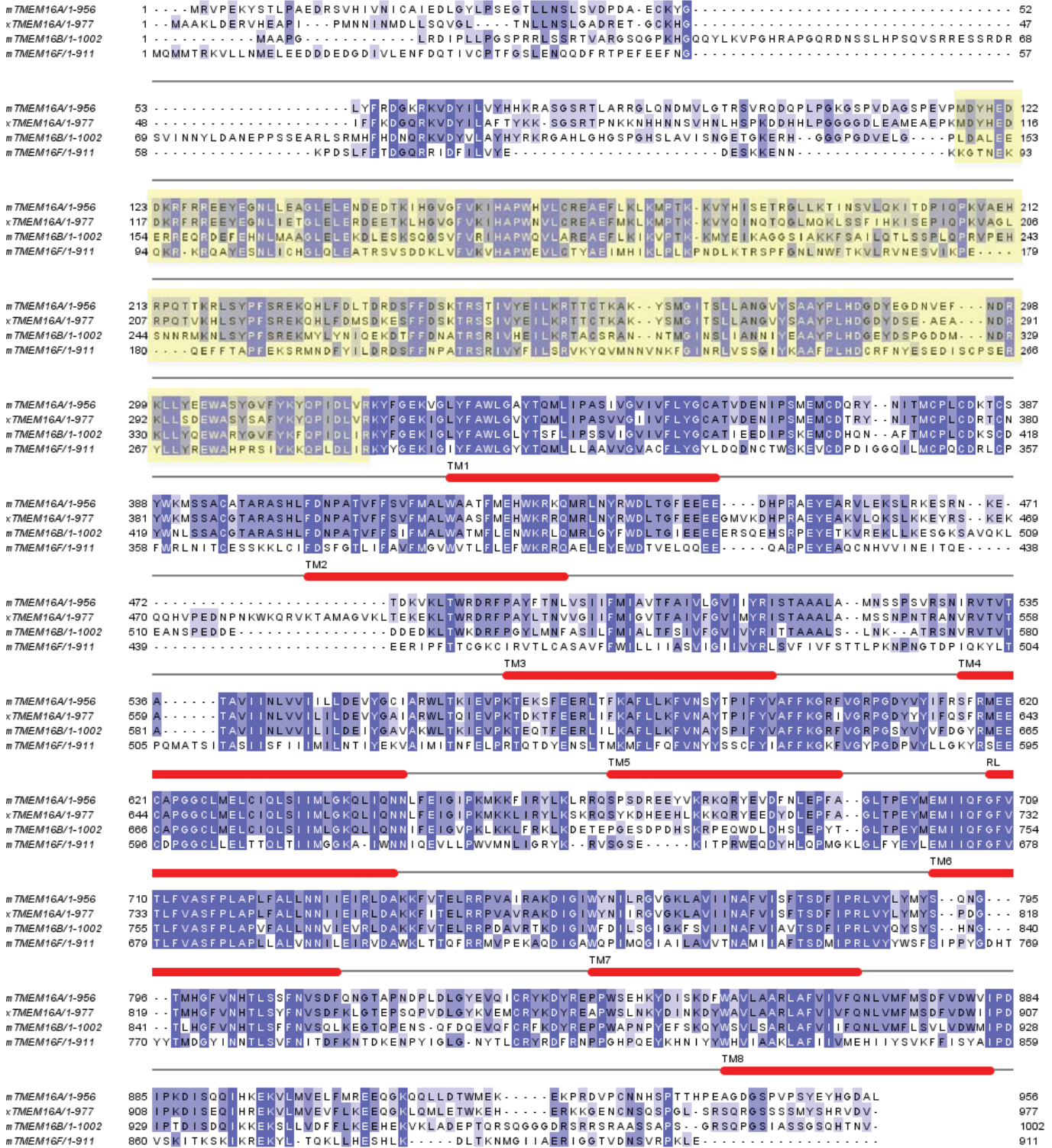
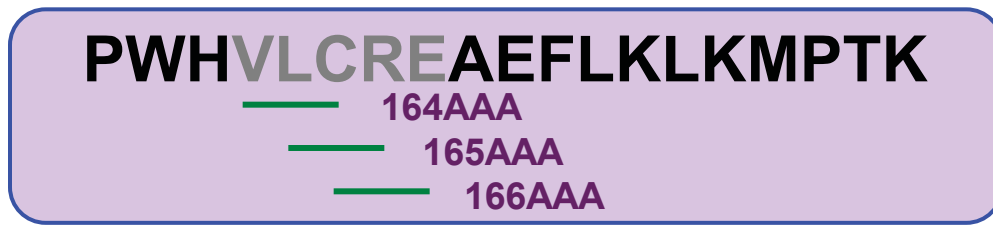
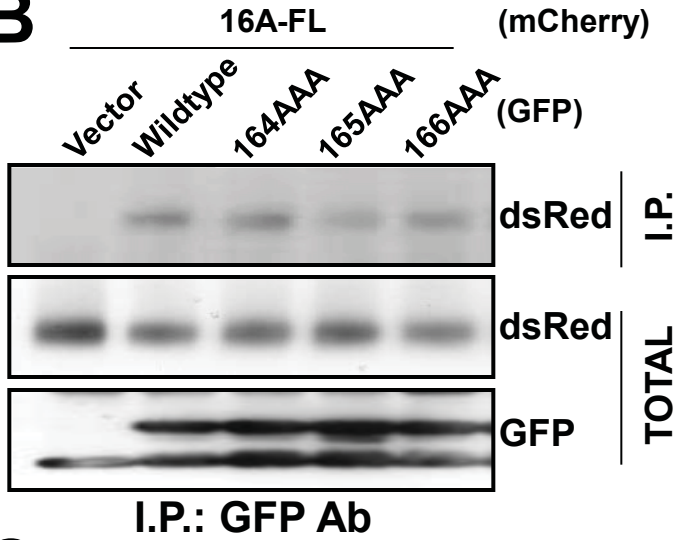


Figure 2.S3

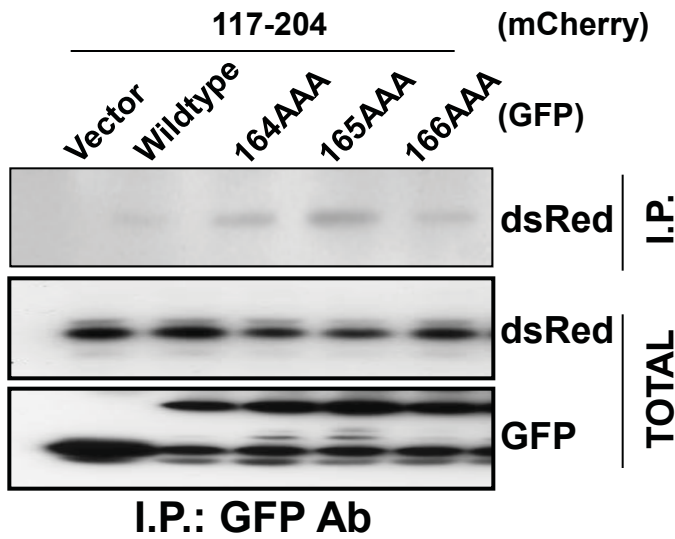
A



B



C



D

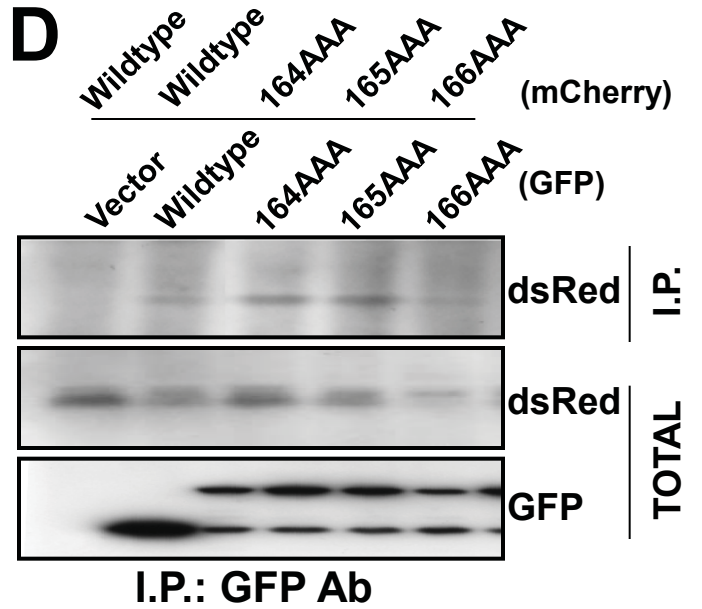


Figure 2.S4

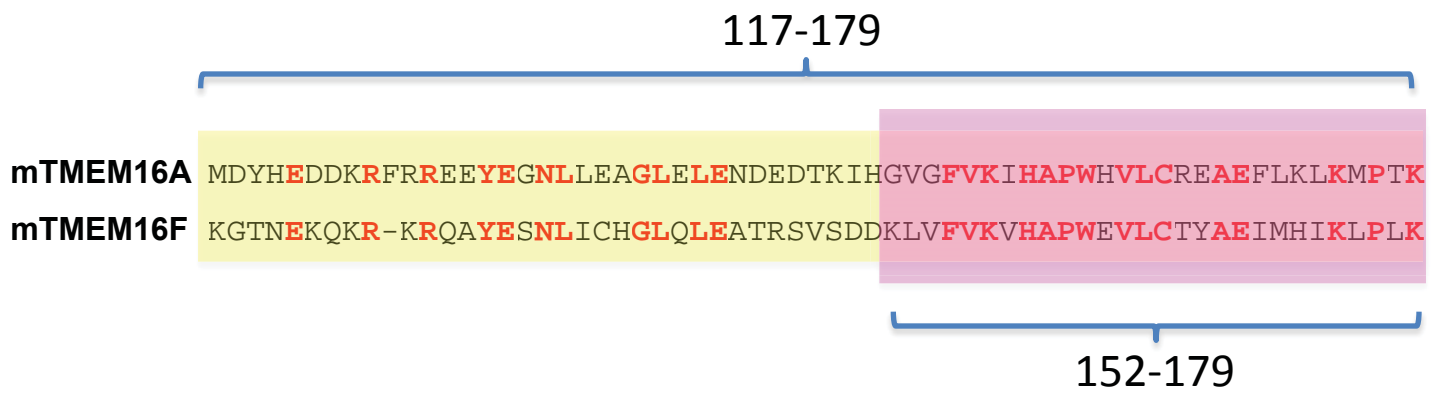


Figure 2.S5

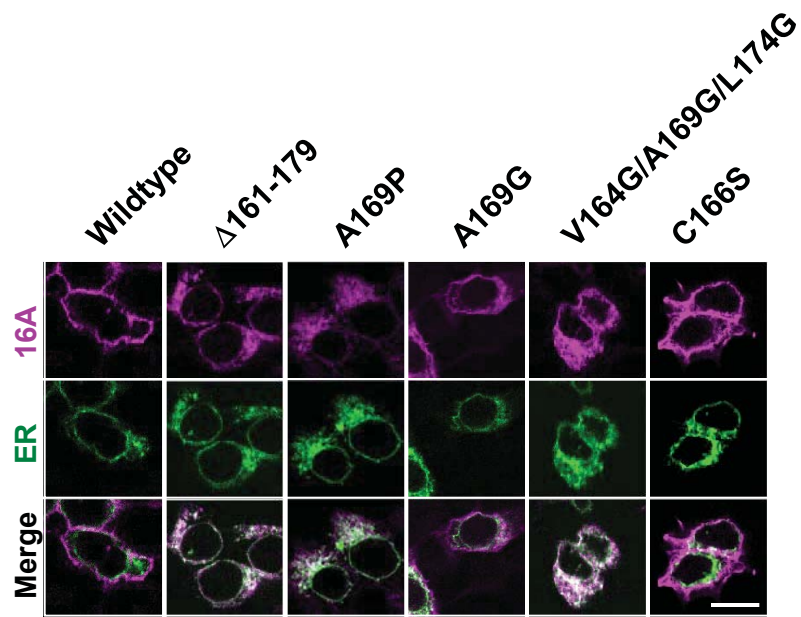


Figure 3.1

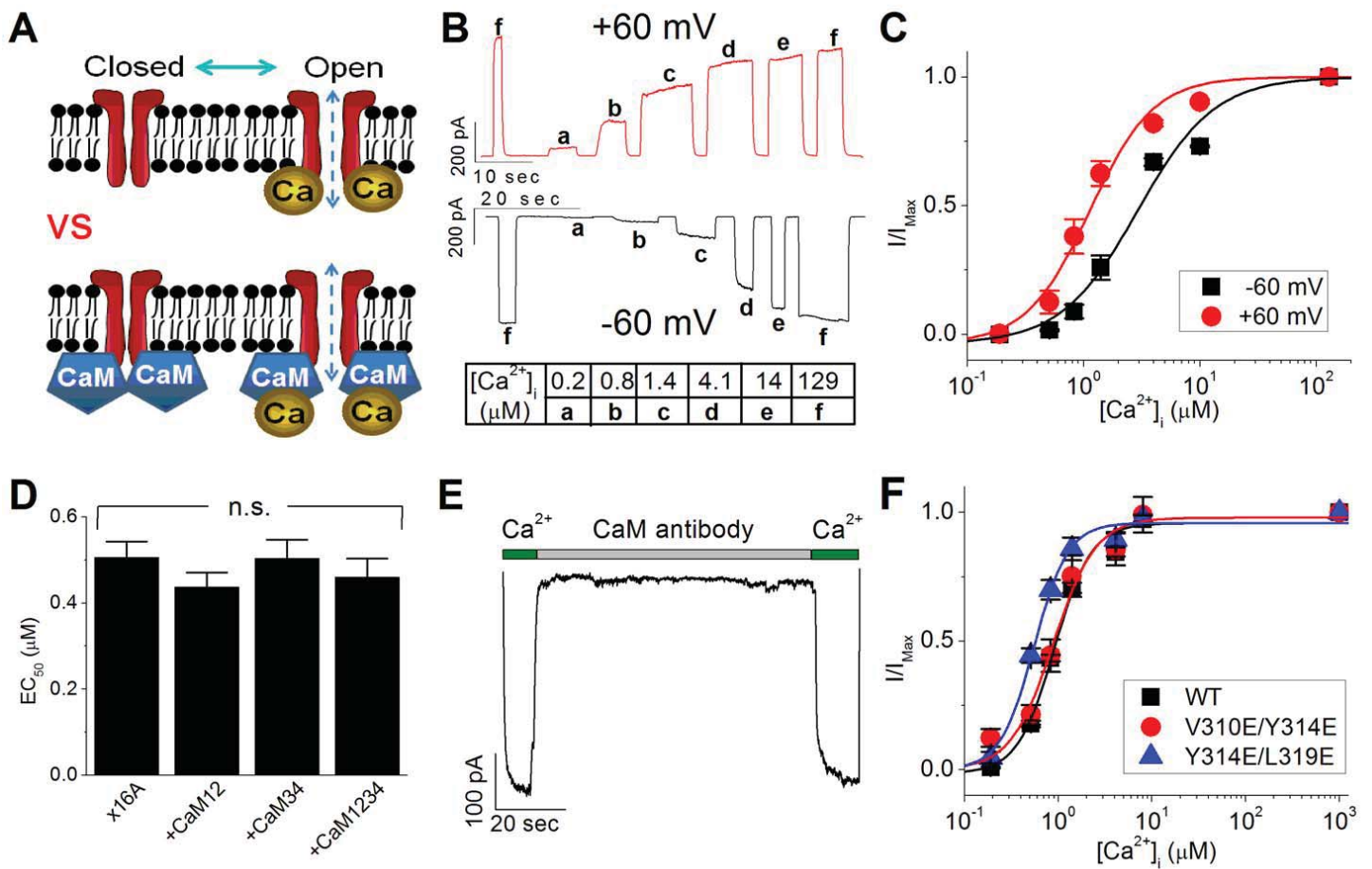


Figure 3.2

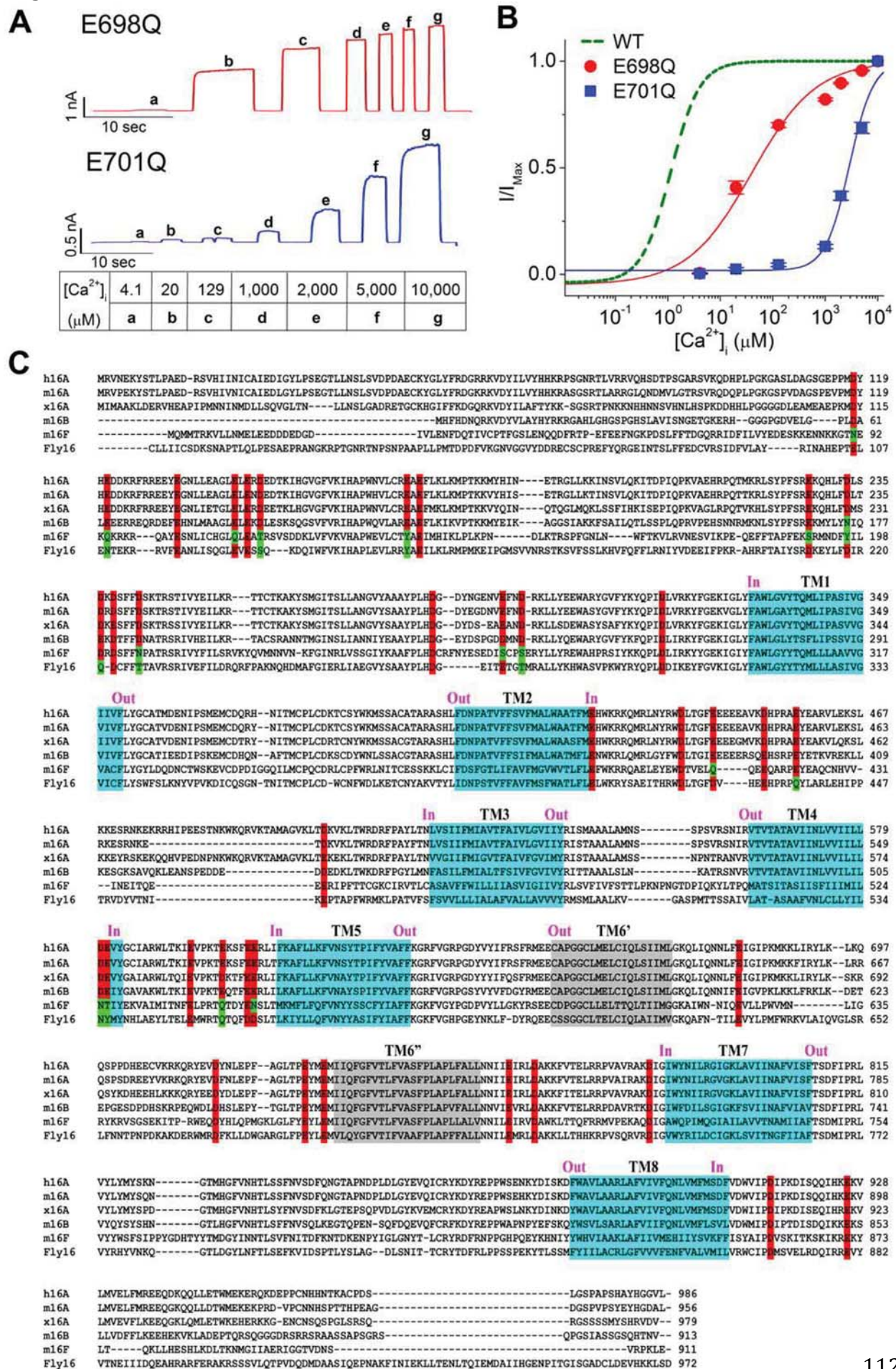


Figure 3.3

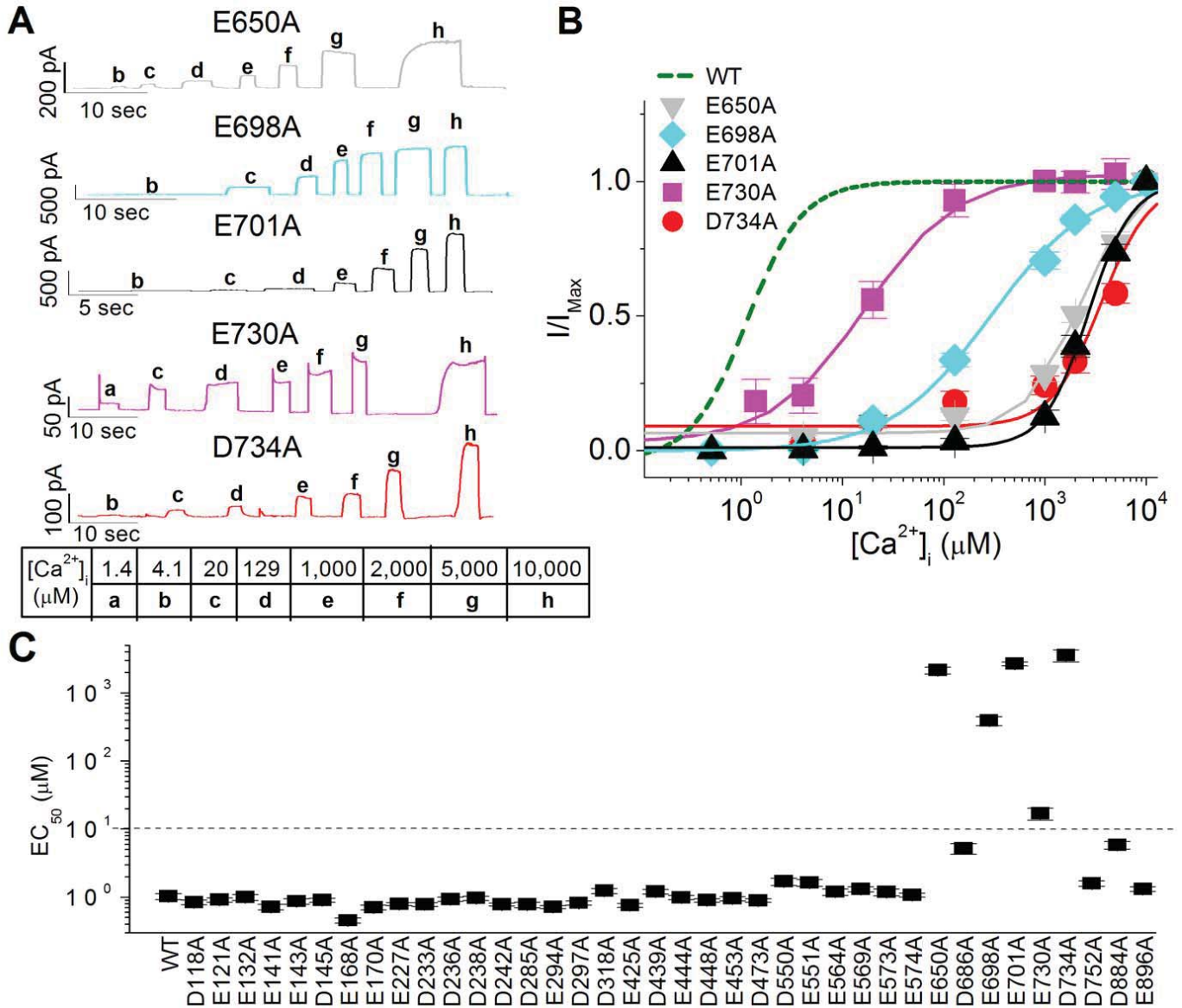


Figure 3.4

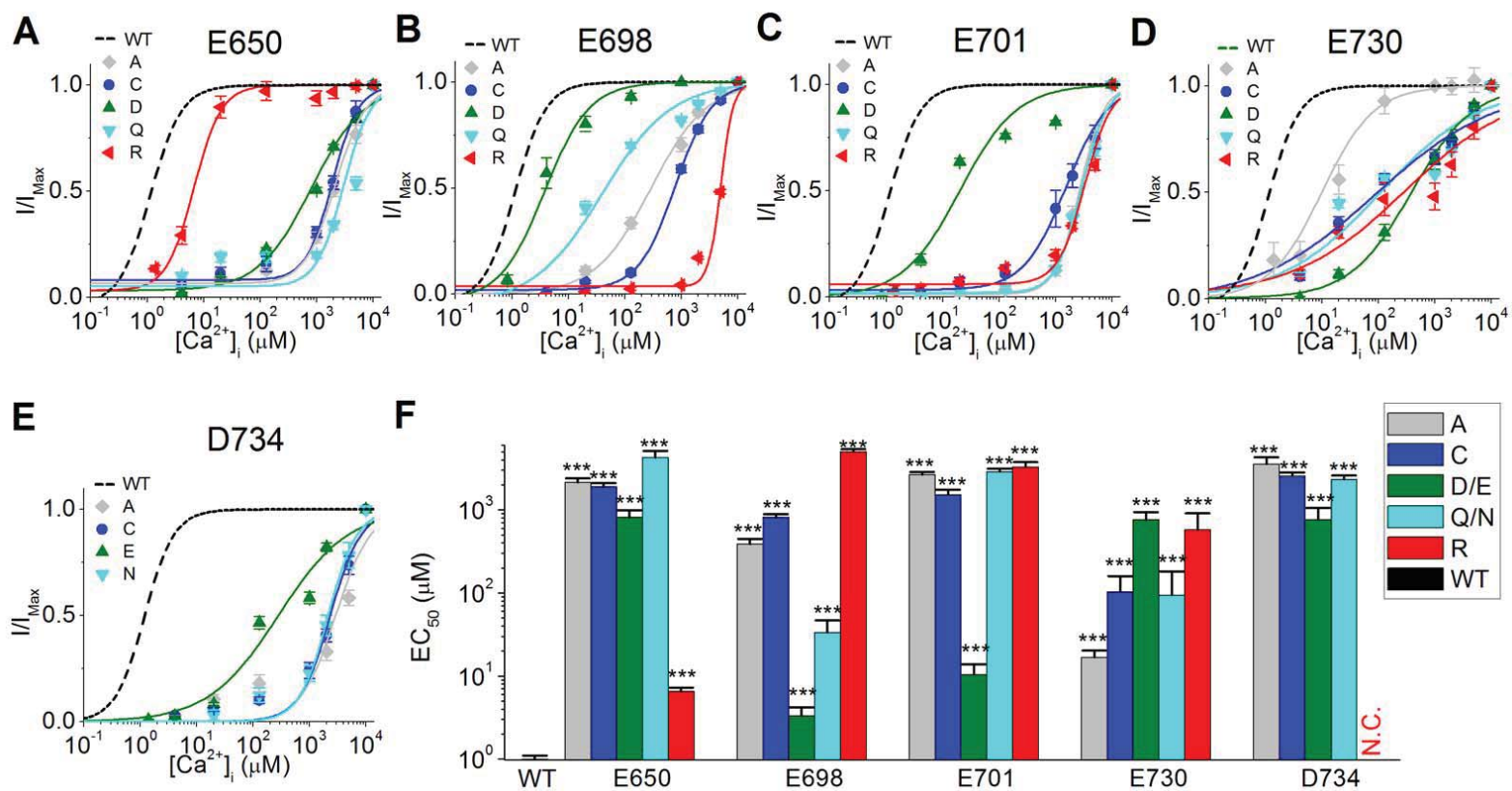


Figure 3.5

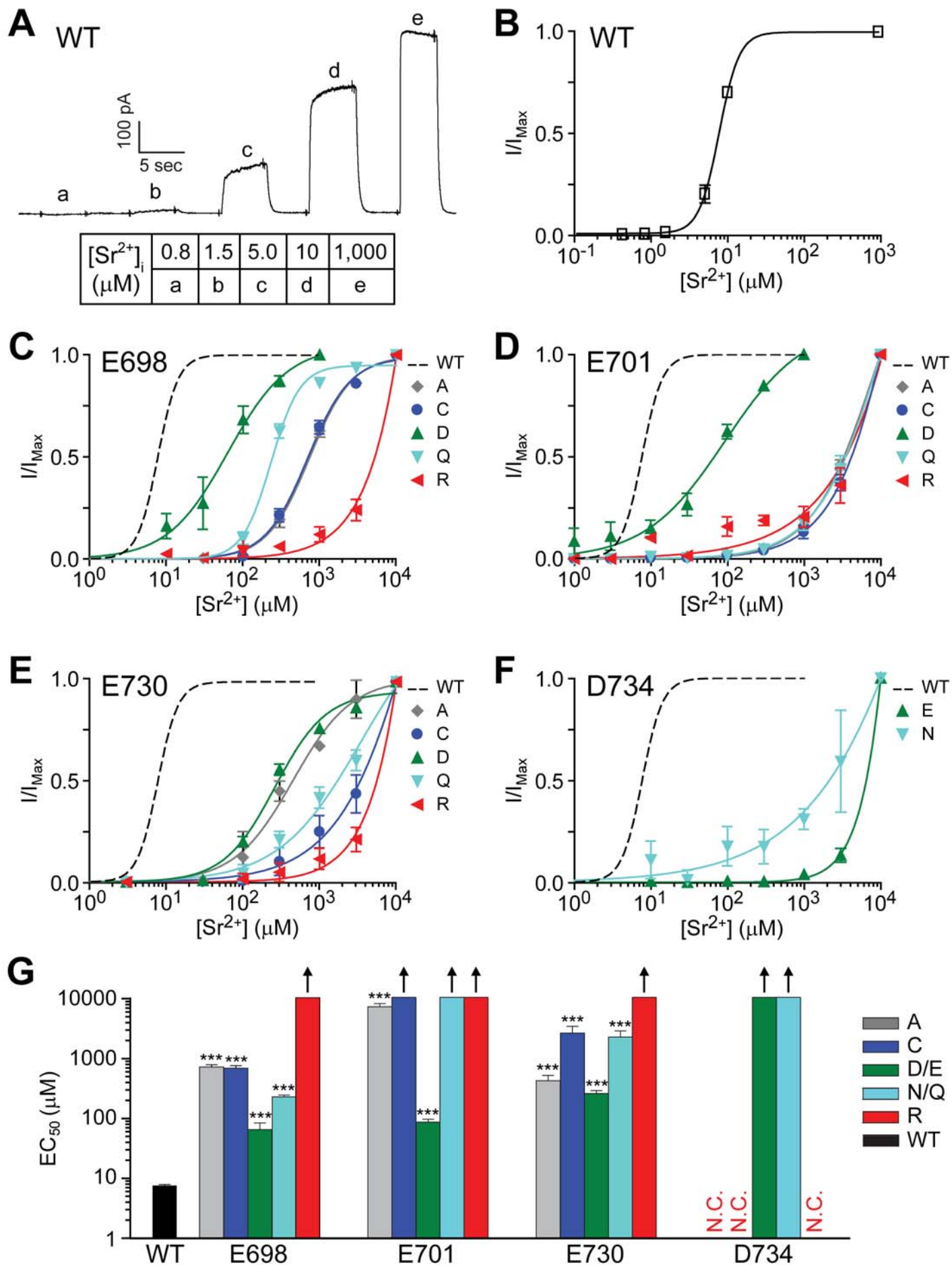


Figure 3.6

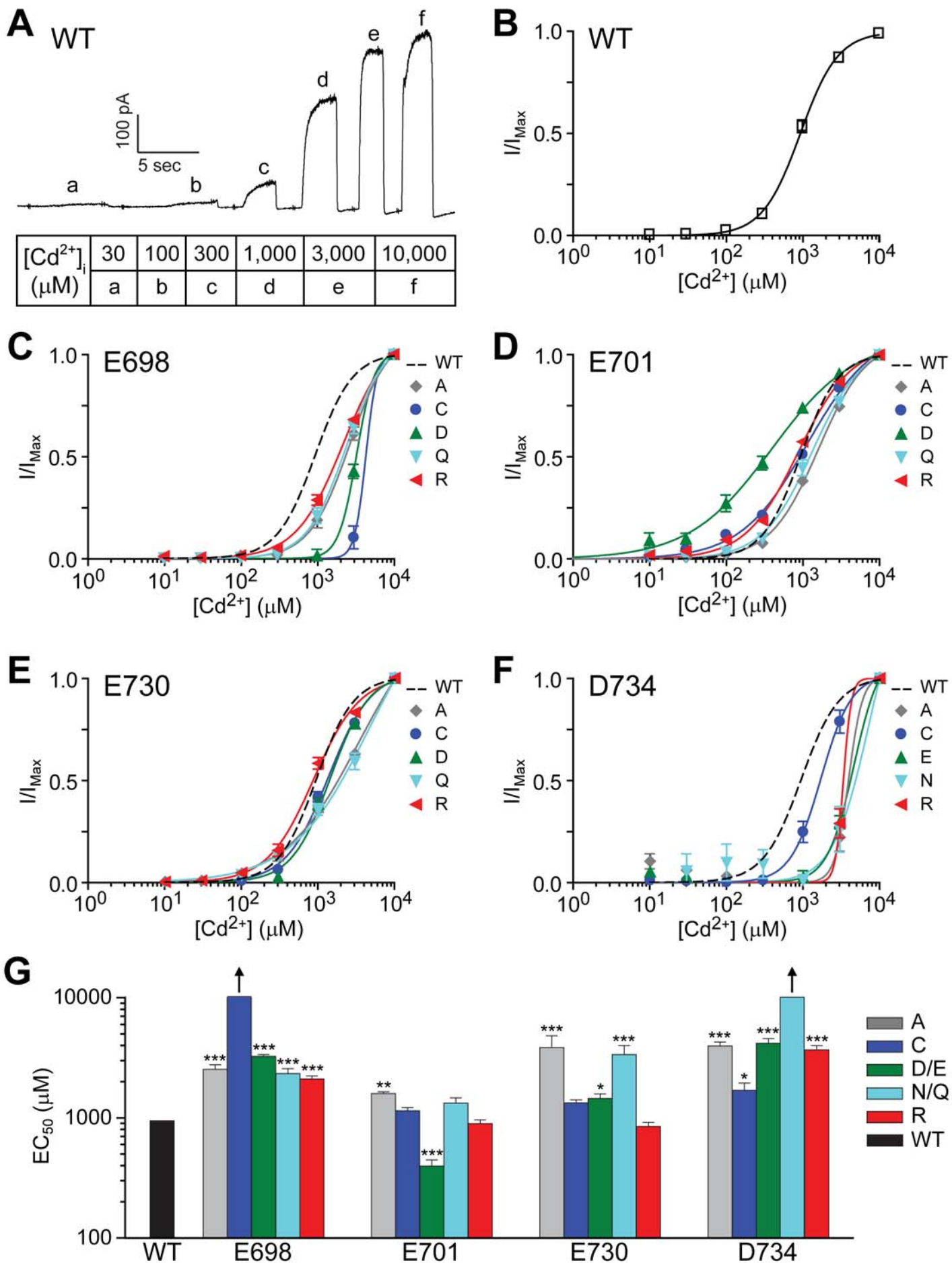


Figure 3.7

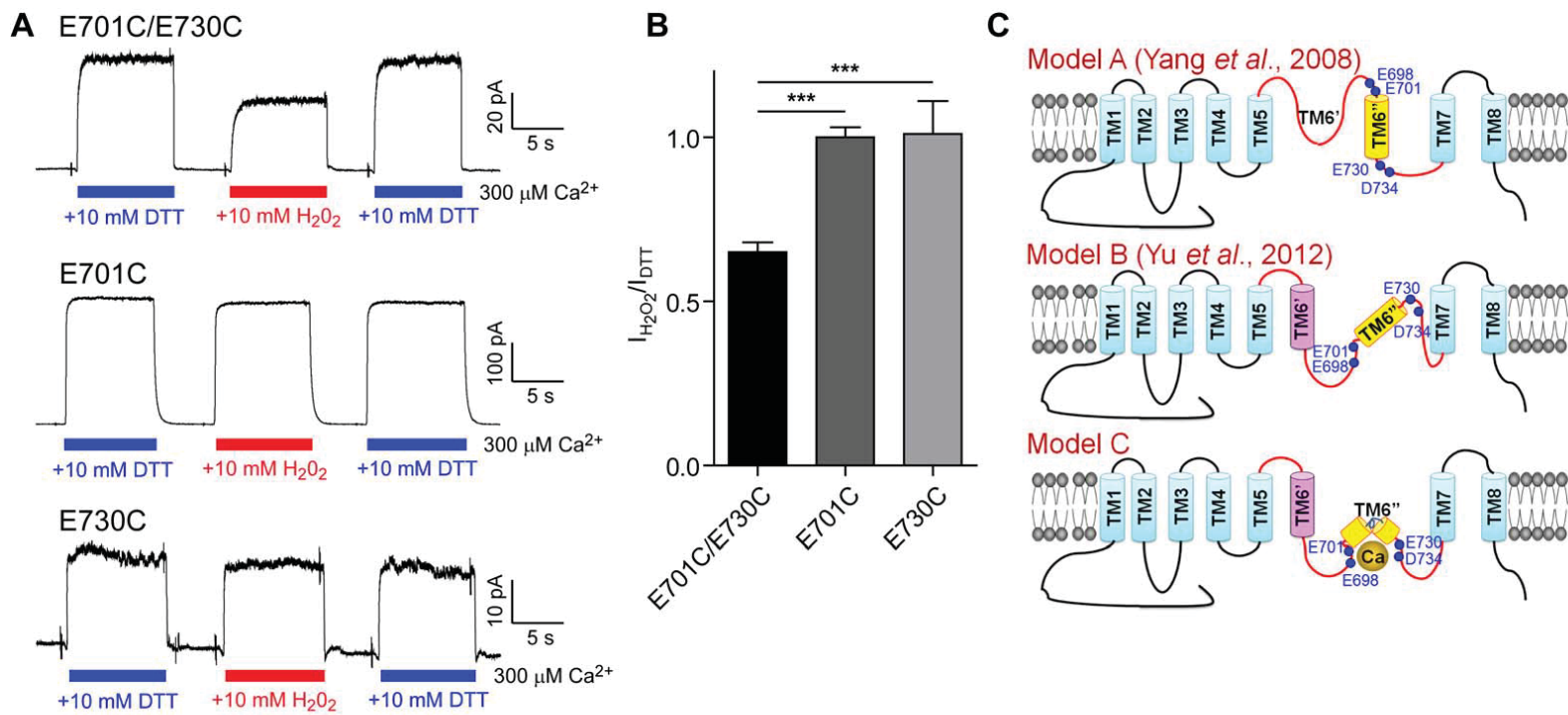
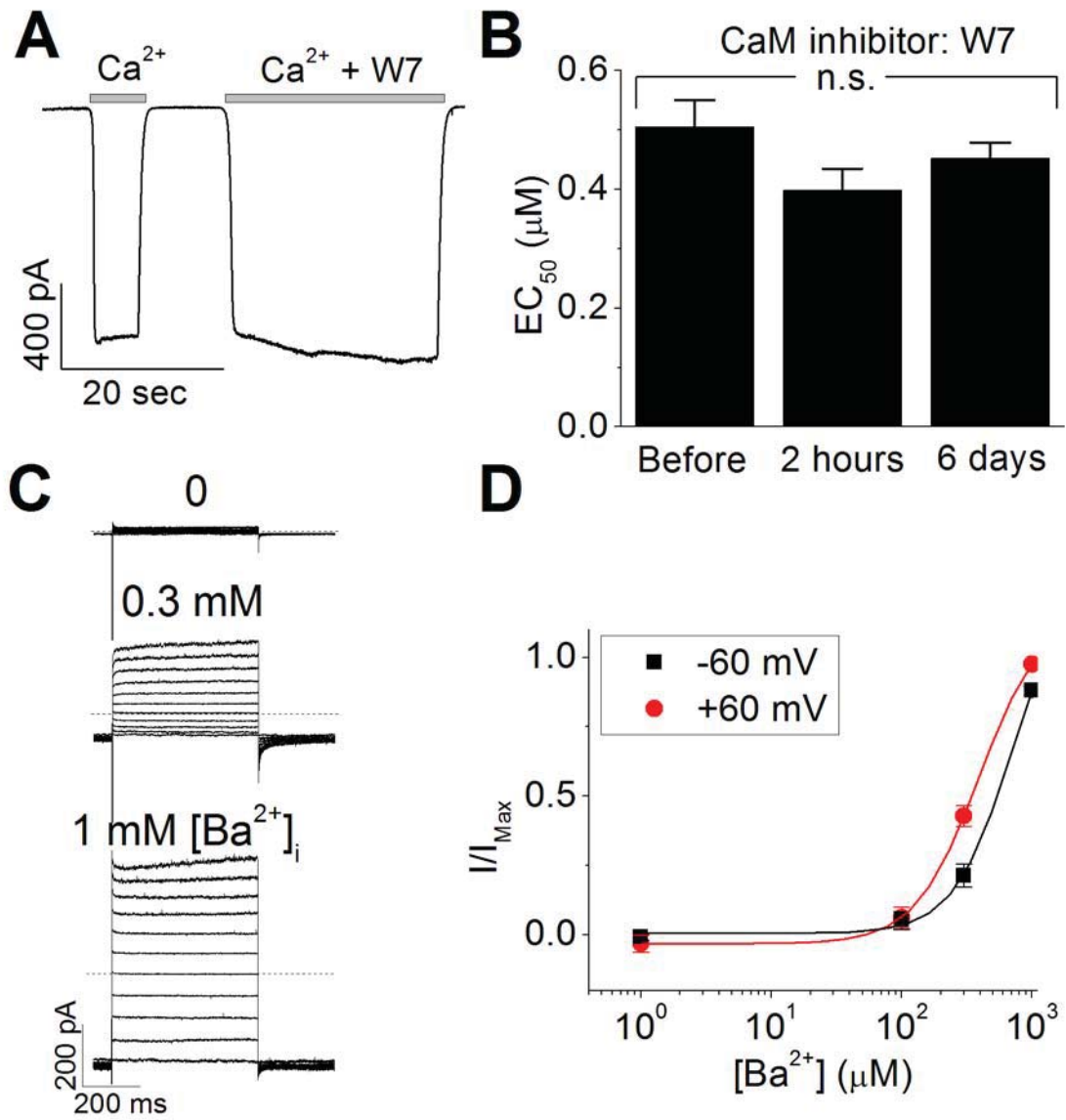


Figure 3.S1



Publishing Agreement

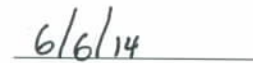
It is the policy of the University to encourage the distribution of all theses, dissertations, and manuscripts. Copies of all UCSF theses, dissertations, and manuscripts will be routed to the library via the Graduate Division. The library will make all theses, dissertations, and manuscripts accessible to the public and will preserve these to the best of their abilities, in perpetuity.

Please sign the following statement:

I hereby grant permission to the Graduate Division of the University of California, San Francisco to release copies of my thesis, dissertation, or manuscript to the Campus Library to provide access and preservation, in whole or in part, in perpetuity.



Author Signature



Date